



**HAL**  
open science

# Molecular insights in tracking optical properties and antioxidant activities of polyphenols

Michal Biler

► **To cite this version:**

Michal Biler. Molecular insights in tracking optical properties and antioxidant activities of polyphenols. Other. Université de Limoges; Univerzita Palackého (Olomouc, République Tchèque), 2017. English. NNT: 2017LIMO0001 . tel-01544039

**HAL Id: tel-01544039**

**<https://theses.hal.science/tel-01544039v1>**

Submitted on 21 Jun 2017

**HAL** is a multi-disciplinary open access archive for the deposit and dissemination of scientific research documents, whether they are published or not. The documents may come from teaching and research institutions in France or abroad, or from public or private research centers.

L'archive ouverte pluridisciplinaire **HAL**, est destinée au dépôt et à la diffusion de documents scientifiques de niveau recherche, publiés ou non, émanant des établissements d'enseignement et de recherche français ou étrangers, des laboratoires publics ou privés.



Palacký University  
Olomouc



Université  
de Limoges

PALACKÝ UNIVERSITY OLOMOUC, Czech Republic  
Department of Biophysics, Faculty of Science

LIMOGES UNIVERSITY, France  
École Doctorale Gay Lussac – Science pour l'Environnement  
INSERM UMR-S 850, Faculty of Pharmacy

Specialty:  
Biophysics / Theoretical chemistry

## **Molecular insights in tracking optical properties and antioxidant activities of polyphenols**

(Doctoral Thesis)  
2013 - 2017

**Presented and defended by:** Michal Biler

**Date:** 8<sup>th</sup> February 2017

### **Reviewers:**

Pr. Johannes Gierschner  
Pr. Martin Hof

IMDEA Nanoscience Madrid, Spain  
J. Heyrovský Institute of Physical Chemistry  
of the ASCR, v.v.i. Prague. Czech Republic

### **Examinators:**

Assoc. Pr. Martin Kubala (supervisor)  
Pr. Patrick Trouillas (supervisor)  
Dr. Florent Di Meo  
Pr. Petr Ilík  
Assoc. Pr. Dušan Lazár

Palacký University Olomouc, Czech Republic  
Limoges University, France  
Limoges University, France  
Palacký University Olomouc, Czech Republic  
Palacký University Olomouc, Czech Republic

*'A journey of a thousand mile begins with a smile.'*

*--- Bernard Kelvin Clive ---*

## TABLE OF CONTENT

ACKNOWLEDGMENT .....	V
PROCLAMATION .....	VII
ABSTRACT .....	VIII
SHRNUTÍ .....	IX
RÉSUMÉ .....	X
LIST OF ABBREVIATIONS .....	XI
LIST OF PUBLICATIONS .....	XIII
1. INTRODUCTION .....	14
2. FLAVONOID DERIVATIVES .....	17
2.A. Introduction .....	17
2.B. Generalities about flavonoids .....	18
2.C. Flavonolignans .....	21
2.D. Generalities about anthocyanins .....	23
2.E. Charge states in anthocyanins .....	26
2.F. Pyranoanthocyanins .....	28
2.G. Copigmentation .....	29
3. THEORETICAL CHEMISTRY METHODS .....	32
3.A General concepts of theoretical chemistry .....	32
3.A.a The Born-Oppenheimer approximation .....	32
3.A.b The Hartree-Fock approximation .....	33
3.A.c Post Hartree-Fock methods .....	34
3.A.d Basis sets .....	36
3.B Density functional theory .....	37
3.B.a Hohenberg and Kohn theorems .....	38
3.B.b Kohn-Sham approach .....	39
3.B.c Exchange-correlation functionals .....	40
3.B.d Dispersion correction of DFT .....	42
3.C QM/MM .....	44
4. HOW TO CALCULATE EXPERIMENTAL OBSERVABLES? .....	47
4.A Sampling the conformational space .....	47
4.B Molecular spectroscopy: TD-DFT .....	48

4.B.a	Runge-Gross theorem	48
4.B.b	Selection rules for absorption spectroscopy	49
4.B.c	Energies between ground and excited states	51
4.B.d	Different methods for evaluation of the excited states	52
4.C	Reactivity of –OH groups	53
5.	RESULTS AND DISCUSSION	56
5.A.	Redox properties of polyphenols	57
5.A.a.	Flavonolignans and their 2,3-dehydroderivatives	57
5.A.b.	Novel flavonolignan hybrid antioxidants	60
5.B.	UV/Vis absorption properties of polyphenols	62
5.B.a.	Tunable optical properties of silymarin flavonolignans	62
5.B.b.	p-Hydroxyphenyl-pyranoanthocyanins – acid-base properties and molecular interactions	66
5.C.	Interaction with biomolecules	70
5.C.a.	Novel flavonolignan hybrid antioxidants in lipid bilayers	70
5.C.b.	Flavonolignans as a novel class of sodium pump inhibitors	71
6.	ONGOING PROJECT - SAMPLING CONFORMATIONAL FEATURES OF COPIGMENTATION COMPLEXES	74
6.A.	Introduction	74
6.B.	Methodology	75
6.C.	Results and Discussion	81
7.	CONCLUSION	90
8.	REFERENCES	92
9.	APPENDIX	105

## ACKNOWLEDGMENT

I would like to express my big thanks to my Czech supervisor Martin Kubala for helping me and guide me since my undergraduate studies. You have been a great adviser. You have been precisely leading my research including writing all papers and this thesis. Děkuji také za přátelskou atmosféru v naší kanceláři.

My second big thanks belongs to my French supervisor Patrick Trouillas. I truly appreciate your kind welcome in your lab. It has been pleasure to work under your supervision. You kindly introduced me to theoretical calculations and you have made me think about and see scientific issues in different angles. You have always acted and spoken straight to me as it is and I am very grateful for that. Thank you so much for all help including introducing me to many researchers, writing all publications and this manuscript.

I could not have asked for better supervisors of my thesis!

I also thank to French Embassy in the Czech Republic and Campus France for the scholarship and the opportunity to study in both France and the Czech Republic.

My next thanks goes to my friends, colleagues and classmates: Petra (i když to vypadalo, že jsme na sebe jen ‘zbyli’, stali jsme se dobrými přáteli a já jsem za to velmi rád; hodně krát jsi mi pomohla, zvedla náladu a byla tam, když bylo potřeba), Jarka (zdravé soupeření a malé rozepře nezmění nic na tom, že když je potřeba, jsme tam jeden pro druhého), Nelča (se kterou jsme si užili hromadu legrace), Tibor (za jeho neustále průpovídky) a všichni další z naší katedry KBF, jejichž jmenování by zabralo mnoho stran.

Many thanks to my dear friends and colleagues in France – Florent (thank you for your time and patiently teaching and explaining new theoretical approaches to me; thank you for helpful and fruitful scientific discussions and for correcting the PE part), Tahani (merci à toi, merci pour toutes les discussions et pour faire notre labo comme il était, et en plus, tu as toujours une bonne humeur; comme tu toujours dit: La vie est dure.), Gabin (for your help with all computer and operating system related issues and for welcome everyone in the lab as (s)he is a part of the group), Benjamin (for your kindly help with the projects, je te remercie aussi pour tous les mots et expressions en francais que tu m’as appris), Imène (pour sa amitié et des aides au debut de mon séjour au labo), Erell (for a great online company during writing the thesis and for all scientific work, I have had chance to work with you) et tout les autres gens qui travaille dans la 2ème étage.

I also want to thank to all people, we have collaborated with. Mainly, Jenda Vacek who also was here since my undergraduate studies and thanks to whom, I was able to manage some of my projects.

Také děkuji Barči a Adélce, které tady vždy pro mě byly, a podporovaly mě. V neposlední řadě také děkuji své rodině, která mě během studií podporovala.

## PROCLAMATION

I claim that I wrote this PhD thesis by myself under the supervision of my mentors Martin Kubala and Patrick Trouillas; I also claim that I read and used the articles quoted at the end of this thesis.

In Olomouc ..... 20...

.....

Michal Biler



## **ABSTRACT**

Polyphenols are abundantly found in many fruit, vegetables, beverages, *etc.* and they possess many potential health benefits. Computational methods were thoroughly used through this thesis to rationalize, describe and predict physical chemical properties of flavonolignans and pyranoanthocyanins. Here, we aim at an understanding of polyphenol biological actions at a molecular level. All outcomes from the theoretical computations were discussed with respect to experimental data. The properties related to antioxidant activity of flavonolignans were investigated by density functional theory (DFT) methods. The pH dependence of ultraviolet/visible (UV/Vis) absorption properties of flavonolignans and pyranoanthocyanins were evaluated by time dependent (TD-) DFT methods, and noncovalent interactions were investigated within dispersion-corrected DFT methods. A short overview is also given on interaction of such compounds with biomolecules. Chapter 6 presents yet not published results of several noncovalent pigment: copigment systems. This part of the results serves as a good starting point to search for 'the best copigment'.

Keywords: Polyphenols; DFT; Noncovalent interactions; UV/Vis absorption; Antioxidants.

## SHRNUTÍ

Polyfenoly jsou hojně zastoupeny v mnoha druzích ovoce, zeleniny, nápojů atd. a mají mnoho biologických aplikací. Tato disertační práce využívá výpočetní kvantové metody k popisu a racionalizaci fyzikálně-chemických vlastností flavonolignanů a pyranoantokyaninů pro lepší porozumění jejich biologických účinků na molekulární úrovni. Všechny výstupy z teoretických výpočtů jsou diskutovány vzhledem k experimentálním datům. Metody funkcionálu hustoty (DFT) byly použity při studiu antioxidační aktivity daných sloučenin. Časově závislé TD-DFT metody posloužily pro popis UV/Vis absorpčních spekter flavonolignanů a pyranoantokyaninů a jejich pH závislosti, a disperzně-korigované DFT-D metody byly využity při popisu nekovalentních interakcí. Stručně jsou také popsány interakce těchto molekul s biomolekulami. Kapitola 6 představuje zatím nepublikované výsledky týkající se nekovalentních interakcí v systémech pigment: kopigment, které poslouží pro budoucí studie k nalezení ‚nejlepšího‘ kopigmentu.

Klíčová slova: Polyfenoly; DFT; Nekovalentní interakce; UV/Vis absorpce; Antioxidanty.

## RESUMÉ

Les polyphénols sont abondamment trouvés dans de nombreux fruits, légumes, boissons *etc.* et ils possèdent de nombreux effets bénéfiques pour la santé. Les méthodes de calcul ont été utilisées dans le cadre de cette thèse pour rationaliser, décrire et prédire les propriétés physiques et chimiques des flavonolignanes et des pyranoanthocyanines pour la compréhension de leurs actions biologiques au niveau moléculaire. Tous les résultats des calculs théoriques ont été discutés par rapport aux données expérimentales. Les propriétés liées à l'activité antioxydante des flavonolignanes ont été étudiées par les méthodes de la théorie de la densité fonctionnelle (DFT). La dépendance au pH des propriétés d'absorption UV/Vis des flavonolignanes et des pyranoanthocyanines ont été évaluée par des méthodes DFT dépendante du temps (TD-), et les interactions non-covalentes ont été étudiées avec les méthodes de DFT incluant la correction de dispersion. Un bref aperçu est également donné sur l'interaction de ces composés avec des biomolécules. Le chapitre 6 présente des résultats non encore publiés de plusieurs systèmes non-covalents pigment: copigment. Cette partie des résultats constitue un bon point de départ pour la recherche du 'meilleur copigment'.

Mots-clés : Polyphénols, DFT, Interactions non-covalentes, Absorption UV/Vis, Antioxydantes.

## LIST OF ABBREVIATIONS

AA	L-Ascorbic acid
ABTS	2,2'-Azinobis-(3-Ethylbenzothiazoline-6-Sulfonic Acid)
AF	Adduct Formation
BDE	Bond Dissociation Enthalpy
CASP	Complete-Active-Space Perturbation Theory
CAS-PT2	Complete-Active-Space Second-Order Perturbation Theory
CC	Coupled Cluster
CI	Configuration interaction
CIS	Configuration Interaction Singles
Cy	Cyanidin
DFT	Density Functional Theory
DFT-D	Dispersion-corrected Density Functional Theory
DHSB	Dehydrosilybin
DHSCH	Dehydrosilychristin
DHSD	Dehydrosilydianin
Dp	Delphinidin
DPPH	1,1-Diphenyl-2-Picrylhydrazyl
ES	Excited State
ET	Electron Transfer
ETE	Electron Transfer Enthalpy
ET-PT	Electron Transfer – Proton Transfer
FCR	Folin-Ciocalteu Reagent
FF	Force Field
GEA	Gradient Expansion Approximation
GGA	Generalized Gradient Approximation
GS	Ground State
GTO	Gaussian-type Orbital
HAT	Hydrogen Atom Transfer
HF	Hartree-Fock
HIV	Human Immunodeficiency Virus
HOMO	Highest Occupied Molecular Orbital
IP	Ionization Potential
KS	Kohn-Sham
LCAO	Linear Combination of Atomic Orbitals
LDA	Local Density Approximation
LUMO	Lowest Unoccupied Molecular Orbital

MD	Molecular Dynamics
MM	Molecular Mechanics
MM/GBSA	Molecular Mechanics/Generalized Born Surface Area
MM/PBSA	Molecular Mechanics/Poisson-Boltzmann Surface Area
MP	Möller-Plesset
MP1	First Order Möller-Plesset
MP2	Second Order Möller-Plesset
MP3	Third Order Möller-Plesset
MP4	Forth Order Möller-Plesset
MR-CI	Multi-Reference Configuration Interaction
Mv	Malvidin
NKA	Na <sup>+</sup> /K <sup>+</sup> -ATPase
PA1	Catechyl-Pyranomalvidin-3-O-Glucoside
PCET	Proton-Coupled Electron Transfer
PCM	Polarizable Continuum Model
PE	Polarizable Embedding
Pg	Pelargonidin
Pn	Peonidin
Pt	Petunidin
PT	Proton Transfer
QM	Quantum Chemistry/Mechanics
QM/MM	Quantum Mechanics/Molecular Mechanics
ROS	Reactive Oxygen Species
SAC-CI	Symmetry Adapted Cluster Configuration Interaction
SCF	Self-Consistent Field
SB	Silybin
SCH	Silychristin
SD	Silydianin
SET-PT	Sequential Electron transfer – Proton Transfer
SPLET	Sequential Proton-Loss-Electron-Transfer
STO	Slater-type Orbital
SWV	Square-Wave Voltammetry
TD-DFT	Time Dependent Density Functional Theory
UV	UltraViolet
UV/Vis	UltraViolet/Visible
ZINDO	Zerner's Intermediate Neglect of Differential Overlap
ZPVE	Zero-Point Vibrational Energy

## LIST OF PUBLICATIONS

This PhD thesis is based on the following papers, which are quoted in text by their Roman numerals I – V. The full articles are attached into the Appendix.

- I. M. Pyszková, **M. Biler**, D. Biedermann, K. Valentová, M. Kuzma, J. Vrba, J. Ulrichová, R. Sokolová, M. Mojovic, A. Popovic-Bijelic, M. Kubala, P. Trouillas, V. Křen, J. Vacek, *Flavonolignan 2,3-dehydroderivatives: Preparation, antiradical and cytoprotective activity*. Free Radical Biology and Medicine 90 (2016) 114-125; doi: 10.1016/j.freeradbiomed.2015.11.014
- II. E. Vavříková, V. Křen, L. Jezova-Kalachova, **M. Biler**, B. Chantemargue, M. Pyszková, S. Riva, M. Kuzma, K. Valentová, J. Ulrichová, J. Vrba, P. Trouillas, J. Vacek, *Novel flavonolignan hybrid antioxidants: From enzymatic preparation to molecular rationalization*. European Journal of Medicinal Chemistry. Submitted.
- III. **M. Biler**, P. Trouillas, D. Biedermann, V. Křen, M. Kubala, *Tunable optical properties of silymarin flavonolignans*. Journal of Photochemistry and Photobiology A: Chemistry 328 (2016) 154-162; doi: 10.1016/j.jphotochem.2016.05.024
- IV. A. Vallverdú-Queralt, **M. Biler**, E. Meudec, Ch. Le Guernevé, A. Vernhet, J.-P. Mazauric, J.-L. Legras, M. Loonis, P. Trouillas, V. Cheynier, O. Danglese, *p-Hydroxyphenyl-pyranoanthocyanins: an experimental and theoretical investigation of their acid – base properties and molecular interactions*. International Journal of Molecular Sciences 17 (2016) 1-19; doi: 10.3390/ijms17111842
- V. M. Kubala, P. Čechová, J. Geletičová, **M. Biler**, T. Štenclová, P. Trouillas, D. Biedermann, *Flavonolignans as a novel class of sodium pump inhibitors*. Frontiers in Physiology 7 (2016) 1-10; doi: 10.3389/fphys.2016.00115

## 1. INTRODUCTION

Polyphenols are natural compounds containing at least one -OH phenolic group and they are found in many plants and plant products. Polyphenols are powerful antioxidants and their capacity to exhibit efficient protective effects against oxidative stress is crucial for their potential use in pharmaceutical applications. As polyphenols contain relatively extended systems of  $\pi$ -conjugated electrons, they absorb light in the ultraviolet/visible (UV/Vis) region. Consequently, they can play an important role as natural sunscreens, or natural colorants in food and beverages.

Our work is mainly focused on flavonoid derivatives, which are introduced in Chapter 2. The first examined subfamily is flavonolignans, which are conjugates of flavonoids and lignans. Flavonolignans are abundantly found in the plant extract known as silymarin, obtained from the seeds of milk thistle. Silymarin possesses many potential health benefits and it has widely been used to treat, *e.g.*, various liver disorders. The second examined subfamily is pyranoanthocyanins, which are formed during wine aging. Anthocyanins and derivatives have a huge impact on human health as well as in plants themselves, as they act as attractants and they have a role in plant resistance against external attacks.

Despite general agreement that polyphenol-rich diet is beneficial for the human health, the molecular mechanisms of action have not been fully rationalized for most of polyphenols. They are usually larger polycyclic molecules with several degrees of freedom, and their physical and chemical properties are strongly influenced by interactions with surrounding molecules, *e.g.*, solvent, other small solute, or large molecular systems, such as proteins, membranes, nucleic acid, *etc.*

In Chapter 2, the copigmentation process is described, which corresponds to anthocyanins' color stabilization by another phenolic derivatives (copigment). This process has recently attracted much interest, as stabilization and modulation of anthocyanins' color has become an important challenge in food industry. The comprehensive understanding of intermolecular interactions in copigmentation is mandatory to better rationalize the color plant-derived food products including beverages. Theoretical methods have become sufficiently accurate to tackle noncovalent interactions in copigmentation complexes and predict the main related observable features.

Quantum-chemistry calculation methods are a powerful tool to support, rationalize and predict experimental data and to better understand biological, physical and chemical phenomena at the atomic scale. However, it is impossible to calculate analytical solution of the Schrödinger equation for such big molecules. Therefore, depending on the size of the computed molecular system, numerous simplified methods are used, with different degrees of approximation. These methods are briefly introduced in Chapter 3.

It is important to evaluate agreement of theoretical methods with respect to real experimental data. Typically, the structure that is identified as the most energetically favorable is used as a starting point for calculation of parameters that can be directly compared to experimental observables. Chapter 4 describes the methods for calculation of redox-, acid base- and optical properties, which were used in our work. These parameters can be directly compared to the experimental data from electrochemistry or UV/Vis absorption spectroscopy. Moreover, the calculated structures can serve as a benchmark for further computations, aimed at interaction with other small molecules (copigmentation) or with large biomolecular systems, such as lipid bilayers or enzymes.

This thesis mainly aims at characterizing polyphenols and polyphenol-polyphenol interactions by quantum chemistry methods; namely redox properties of flavonolignans and other conjugates, optical properties of flavonolignans and pyranoanthocyanins and their pH dependence, and interactions of flavonolignans with the lipid membrane and Na<sup>+</sup>/K<sup>+</sup>-ATPase pump were investigated. Results are closely discussed with experimental data, which were mostly performed by other collaborators. Some of the experimental measurements (absorption properties of flavonolignans) were performed by author of this thesis.

The major highlights of this work are summarized in Chapter 5. Subsection A shows how theoretical methods have succeeded in the evaluation of antioxidant properties of flavonolignans and how they have unraveled conformational features related to mechanisms of action of newly synthesized flavonolignan-conjugates, which have appeared promising agents to real pharmaceutical applications.

In subsection B, time dependent density functional theory (TD-DFT) calculations and molecular orbital analysis fully rationalized UV/Vis absorption properties of flavonolignans. We identified and rationalized the major structural and environmental factors that can induce spectral changes. TD-DFT methods also succeeded in description of pyranoanthocyanins and we have rationalized a non-typical (blue) hypsochromic shift of the neutral base compared to



the cation form, which was observed experimentally. In this section, quantum chemistry calculations have also shed light on copigmentation and self-association of pyranoanthocyanins and they perfectly evaluated different noncovalent conformers and their corresponding association energies with respect to the isolated fragments. A better understanding of these interactions should support the control of color modulation. Quantum mechanics/molecular mechanics (QM/MM) methods treat noncovalent interactions differently in terms of local environment and they approach to the ‘real’ behavior of these molecules with possible biological and food industry applications.

Subsection C is devoted to molecular interactions of polyphenols with lipid membranes and the Na<sup>+</sup>/K<sup>+</sup>-ATPase (NKA) pump.

To establish structure-copigmentation relationships, further computational results on explicit description of solvent molecules are discussed in Chapter 6.

## 2. FLAVONOID DERIVATIVES

### 2.A. Introduction

Polyphenols are secondary metabolites biosynthesized in plants. They are found in many plants and in various parts including fruit, vegetables and leaves, and consequently, they are also found in beverages (*e.g.*, wine, fruit juices, and beer). Among other roles in plants, some polyphenols contribute to their color. They are indeed  $\pi$ -conjugated compounds containing -OH phenolic groups; due to their extended  $\pi$ -conjugated system, they absorb in the UV/Vis range<sup>1</sup>. They are also involved in the protection against ultraviolet (UV) radiation. Over the past decades, they have attracted interest for their potential health benefits, as they possess numerous biological activities (Figure 1). They are particularly known for their antioxidant properties. They have been described for their potential role in prevention of various diseases including cancers, liver diseases, or cardiovascular diseases.<sup>2-5</sup> They have also exhibited defense activities against many pathogens (*e.g.*, viruses, fungi).<sup>6-8</sup> As antioxidants, polyphenols can scavenge free radicals by donating electrons or hydrogen atoms, thus inhibiting their action.<sup>9</sup> As antioxidants, they also act as metal chelators (*e.g.*,  $\text{Fe}^{2+}$ ) or as inhibitors of enzymes involved in oxidative stress.<sup>6,10-12</sup> Polyphenols are known to modulate the activity of a wide range of enzymes and cell receptors,<sup>13</sup> thus exhibiting indirect antioxidant action.

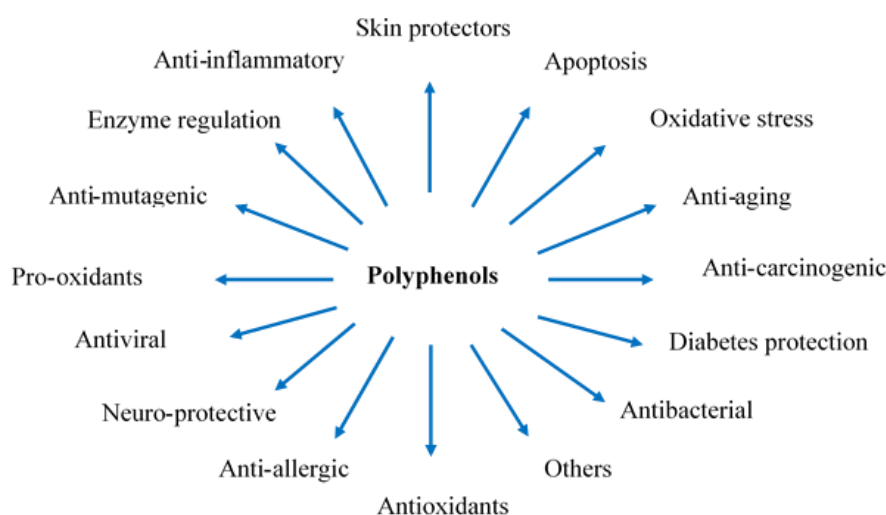


**Figure 1.** Biological activities of polyphenols.<sup>6,14-16</sup>

Certain polyphenols such as quercetin are found in many plant products, whereas others are specific to particular food products (*e.g.*, flavanones in citrus fruit, isoflavones in soya, phloridzin in apples).<sup>12,17</sup> The polyphenol composition of many plants and derived products (*e.g.*, in some exotic fruit, black tea, or some cereals) is still under scrutiny and it can be affected by many factors, namely: ripeness at harvest time; storage conditions and related oxidation possibility; processing and methods of culinary preparation; environmental factors, such as soil type, sun exposure or rainfall; agronomic factors such as planting in greenhouses or fields.<sup>12</sup> Several polyphenols are also found in the skin of fruit and vegetables and peeling may eliminate a significant portion of polyphenols. Polyphenols are grouped into different classes (*e.g.*, phenolic acids, flavonoids, stilbenoids and lignans) according to the carbon skeleton and the number and position of phenol groups. Here we focus on the large class of flavonoids and closely related derivatives.

## **2.B. Generalities about flavonoids**

Flavonoids are divided into several subclasses<sup>6,10,12</sup> (*i.e.*, flavones; flavonols; flavanones; flavanonols; flavanols; isoflavones; chalcones; anthocyanidins) according to aromaticity of the heterocycle (C-) ring, functional groups, mainly at C4 and C3, and oxidation state (Figure 2).

Flavones (2-phenylchromen-4-one) are characterized by the presence of a 2,3-double bond and a keto group in C-ring. They include *e.g.*, luteolin, apigenin, chrysin and they are mainly identified in parsley and celery.<sup>12,18</sup> Cereals (such as millet or wheat) contain C-glycosides of flavones.<sup>19,20</sup> Polymethoxylated flavones are the most hydrophobic flavonoids and they are largely found in the skin of citrus fruit.<sup>12,21,22</sup>

Flavonols (3-hydroxy-2-phenylchromen-4-one = 3-hydroxyflavone) are flavone derivatives having a hydroxyl group at C3. The main representatives are quercetin, kaempferol, galangin and isorhamnetin. Onions, leeks, broccoli, blueberries, red wine and tea contain large quantities of flavonols. Their biosynthesis is stimulated by light, therefore, they accumulate in the outer and aerial part of tissues.<sup>12,23,24</sup>

Flavanones (2,3-dihydro-2-phenylchromen-4-one) are 2,3-dihydroflavones derivatives, with hesperetin, naringenin and eriodictyol as the most representative compounds. They are present

in tomatoes, mint or citrus fruit in high concentration (naringenin, hesperetin, and eriodictyol in grapefruit, orange and lemon, respectively).<sup>12,17</sup>

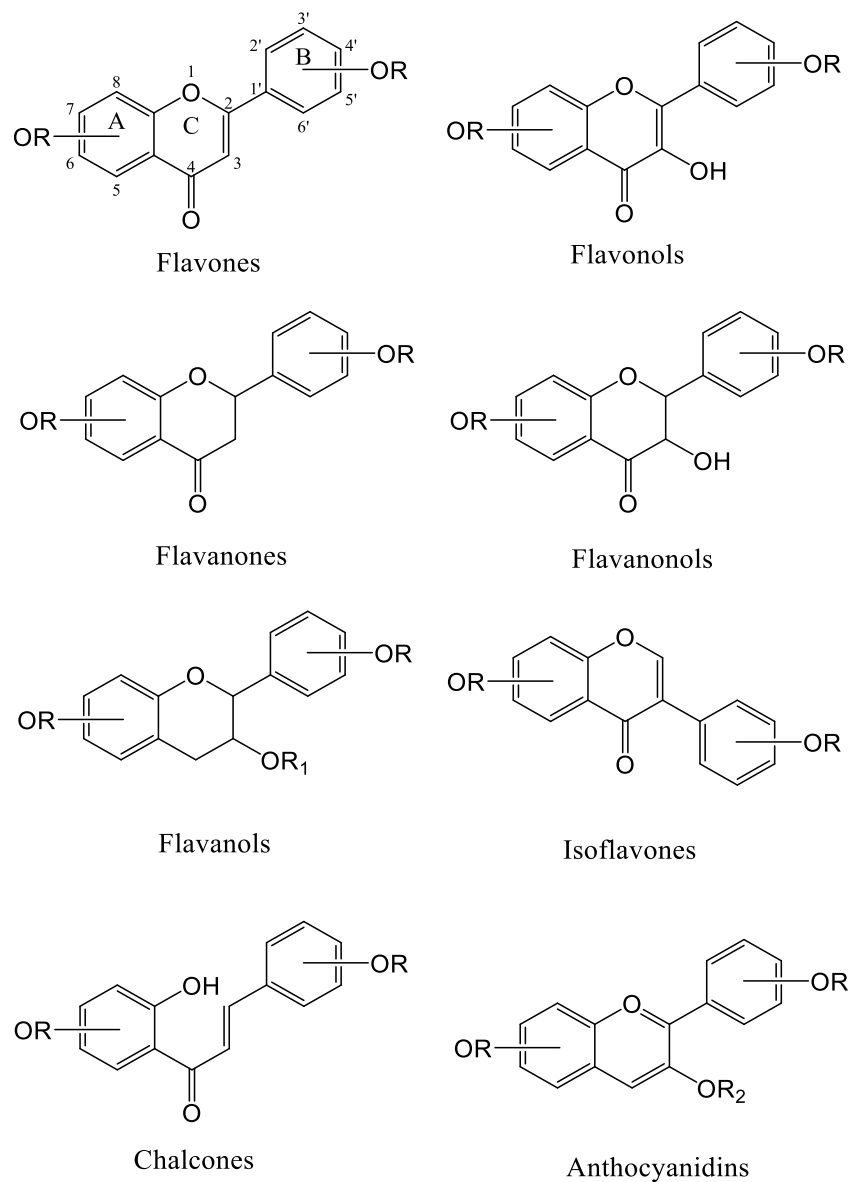


**Figure 2.** Structures of the main flavonoid subclasses. Numbering for the structures is similar to that for flavones. For the main representatives of the groups, R represents -H or -CH<sub>3</sub> group(s), which can be attached somewhere to the A- and/or C- rings, R<sub>1</sub> corresponds to H-atom, -CH<sub>3</sub> group, a gallate moiety, a sugar moiety or another polyphenol, alternatively R, R<sub>1</sub> may also correspond to a sugar moiety for glycosides.

Flavanonols (3-hydroxy-2,3-dihydro-2-phenylchromen-4-one) are 2,3-dihydroflavonols and 3-hydroxyflavanones. The main representative compound is taxifolin (dihydroquercetin) found in citrus fruit.<sup>12,17</sup>

Flavanols are a group of flavan-3-ols, flavan-4-ols, flavan-3,4-diols. They are characterized by the lack of both a 2,3-double bond and a carbonyl group at C4. They can also be characterized by the presence of hydroxyl group at C3, which makes flavonols two chiral centers at C2 and C3 (similarly to flavanonols). This subclass includes catechin (isomer with *trans* configuration of C2-C3), epicatechin (isomer with *cis* configuration of C2-C3), catechin 3-gallate, epicatechin 3-gallate, *etc.* Flavanols are often found in seeds of leguminous plants and many fruit (*e.g.*, apricots, the skin of grapes, apples and blueberries, tea leaves and cacao beans). Flavanols exist in polymeric forms that are called proanthocyanidins. These polymer forms are often found in cider apples, where the averaged degree of polymerization is ranging from 4 to 11. For instance, tannins are responsible for the astringency and bitterness of certain fruit, beverages and other food as a result of formation of complexes with salivary proteins.<sup>25-31</sup>

As for flavones, the 3-phenylchromen-4-one skeleton also characterizes isoflavones, however the B-ring is attached at C3 instead of C2. They are mostly found in the leguminous plant family, soybeans being the main source of isoflavones in the human diet.<sup>10,32</sup> The major isoflavones are genistein, daidzein and glycitein. They have attracted interest because of their structural similarities to estrogens with pseudohormonal properties (capacity to bind to estrogen receptors).<sup>12,33-35</sup>

Unlike the compounds mentioned above, anthocyanidins bear a flavylium cation moiety. They are major components in many beverages, fruit, vegetables, flowers or leaves, including red wines, berries, violet plums, figs, blue tomatoes, red cabbages, radishes, red onions, tulips and orchids.<sup>36,37</sup> Their glycosidic forms are called anthocyanins, with the sugar moiety being mostly but not necessary located at C3. According to the pH values, they exist in different colored and uncolored chemical forms and they are stabilized by the formation of complexes with other flavonoids, see below for more details.

Our work has mainly focused on flavonolignans, which are conjugates of flavonoids and lignans (publications **I**, **III**, **V**), conjugates of flavonolignans with other molecules (publication **II**) and pyranoanthocyanins, which are anthocyanin derivatives (publication **IV**); these subclasses are described in details below.

## 2.C. Flavonolignans

Lignans are a complex class of polyphenols, which are mainly characterized by the presence of a skeleton made of at least one propylbenzene moiety. Their combination with flavonoids makes a specific class of compounds, so-called flavonolignans. The most widely used natural source of flavonolignans is a plant extract obtained from the milk thistle seeds (*Silybum marianum* (L.) Gaertn., Asteraceae), commercially known as silymarin. Silymarin contains approximately 70 – 80 % of flavonolignans (silybin, SB; dehydrosilybin, DHSB; silychristin, SCH; silydianin, SD; isosilybin) and approximately 20 – 30 % of other polyphenols (taxifolin) and polymeric compounds, which is often called the polymeric fraction (Figure 3).<sup>38</sup>

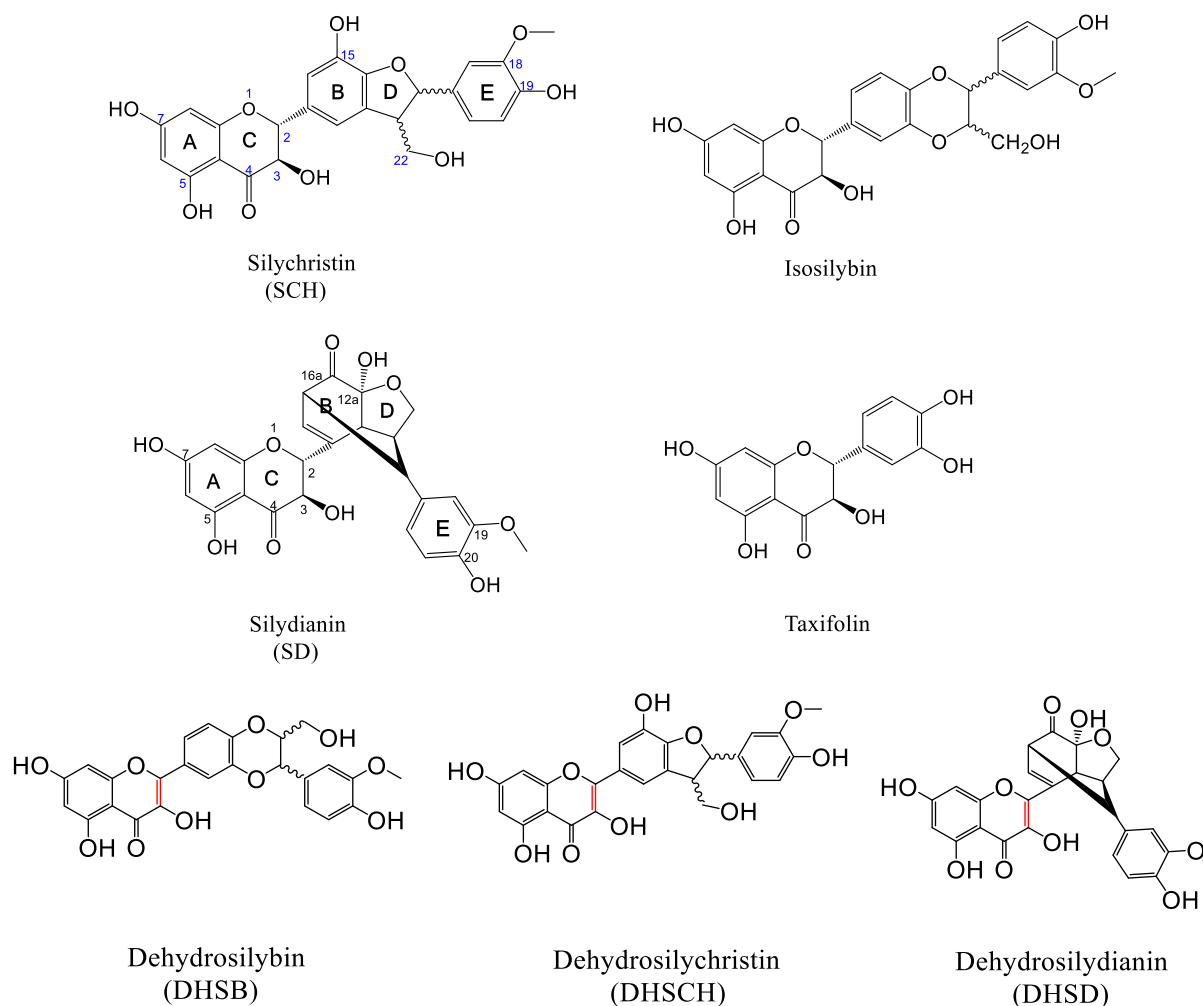


**Figure 3.** Structures of other compounds found in silymarin.

Silybin is the major component of silymarin, the natural form is a mixture of two diastereomers (Figure 4) in approximately 1:1 proportion: silybin A [(2R,3R)-2-((2R,3R)-2,3-dihydro-3-(4-hydroxy-3-methoxyphenyl)-2-(hydroxymethyl)-1,4-benzodioxin-6-yl)-2,3-dihydro-3,5,7-trihydroxy-4H-1-benzopyran-4-one], and silybin B [(2R,3R)-2-((2S,3S)-2,3-dihydro-3-(4-hydroxy-3-methoxyphenyl)-2-(hydroxymethyl)-1,4-benzodioxin-6-yl)-2,3-dihydro-3,5,7-trihydroxy-4H-1-benzopyran-4-one]. SB is easily oxidized and forms 2,3-dehydrosilybin. SCH exists as two diastereoisomers too, but the ratio between stereoisomers A and B is 95:5. SD exists as a single diastereomer.<sup>38</sup>

SB possesses five hydroxyl groups, which can be divided into three categories according to their nature: three phenolic OH groups, one secondary and one primary alcoholic OH group. The hydroxyl group at C5 forms a strong hydrogen bond with the oxo-group of the C-ring. The secondary alcoholic OH group at C3 can be easily oxidized to yield 2,3-DHSB, with the 3-OH group being the most active radical-scavenging moiety, whereas the most active radical-scavenging moiety of SB is the 20-OH group. This group is also an important group in lipoperoxidation inhibitory activity. The aryloxy radicals formed upon oxidation (especially at C7) may contribute to pro-oxidant activity. Owing to the 2,3-double bond, DHSB is a much better antioxidant than SB. It is 25-fold better radical scavenger and 10-fold better inhibitor of lipid peroxidation than SB.<sup>38-42</sup>

Silymarin has exhibited many biological activities, which makes it active in both *in vivo* and *in vitro*, with a few possible therapeutic usages, as it has already been used in patients.<sup>16,43,44</sup>

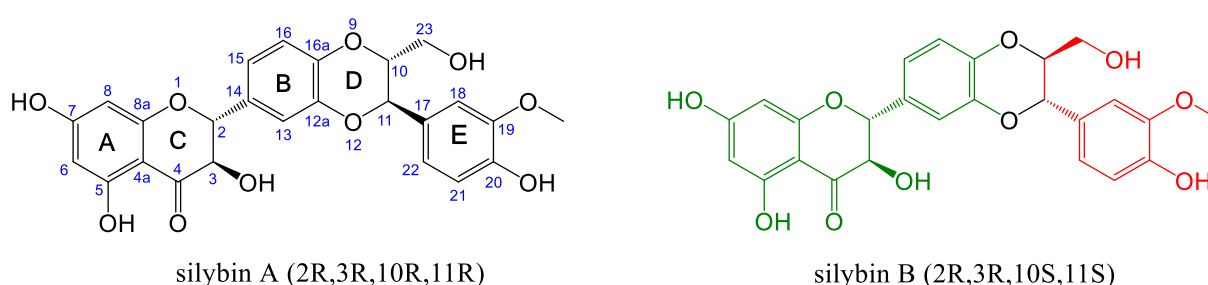


**Figure 4.** Structure of silybin A and silybin B with the nomenclature. Green and red colors are used to distinguish the flavonoid and the lignan moieties, respectively.

The health benefits of milk thistle have been known for a long time, *i.e.*, already in the ancient Greece, but better understanding of their medicinal properties has only been rationalized in the past few years owing to modern technologies. Silymarin has been widely used to treat various liver<sup>4,45</sup> and gall bladder<sup>46</sup> disorders and to protect liver against poisoning effects of chemical and environmental toxins. It possesses antioxidant, hypocholesterolemic, estrogenic, anti-atherosclerotic chemoprotective, canceroprotective,<sup>2,5</sup> renoprotective,<sup>47</sup> neuroprotective<sup>48</sup> and neurotropic activities.<sup>16,43,44</sup> It has been used in the treatment and prevention of cardio-pulmonary and gastrointestinal<sup>49,50</sup> disorders as a skin protector<sup>44,51–54</sup>, in regulation of apoptosis<sup>46,51,52,55,56</sup> and inflammation processes<sup>48</sup>. SB, the major component of silymarin has exhibited activities in the treatment of various disorders of prostate including adenocarcinoma, lung problems as well as kidney diseases, pancreas problems and glycemia balance.<sup>16,43,44</sup> It has been used in dermatology and cosmetics and it can also have an influence in modulation of drug transport.<sup>16,43,44</sup> SB has shown a potential usage with patients infected with the human immunodeficiency virus (HIV) as a complementary alternative medicine.<sup>57,58</sup> Only a few articles have been published on its adverse effects – gastroenteritis symptoms (diarrhea and vomiting), anaphylactic reactions<sup>59</sup> after ingestion of *Silybum marianum* tea and dermatological symptoms and headaches.<sup>16</sup> It is important to note that the frequency of occurrence of these negative effects was very low and the treatment with milk thistle has appeared to be safe and well tolerated.<sup>4</sup>

## **2.D. Generalities about anthocyanins**

Anthocyanins (anthos = flower, kyanos = blue in Greek) are water-soluble pigments in plants and they are described as glycosides of polyhydroxy and polymethoxy derivatives of the 2-phenylbenzopyrylium moiety (so-called flavylum salt).<sup>60</sup> They bear a C6-C3-C6 skeleton and they consist of the aromatic A-ring bonded to the heterocyclic C-ring, which contains oxygen at C1. The C-ring is also connected to the third aromatic B-ring by a carbon–carbon bond (Figure 5). There exists a huge variety of anthocyanins in nature. Both the number/position of hydroxyl, methoxyl and sugar groups, and the nature/number of aliphatic or aromatic acids attached to sugars define the main differences between individual anthocyanins or anthocyanidins (see Table 1).<sup>60</sup>



There exist several anthocyanidins, but only six of them are common in higher plants (Table 1) – pelargonidin (Pg), cyanidin (Cy), delphinidin (Dp), peonidin (Pn), petunidin (Pt) and malvidin (Mv) with cyanidin being the most distributed anthocyanidin in the edible parts of plants. The glycosides of anthocyanidins (with a sugar moiety in its structure) are called anthocyanins and common glycosylation occurs as 3-monosides, 3-biosides, 3,5-diglycosides and 3,7-diglycosides, with 3-glycosides occurring about two and half times more frequently than 3,5-diglycosides.<sup>37,60</sup>

Anthocyanins are extracted from grapes, berries, blue tomatoes, red cabbages, red apples, red onions, red-skinned and purple sweet potatoes, radishes, tulips, roses, orchids and many other plants and plant organs. They act as attractants, therefore playing a role in the attraction of animals for pollination and seed distribution, and in the resistance of plants against insect attack.<sup>60</sup> Due to their occurrence, they may strongly impact plant-derived products (*e.g.*, beverage, jam, purée).

Similar to flavonoids, anthocyanins are known for their many biological activities that may have beneficial impact on human health. Due to their antioxidant activity, they exhibit the capacity to scavenge reactive oxygen species (ROS), so to control oxidative stress, which may play a role in the prevention of many diseases (neuronal and cardiovascular diseases, mutagenesis and carcinogenesis inhibitor and/or diabetes treatments). The antioxidant activity of berries for human low-density lipoproteins was directly associated with the anthocyanin content.<sup>61</sup> Anthocyanidins are also promising compounds, which might be used in chemoprevention, as they exhibit potent inhibitors of human tumor cell growth *in vitro*.<sup>62</sup> They are important in protecting plants against UV-induced damage.

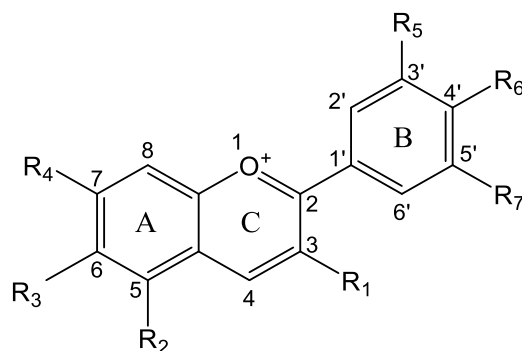


**Figure 5.** Anthocyanidin skeleton

**Table 1.** Structures of naturally occurring anthocyanidins. Data adapted from refs. 17, 36, 63.

	R <sub>1</sub>	R <sub>2</sub>	R <sub>3</sub>	R <sub>4</sub>	R <sub>5</sub>	R <sub>6</sub>	R <sub>7</sub>
<b><i>Common Anthocyanidins</i></b>							
Pelargonidin	OH	OH	H	OH	H	OH	H
Cyanidin	OH	OH	H	OH	OH	OH	H
Delphinidin	OH	OH	H	OH	OH	OH	OH
Peonidin	OH	OH	H	OH	OCH <sub>3</sub>	OH	H
Petunidin	OH	OH	H	OH	OCH <sub>3</sub>	OH	OH
Malvidin	OH	OH	H	OH	OCH <sub>3</sub>	OH	OCH <sub>3</sub>
<b><i>6-Hydroxylated Anthocyanidins</i></b>							
6-Hydroxypelargonidin (Aurantidin)	OH	OH	OH	OH	H	OH	H
6-Hydroxycyanidin	OH	OH	OH	OH	OH	OH	H
6-Hydroxydelphinidin	OH	OH	OH	OH	OH	OH	OH
<b><i>Methylated Anthocyanidins</i></b>							
5-Methylcyanidin	OH	OCH <sub>3</sub>	H	OH	OH	OH	H
7-Methylpeonidin (Rosinidin)	OH	OH	H	OCH <sub>3</sub>	OCH <sub>3</sub>	OH	H
5-MethylDelphinidin (Pulchellidin)	OH	OCH <sub>3</sub>	H	OH	OH	OH	OH
5-Methylpetunidin (Europinidin)	OH	OCH <sub>3</sub>	H	OH	OCH <sub>3</sub>	OH	OH
5-Methylmalvidin (Capensinidin)	OH	OCH <sub>3</sub>	H	OH	OCH <sub>3</sub>	OH	OCH <sub>3</sub>
7-Methylmalvidin (Hirsutidin)	OH	OH	H	OCH <sub>3</sub>	OCH <sub>3</sub>	OH	OCH <sub>3</sub>
<b><i>Others</i></b>							
Carajurin	H	OCH <sub>3</sub>	OH	OH	H	OCH <sub>3</sub>	H
Arrabidin	H	H	OH	OH	H	OH	OCH <sub>3</sub>
3'-Hydroxyarrabidin	H	H	OH	OH	OH	OH	OCH <sub>3</sub>
Apigenin	H	OH	H	OH	H	OH	H
Luteolin	H	OH	H	OH	OH	OH	H
Tricetinidin	H	OH	H	OH	OH	OH	OH
Riccionidin A *	OH	H	OH	OH	H	OH	H

\* Ring closure on the basis of ether linkage between the 3- and 6'-positions and an additional OH-group in the 2'-position.

## 2.E. Charge states in anthocyanins

The color and structure of anthocyanins strongly depend on pH values, but also on the presence of other polyphenols (copigments, see below the Copigmentation section). Depending on the pH values, anthocyanins are found in different chemical forms through hydration, proton transfer or tautomerization. The major structures and abundance ratio of anthocyanins at different pH values are shown in Figures 6 and 7. At pH between 1 and 2, anthocyanins exist in their flavylium cation form, which is mainly responsible for red color. In protic solvents, the flavylium cation is indeed red (occurrence as monomers), whereas in aprotic solvents the color turns to yellow (explained by the presence of homo-dimers). It was also observed that when increasing the water proportion in acetonitrile, the monomer was transformed into a green dimer.<sup>36</sup> At pH between 2 and 4, the cation form undergoes deprotonation and blue/purple-colored neutral quinonoidal bases are predominant species in solution. At higher pH values, these quinonoidal bases lose a second proton to form the anionic (blue) quinonoidal bases. Above pH values of 2, the flavylium cation is also prone to water addition (hydration) at C2 to form colorless hemiketals that are in fast equilibrium with a (yellowish) *cis*-chalcone tautomer, itself in slow equilibrium with the corresponding *trans*-chalcone. Aldehydes and phenolic acids can also be oxidative products of anthocyanins. The number of hydroxyl and methoxyl groups also affects the color of anthocyanins. The color is generally more blueish when increasing the number of hydroxyl groups (*e.g.*, delphinidin with three OH groups attached to the B-ring with respect to pelargonidin with only one OH group in the B-ring), whereas the red color increases when the number of methoxyl groups increases.<sup>37</sup>

The stability of anthocyanins is affected not only by the pH values, but also by other factors including temperature, chemical structure, concentration, light, oxygen, solvents, as well as the presence of enzymes, proteins, metal ions or other phenolic compounds including flavonoids and phenolic acids, which induce copigmentation (see the related section below).<sup>37,63</sup>

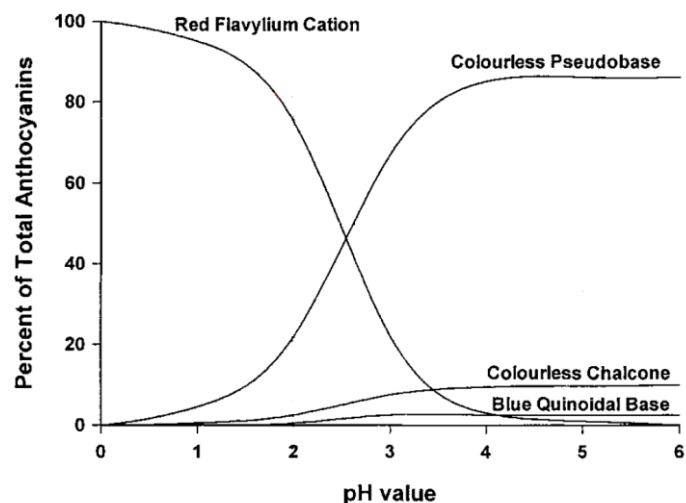


**Figure 6.** Abundance ratio diagram of the different forms of anthocyanins according to pH values (adapted from ref. 64).

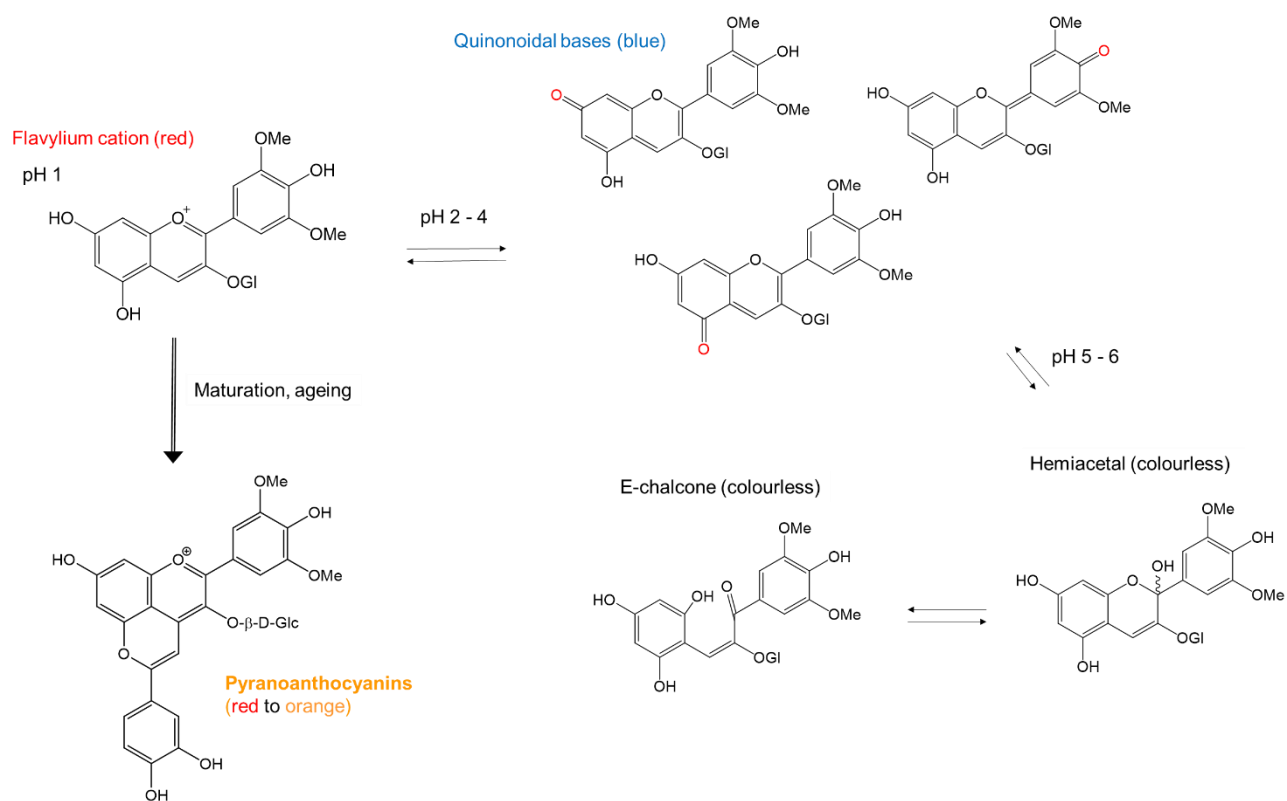


**Figure 7.** Different forms of anthocyanins vs. pH values

## 2.F. Pyranoanthocyanins

During wine aging and maturation, anthocyanins can form oligomers, which may lead to the formation of other anthocyanin-derived pigments including pyranoanthocyanins (Figure 7), which are thought to be of major importance for the color of certain aged wines. Their description is relatively new, and they have attracted much interest over the past decade. Their structure results from the cycloaddition of diverse wine nucleophiles at C4 and C5 of the native flavylum nucleus, yielding a fourth ring (pyrene D-ring) that is responsible for the higher stability to hydration compared to the native anthocyanins. They can react with small molecules as flavanols, aldehydes (*e.g.*, acetaldehyde), acetoacetic acid, pyruvic acid, hydroxycinnamic acids, vinyl-phenol, vinyl-guaiacol, vinyl-catechol. Over the past years, several classes<sup>65-74</sup> have been identified such as vitisins (A-, B- type), portisins, vinylflavanol-, methyl-, hydroxyphenyl-pyranoanthocyanins or pyranoanthocyanin dimers. Pyranoanthocyanins exhibit yellowish and orange-ish colors, except portisins<sup>67</sup>, which exhibits bluish hue.

The simplest pyranoanthocyanins detected in red wines are B-type vitisins, which are formed from the reaction with acetaldehyde. The A-type of vitisins (carboxy-pyranoanthocyanins) are detected in Port wine after only one year of ageing and they are formed by the reaction between anthocyanins and pyruvic acid. Both vitisin A and vitisin B are hypsochromically shifted in UV/Vis spectra and they exhibit much less sensitivity to pH value with respect to their anthocyanin counterpart (malvidin-3-glucoside); this allows greater color expression at higher pH values. Vitisin A is resistant to bleaching by sulfur dioxide, which is known to instantly bleach anthocyanins with reversible formation of colorless compounds. On the other hand, vitisin B is partly bleached but still more resistant than malvidin-3-glucoside, which is almost fully decolorized.<sup>65</sup>

Methyl-pyranoanthocyanins were detected in 3-year old Port wine and its presence in red wines arises from the reaction with acetoacetic acid.<sup>69</sup> Vinyl-pyranoanthocyanin-phenolics (A-, B-type of portisins) are detected in 2-year old Port wine<sup>68</sup> and pyranoanthocyanin dimers (turquoise blue color) were found in 9-year old Port wine<sup>73,75</sup>.

## 2.G. Copigmentation

Copigmentation plays a crucial role in stabilizing many hues in flowers, certain fruit and related beverages, *e.g.*, in some wines. It is very important in food chemistry science, as color and stability are major descriptors of the final food products. Copigmentation is a phenomenon in which pigments (anthocyanins) form noncovalent complexes with copigments. It stabilizes the flavylium cation form of the pigment, causing changes in color and/or brightness. In particular, copigmentation stabilizes the red color of the flavylium cation, which can occur at higher pH values, where it should normally undergo other chemical reactions that lead to color degradation (see explanation above). Efficient copigments are electron-rich systems, which are prone to associate with the (electron-poor) flavylium cation. Copigments are generally colorless phenolic compounds, *e.g.*, flavonols, phenolic acids, and more rarely other flavonoids and alkaloids. They should bear sufficiently extended  $\pi$ -conjugated system, which is prone to favor  $\pi - \pi$  stacking interactions with the pigment. Increasing the number of hydroxyl and methoxyl substituents modifies the efficiency of stability of copigmentation complexes. Chlorogenic, ferulic, *p*-coumaric and other hydroxycinnamic acids are relatively efficient copigments and they are more efficient copigments than benzoic acids. Flavonols (*e.g.*, quercetin, kampferol) are the most efficient copigments.<sup>76-79</sup>

Copigmentation is often accompanied by formation of complexes with charge-transfer character, *i.e.*, in which the electron density is transferred from the electron-rich to the electron-poor moiety in the copigmentation complexes, in the excited state. This partially rationalizes the spectral changes observed in UV/Vis absorption spectra (hypo-/hyper- and hypso-/bathochromic effects).<sup>36,76</sup>

Besides intermolecular associations, intramolecular stacking can also exist. This occurs when both the pigment and copigment are covalently linked with a flexible linker, allowing a folding and close contact between both partners to make intramolecular copigmentation. Copigmentation complexes can also be stabilized by metal ions, which may be responsible for blue color of metal-anthocyanin complexes.<sup>76,77,80</sup> Self-association (so-called homo-molecular intermolecular complexation) may be seen as a special case of copigmentation, also allowing anthocyanins to remain stable at higher pH values.

Depending on external conditions and thus the charge state, anthocyanins absorb either in the UV or the visible region. Pyranoanthocyanins express their maximal color intensity at pH value

of about 3.6 (pH of wine) and they can absorb visible light twice or three times more than at pH = 1.0, whereas, anthocyanins absorb visible light (for given wavelengths) more strongly under acidic conditions. The presence of certain copigments influences color stability. It has been shown that phenolic acids enhance color stability in *e.g.*, strawberries, raspberries, cranberries and other juices during storage.<sup>76,77</sup> Rutin and other flavonols glycosides also exhibit positive effects in color stabilization.<sup>81</sup>

Copigmentation is also strongly influenced by structures and charge states of copigments. The negatively charged 7-*O*-sulfoquercetin is an efficient copigment of the malvin flavylium cation not only due to  $\pi$ - $\pi$  stacking interactions but also due to ionic interactions between charged forms of molecules. The enhancement of charge transfer between the pigment and copigment is observed for ferulate ion, which is more prone to bind to malvin than ferulic acid in its neutral form. The B-ring substitution influences the copigmentation effect as it was reported that pigments having hydroxyl groups in the B-ring tend to bind copigments less efficiently than the pigments having methoxyl groups.<sup>76</sup>

Copigmentation is influenced not only by pH values, concentrations, structure of molecules, but also by environment. Hydrophobic effects have a crucial contribution to these effects and they also are a crucial driving force of copigmentation. Hydrophobic effect is a complex combination of solute-solvent and solute-solute interactions (enthalpic contribution) but also a matter of solute-solvent reorganization (entropic contribution). From a theoretical point of view, one should mention that to properly and efficiently evaluate such effects, solvent should be described explicitly.

Copigmentation is mainly observed in water; a decrease in water content (*i.e.*, adding co-solvent) always leads to a decrease in the copigmentation effect, no matter the nature of the organic co-solvent added to water (ethanol or other alcoholic co-solvents reduce the amount of complexation).<sup>82</sup> Whereas methanol is less damaging to the copigmentation than ethanol and acetone, further increase in the amount of the latter co-solvents makes the copigmentation effect vanish.<sup>82</sup>

As mentioned above, dispersion ( $\pi$ - $\pi$  stacking) interaction strongly contributes to the stabilization, and in a lesser extent H-bonding interactions or CH- $\pi$ , OH- $\pi$ , cation- $\pi$  and anion- $\pi$  interactions. Electrostatic interactions are very important to predict the geometries with three

main types of  $\pi$ -stacking arrangements – stacked (sandwich), displaced-stacked (face-to face) and edge-to-face (T-shape) aromatic interactions (Figure 8).<sup>83-86</sup>

Theoretical chemistry methods have become very useful and important to support experimental results as they shed light on driving forces of copigmentation and rationalization of subsequent spectral changes. Moreover, more demanding QM/MM methods (Section 3.C.) can be used to evaluate structural features and electronic description with explicit solvent molecules.

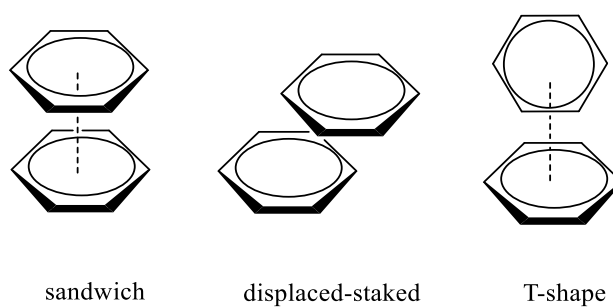


**Figure 8.** Types of stacking interactions.



### 3. THEORETICAL CHEMISTRY METHODS

#### 3.A. General concepts of theoretical chemistry

##### 3.A.a. The Born-Oppenheimer approximation

The time-independent Schrödinger<sup>87</sup> equation describing the energy and the motion of systems is given as follows:

$$\hat{H}\Psi = E\Psi \quad (1)$$

where  $\hat{H}$  is the Hamiltonian operator acting on the wave function  $\Psi$  and  $E$  corresponds to the total energy of the electronic system. The Hamiltonian operator is given by:

$$\hat{H} = -\sum_{i=1}^N \frac{1}{2} \nabla_i^2 - \sum_{A=1}^M \frac{1}{2M_A} \nabla_A^2 - \sum_{i=1}^N \sum_{A=1}^M \frac{Z_A}{r_{iA}} + \sum_{i=1}^N \sum_{j>i}^N \frac{1}{r_{ij}} + \sum_{A=1}^M \sum_{B>A}^M \frac{Z_A Z_B}{r_{AB}} \quad (2)$$

where  $i, j$  are numbering of electrons and  $A, B$  are numbering of nuclei;  $r_{iA}$ ,  $r_{ij}$ ,  $r_{AB}$  are the electron-nucleus, electron-electron and nucleus-nucleus distances, respectively;  $M_A$  and  $Z_A$  are the atomic mass and number, respectively. The first two terms describe the kinetic energies for electrons ( $T_{elec}$ ) and nuclei ( $T_N$ ), respectively. The other three terms are the electron-nucleus ( $V_{eN}$ ), electron-electron ( $V_{ee}$ ) and nucleus-nucleus ( $V_{NN}$ ) potential energies, respectively.

The solution of the Schrödinger equation for many-electron system can only be achieved from approximations. The Born-Oppenheimer approximation<sup>87,88</sup> is such a way to facilitate the solution of the Schrödinger equation. It is based on the fact that nuclei are much heavier than electrons, therefore electron distribution is instantly adjusted to any new potential created by the slow movements of nuclei. In other words, electrons move in a field of almost motionless atom nuclei. As a consequence, the movements on both nuclei and electrons are decoupled and two Schrödinger equations can be written for both types of particles. When dealing with electrons, the equation  $\hat{H}_{elec}\Psi_{elec} = E_{elec}\Psi_{elec}$  allows solving electronic wave function, whereas  $T_N$  is neglected and  $V_{NN}$  is a constant. The total energy  $E$  is calculated as the sum of the resolved electronic energy  $E_{elec}$  and the constant repulsion between the fixed nuclei.

### 3.A.b. The Hartree-Fock approximation

Each electron is described by a spin-orbital ( $\chi$ ) – a function, which depends on space distribution ( $\varphi$ ) and spin ( $\alpha$  or  $\beta$ ) of electrons:

$$\chi(x_i) = \varphi(r_i)\alpha(\omega_i) \quad \text{or} \quad \chi(x_i) = \varphi(r_i)\beta(\omega_i) \quad (3)$$

The total wave function of a given n-electron system can be described by a Slater determinant:

$$\Psi(x_1, x_2, \dots, x_n) = \frac{1}{\sqrt{n!}} \begin{vmatrix} \chi_i(x_1) & \chi_j(x_1) & \dots & \chi_k(x_1) \\ \vdots & \vdots & & \vdots \\ \chi_i(x_n) & \chi_j(x_n) & \dots & \chi_k(x_n) \end{vmatrix} \quad (4)$$

where  $x_n$  stands for spatial and spin coordinates.

The main idea of the Hartree-Fock (HF) approximation<sup>87,89,90</sup> is to replace the complicated many-electron problem by a one-electron problem, in which all electrons move and see an averaged potential field of all the other electrons. In other words, in this approximation an electron does not explicitly see nearby electrons. Considering this approximation, the HF equations are derived as:

$$\hat{f}_i \chi_i = \varepsilon_i \chi_i \quad (5)$$

where  $f_i$  is the Fock operator and  $\varepsilon_i$  is the energy of a given spin-orbital  $\chi_i$ .

The mono-electronic Fock operator is given as the sum of the mono-electronic core operator  $H_i^{core}$  (describing the kinetic term plus the electron-nuclei interactions) and a mono-electronic operator  $v_i^{HF}$  (describing electron-electron interactions). More precisely, the mono-electronic operator contains the Coulomb interaction  $J_{ij}$ , between electrons in  $i$  and  $j$ , and the exchange term  $K_{ij}$ , which describes correlation between electrons with parallel spin. The HF Hamiltonian can then be written as the sum of all  $f_i$ :

$$H^{HF} = \sum_i^N \underbrace{(H_i^{core} + v_i^{HF})}_{f_i} = \sum_i^N H_i^{core} + \sum_i^N \sum_{j>i}^N (J_j(i) - K_j(i)) \quad (6)$$

### 3.A.c. Post Hartree-Fock methods

The HF approximation has shown many drawbacks. The major limitation is that electron correlation is not fully taken into account in this formalism<sup>90</sup>. In particular, the correlation attributed to electrons having antiparallel spin is totally ignored. The missing term is called the correlation energy and it is given by:

$$E_{corr} = E_{exact} - E_{HF} \quad (7)$$

which is defined as the difference between the exact non-relativistic energy of the system and the HF energy limit. The post-HF methods<sup>87</sup> based on configuration interaction<sup>90-92</sup>, coupled cluster<sup>90,92</sup> and perturbation theory<sup>90,93,94</sup> assess  $E_{corr}$  estimates, so to approach the exact energy, which is unknown for many-electron systems.

The configuration interaction (CI) method uses an excited determinant to obtain a set of n-electron trial functions and a linear combination of these trial functions describes the exact wave function. The best estimate of the HF ground state is a single Slater determinant generated from the n spin-orbitals:

$$|\psi_0\rangle = |\chi_1\chi_2 \dots \chi_a\chi_b \dots \chi_n\rangle \quad (8)$$

therefore a single excited state determinant is such that one electron occupies a virtual orbital (transition from  $\chi_a$  to  $\chi_r$ ) and the Slater determinant of the corresponding excited state is given by:

$$|\psi_a^r\rangle = |\chi_1\chi_2 \dots \chi_r\chi_b \dots \chi_n\rangle \quad (9)$$

similarly a double excited state determinant (transition from  $\chi_a\chi_b$  to  $\chi_r\chi_s$ ) can be written as:

$$|\psi_{ab}^{rs}\rangle = |\chi_1\chi_2 \dots \chi_r\chi_s \dots \chi_n\rangle \quad (10)$$

Eventually, the exact wave function is calculated as a linear combination of all single-excited determinants, all double-excited determinants *etc.*:

$$|\Psi\rangle = c_0 |\psi_0\rangle + \sum_r \sum_a c_a^r |\psi_a^r\rangle + \sum_a \sum_{b>a} \sum_r \sum_{s>r} c_{ab}^{rs} |\psi_{ab}^{rs}\rangle + \dots \quad (11)$$

The coupled cluster (CC) method uses an exponential operator defining the exact wave function  $\Psi$  as:

$$\Psi = e^{\hat{T}} \Phi_0 \quad (12)$$

in which  $\hat{T} = \hat{T}_1 + \hat{T}_2 + \dots + \hat{T}_n$  is the cluster operator, which produces excited determinants from the ground state wave function,  $\hat{T}_1$  is defined by using the mono-excited wave function,  $\hat{T}_2$  by bi-excited wave function, *etc.* The exponential factor can be rewritten as a Taylor series:

$$e^{\hat{T}} = \sum_{i=0}^{\infty} \frac{\hat{T}^i}{i!} \quad (13)$$

The Möller-Plesset (MP) perturbation theory uses a correcting factor (a perturbation term, corresponding to the correlation energy), which is added to the Hamiltonian operator  $\hat{H}_0$  as follows:

$$\hat{H} = \hat{H}_0 + \lambda \hat{V} \quad (14)$$

Depending on the order of the theory, there exist the MP2, MP3, MP4 methods. The first order Möller-Plesset (MP1) method corresponds to the HF energy. The second order MP method (MP2) provides the energy as follows:

$$E_0^{(2)} = \sum_{\substack{\text{possible} \\ \text{diexcitations}}} \frac{|\langle \Psi_{HF} | \sum_{j>i} \frac{1}{r_{ij}} | \Psi^D \rangle|^2}{E_0^0 - E_0^D} = \sum_{s>r} \sum_{b>a} \frac{|(ab|rs)|^2}{(E_r - E_a) + (E_s - E_b)} \quad (15)$$

where  $a$  and  $b$  correspond to the spin-orbital of electrons no. 1 and 2 of the ground state,  $r$  and  $s$  refer to the spin-orbital of electrons in excited state;  $\Psi^D$  is the double-electron excited wave function. The MP2 method provides accurate results with respect to experimental data, but it is computationally time demanding, particularly when using large basis sets. The MP3 is more computationally time demanding than MP2 although it does not provide better results.

### 3.A.d. Basis sets

A basis set<sup>90,95-97</sup> is an ensemble of mathematical functions, which allows a simplified description of atomic orbitals ( $\chi$ ). Molecular orbitals ( $\Phi$ ) are often deduced from atomic orbitals within the linear combination of atomic orbitals (LCAO) approximation:

$$\Phi_i = c_{1i}\chi_1 + c_{2i}\chi_2 + c_{3i}\chi_3 + \dots + c_{ni}\chi_n \quad (16)$$

where  $c_{ji}$  is the coefficient that is weighting the contribution of atomic orbitals  $j$  to molecular orbital  $i$ .

Atomic orbitals are in principle described by Slater-type orbitals (STOs). The STOs decay exponentially with electron-nucleus distance and they accurately describe the long-range overlap between atoms. However, the integration of STO functions is numerically time consuming. To overcome this drawback, orbitals can be alternatively described as a linear combination of mathematical functions easier to integrate; these functions are called contractions. In the Pople's basis sets, contractions are Gaussian functions, *i.e.*, Gaussian-type orbitals (GTOs). All contractions are basis functions and they constitute the basis set. The minimal basis set corresponds to the use of only one contraction (*e.g.*, one Gaussian) per atomic orbital; for instance, only a single 1s orbital describes a hydrogen atom. In GTO, the decay is exponential of squared electron-nucleus distance. This mathematical difference makes that a minimum of three Gaussian functions is required to somewhat mimic STOs (*i.e.*, STO-3G basis set). In general, atomic orbitals are therefore described as a linear combination of multiple Gaussian functions:

$$\chi_n = d_1g_1 + d_2g_2 + d_3g_3 + \dots + d_ng_n \quad (17)$$

where  $g_n$  are the Gaussian functions.

Minimal basis sets are currently rarely used, as they do not provide accurate electronic description. Among the most relevant improvement that has been made in Pople's basis, was to separate the description of core and valence electrons (*e.g.*, in a 6-31G basis set, six contractions are used for core electrons while two atomic orbitals made of three and one contractions are used for valence electrons). Moreover, adding polarization functions somehow allows introducing asymmetry in molecular orbital description. One or two asterisks (alternatively quoted d and p) indicate that the polarization functions are added to heavy and light (hydrogen)

atoms, respectively. Adding diffuse functions (marked as ‘+’ in Pople-type or ‘aug’ for augmented in Dunning-type basis sets) improves the description far from the nuclei by using more flat Gaussian basis functions. Diffuse functions can also be added on hydrogen atoms, as quoted by ‘++’.<sup>98</sup>

The 6-311++G\*\* [or 6-311++G(d,p)] basis set consists of one atomic orbital for the inner shell electrons described by six Gaussian functions and three atomic orbitals for the valence electrons – the first being described by three Gaussian functions, the second and the third atomic orbitals being described by one Gaussian function; ++ indicate the presence of polarization functions for heavy and hydrogen atoms; and \*\* [or (d,p)] indicate that diffuse functions are used for all atom types. Beside Pople-type basis sets, correlation consistent (cc)<sup>99</sup> basis sets (Dunning-type) also exist, *e.g.*, cc-pVDZ, cc-pVTZ, cc-pVQZ *etc.* where p stands for polarization function and VxZ describes the valence electrons (Valence Double, Triple or Quadruple Zeta).

As the atoms of interacting molecules get closer to each other, a given molecule can borrow basis set functions from the other molecule. This artificially improves description, which may induce artifacts. This effect is called basis set superposition error and it can be eliminated by the counterpoise method employing ghost orbitals with no electrons or protons, and the calculations are performed using mixed basis sets and the error is then subtracted *a posteriori*.

### 3.B. Density functional theory

The wave function does not have any real physical meaning, except that the square of its modulus  $|\Psi|^2$  is the electron probability density of electron, *i.e.*, describing spatial electron distribution. Although post-HF methods allow description of electron correlation, thus, providing high accuracy, they can only be used for systems with limited number of atoms (up to around 100). The density functional theory (DFT) is an alternative to account for electron correlation, however much less computationally-demanding than post-HF methods, in other words, DFT is adapted to much bigger systems for a reasonable computational time. The DFT formalism does not use the wave function as the main variable, but instead the electron density  $\rho(r_1)$  is used, *i.e.*, the probability of finding an electron at a given position  $r_1$ :

$$\rho(r_1) = \int \dots \int \Psi^*(x_1, x_2, \dots, x_N) \Psi(x_1, x_2, \dots, x_N) dx_2 \dots dx_N \quad (18)$$

As already stated in section 3.A.a., the Hamiltonian is given by:

$$\hat{H}_{elec} = - \sum_{i=1}^N \frac{1}{2} \nabla_i^2 - \sum_{i=1}^N \sum_{A=1}^M \frac{Z_A}{r_{iA}} + \sum_{i=1}^N \sum_{j>i}^N \frac{1}{r_{ij}} \quad (19)$$

where the first term corresponds to the kinetic operator; the middle term corresponds to the external potential  $V_{ext}$  ( $= V_{eN}$ ) mainly corresponding to electron-nuclei interaction potential; and the last term is electron-electron interaction  $V_{ee}$ .

### 3.B.a. Hohenberg and Kohn theorems

The first Hohenberg and Kohn theorem<sup>87,90,100</sup> states that the external potential  $V_{ext}(\mathbf{r})$  is fully determined, within a constant, by the electron density  $\rho(\mathbf{r})$ . As the electron density also determines the number of electrons, it determines the wave function of the system. Consequently  $\rho(\mathbf{r})$  determines all electronic properties of a given system. The total energy is written as a sum of functions of  $\rho(\mathbf{r})$ , itself a function of the wave function, *i.e.*, the total energy is a sum of functionals of the density:

$$E[\rho] = T[\rho] + V_{ext}[\rho] + V_{ee}[\rho] \quad (20)$$

the  $V_{ext}$  term is a system-dependent term corresponding to the interaction between nuclei and electrons.

The second theorem is the variational principle for  $E[\rho]$ . Let us consider  $\rho_0$  as the exact electron density of the ground state and  $E_0$  the corresponding exact energy. For a trial electron density  $\rho_{trial}$ , the corresponding energy  $E$  is always higher (or equal) than (to)  $E_0$ :

$$E_0 \leq E \quad (21)$$

The exact energy can be rewritten with respect to eq. 20 as:

$$E_0[\rho] = F^{HK}[\rho_0] + \int \rho_0 v_{ext}(r) dr \quad (22)$$

where  $F^{HK}$  is the universal Hohenberg-Kohn functional, which is described independently from the external potential  $v_{ext}$ , and which is written as  $T[\rho_0] + V_{ee}[\rho_0]$ . The  $V_{ee}$  term describes electron-electron interactions, given as the classical Coulomb interaction  $J$  between electrons, and the non-classical term including the exchange part and electron correlation ( $E_{XC}(\rho_0)$ ):

$$F^{HK}[\rho_0] = T[\rho_0] + J[\rho_0] + E_{non-classical}[\rho_0] \quad (23)$$

where

$$J[\rho_0] = \frac{1}{2} \iint \frac{\rho_0(r_1) \rho_0(r_2)}{r_{12}} dr_1 dr_2 \quad (24)$$

### 3.B.b. Kohn-Sham approach

Neither  $T[\rho_0]$  nor  $E_{non-classical}[\rho_0]$  are exactly known, so Kohn and Sham<sup>87,90,101</sup> proposed an indirect approach to determine these terms by using Kohn-Sham (KS) orbitals.

The ground state kinetic energy is written as:

$$T = \sum_i^N n_i \left\langle \psi_i \left| -\frac{1}{2} \nabla^2 \right| \psi_i \right\rangle \quad (25)$$

where  $\psi_i$  and  $n_i$  are the natural spin orbitals. T is a functional of the total electron density:

$$\rho(r) = \sum_i^N n_i \sum_s |\psi_i(r, s)|^2 \quad (26)$$

Kohn and Sham simplified eqs. 25 and 26 and used  $n_i = 1$  for all N spin-orbitals. This correspond to a non-interacting N-electron system, somehow similarly to what is stated in HF approximation. The  $\psi_i$  in KS kinetic energy ( $T_{KS}$ ) are called KS orbitals. This energy term is introduced into  $F^{HK}$  (eq. 23) as:

$$F^{HK}[\rho] = T_{KS}[\rho] + J[\rho] + E_{XC}[\rho] \quad (27)$$

where the exchange-correlation energy functional includes the non-classical terms plus the correction to kinetic energy, with  $T[\rho]$  being the exact kinetic energy:

$$E_{XC}[\rho] = (T[\rho] - T_{KS}[\rho]) + E_{non-classical}[\rho] \quad (28)$$



Compared to the HF method, the KS formalism intrinsically incorporates electron correlation. The exact expression of  $E_{XC}[\rho]$  is unknown, and there are many ways to provide an expression for it.

### 3.B.c. Exchange-correlation functionals

Local density approximation (LDA).<sup>87,90,102</sup> In the LDA approximation, the exchange-correlation functional is written as:

$$E_{XC}^{LDA}[\rho] = \int \rho(r) \varepsilon_{XC}(\rho(r)) dr \quad (29)$$

with  $\varepsilon_{XC}(\rho(r))$  being the exchange-correlation energy per particle of a uniform gas of density  $\rho$  at a particular space point  $r$ . The  $\varepsilon_{XC}$  term can be split into two contributions, namely the exchange ( $\varepsilon_X$ ) and the correlation ( $\varepsilon_C$ ) parts, allowing to use different mathematical expressions for both contributions.

The LDA is based on the jellium model (a uniform gas of electron, in which the positive charges are spread out), and in which the electron density is defined locally at a certain  $r$ . It is the best used for homogenous uniform electron gas system and it has provided better results than HF.

Generalized gradient approximation (GGA).<sup>87,90,102</sup> Here, the density gradient  $\nabla\rho$  was introduced to create inhomogeneity, *i.e.*, getting out from the too restrictive local approximation. This was first introduced by gradient expansion approximation (GEA) as:

$$E_{XC}^{GEA}[\rho] = \int \rho \varepsilon_{XC}(\rho) dr + \sum_{\alpha,\beta} \int C_{XC}^{\alpha,\beta}(\rho^\alpha, \rho^\beta) \frac{\nabla\rho^\alpha}{(\rho^\alpha)^{2/3}} \frac{\nabla\rho^\beta}{(\rho^\beta)^{2/3}} + \dots \quad (30)$$

in which  $\alpha, \beta$  correspond to the spin of electrons. This approach did not lead to sufficient accuracy for non-homogenous systems. The GGA approach was developed to solve the mathematical inconsistencies introduced in the GEA functionals. In GGA, the gradient was introduced as follows:

$$E_{XC}^{GGA}[\rho, \nabla\rho] = \int \varepsilon_{XC}^{GGA}[\rho^\alpha, \rho^\beta, \nabla\rho^\alpha, \nabla\rho^\beta] dr \quad (31)$$

The so-called meta-GGA functionals have also been developed, which are including the second derivative of the density.

One of the most popular GGA exchange functionals is Becke88 (B) (it was developed by Becke, the number corresponds to the year of development). Another popular functional is Perdew-Wang (PW91), which was modified PW by Barone and Adamo (mPW), Gill96 (G96), and Perdew-Burke-Ernzerhof (PBE). Some of the examples of the gradient-corrected correlation functionals are LYP (according to Lee, Yang and Parr), Perdew-Wang (PW91), Perdew86 (P86), Berke96 (B96) *etc.* All combinations of exchange and correlation functionals are possible.

Hybrid functionals.<sup>87,90,102</sup> The main idea of hybrid functionals is to describe exchange energy by both the HF and DFT formalisms, the correlation term being only derived from the DFT formalism. A general expression of hybrid functional can be given as:

$$E_{XC} = (1 - a)E_{XC}^{DFT} + a E_X^{HF} \quad (32)$$

When  $a = 0.5$  in eq. 32, the method is so-called half-and-half, because of the use of half HF-exchange and half DFT-exchange. Any functional using any mixture of the different exchange and correlation parts can be developed.

As characteristic examples of hybrid functionals are the B3 functionals using 3 parameters as *e.g.*, B3LYP:

$$E_{XC}^{B3LYP} = (1 - a) E_X^{LSDA} + a E_X^{HF} + b E_X^B + E_C^{LSDA} + c E_C^{LYP} \quad (33)$$

$a = 0.2$ ,  $b = 0.72$  and  $c = 0.81$  (Becke-3-LYP).

The B3P86 uses the P86 correlation functional instead of the LYP, but it still uses the three parameters derived for B3LYP. The PBE0 functional uses 25 % of HF exchange and 75 % of PBE ( $0.25 E_X^{HF} + 0.75 E_X^{PBE} + E_C^{mPW91}$ ).

The CAM-B3LYP functional is an example of hybrid functional with long-range correction, *i.e.*, where electron-electron interactions are separated (in terms of mathematical description) into short- and long-range components<sup>103</sup>. The respective weight of HF-like and DFT-like exchange is different in both components, the full HF-like term being dominant in the latter

component. This has allowed several improvements, such as better description of polarizability of long chains or of charge transfer.

### 3.B.d. Dispersion correction of DFT

Depending on the choice of functional, DFT methods are well adapted to calculate many physico-chemical properties of molecules with reasonable time and reliability. Nevertheless, many DFT functionals fail at description of noncovalent interactions, as almost all gradient-corrected density functionals are not capable to describe dispersive interactions. Therefore, other methods (*e.g.*, DFT-D, DFT-D2, and DFT-D3) have been developed to improve the description of such dispersion interactions.

DFT-D<sup>104,105</sup> – Grimme came to the idea how to improve the DFT energy, and he implemented a parametrized dispersion correction to energy as follows:

$$E_{DFT-D} = E_{DFT} + E_{disp} \quad (34)$$

where the dispersion correction is given by:

$$E_{disp} = -s_6 \sum_{i=1}^{M-1} \sum_{j>j}^M \frac{C_6^{ij}}{R_{ij}^6} f_{dmp}(R_{ij}) \quad (35)$$

where  $s_6$  is a functional dependent scaling factor, which is adjusted to reach accuracy and it should be systematically and carefully parameterized;  $R_{ij}$  are interatomic distances;  $C_6^{ij}$  is the dispersion coefficient for the  $ij$  atom pair, which is derived from the atomic dispersion coefficients  $C_6^i$  and  $C_6^j$ , as:  $2 C_6^i C_6^j / (C_6^i + C_6^j)$ ;  $f_{dmp}$  is the damping function, which corrects the near-singularities (at small interatomic distances  $R_{AB}$ ) and double-counting effects of electron correlation (at intermediate distances)<sup>106</sup>:

$$f_{dmp}(R) = \frac{1}{1 + e^{-d(R/R_0-1)}} \quad (36)$$

where  $d$  is the slope of the damping function ( $d = 23$  for DFT-D) and  $R_0$  is the sum of the van der Waals radii of both involved atoms.

DFT-D2<sup>107</sup> – The DFT-D2 differs from the DFT-D by the slope of the damping function and by the atomic and atom-paired dispersion contribution as  $d = 20$ ,  $C_6^{AB} \approx \sqrt{C_6^A C_6^B}$  and  $C_6^A = 0.05 N I_p^A \alpha_p^{A*}$ , where  $N = 2, 10, 18, 36$  and  $54$  for atoms from rows 1 – 5 of the periodic table;  $I_p^A$  is the ionization potential; and  $\alpha_p^{A*}$  is the static dipole polarizability of atom A. DFT-D2 provides more accurate description of geometries and energies in comparison to the formal 1D dispersion correction.

DFT-D3<sup>108</sup> – A few years later, Grimme proposed an improvement of the previous model, in which he included a three body term and higher-order dispersion terms ( $R^{-8}, R^{-10} \dots$ ) as follows:

$$E_{disp} = E^{(2)} + E^{(3)} \quad (37)$$

where the two-body term is described as:

$$E^{(2)} = \sum_A^{M-1} \sum_{B>A}^M \sum_{n=6,8,10\dots} S_n \frac{C_n^{AB}}{R_{AB}^n} f_{dmp,n}(R_{AB}) \quad (38)$$

The first two sums run over all atom pairs of the system;  $C_n^{AB}$  corresponds to the  $n^{\text{th}}$  order dispersion coefficient for atom pair; AB and  $R_{AB}$  is their internuclear distance. The damping function, numerically stable and convenient for all higher  $n^{\text{th}}$  orders of dispersion, was described by Chai and Head-Gordon as (note: other  $f_{dmp}$  may be used as well, *e.g.*, from Becke-Johnson or Tang-Toennies):

$$f_{dmp,n}(R) = \frac{1}{1 + 6(R/(s_{r,n} R_0^{AB}))^{-\alpha_n}} \quad (39)$$

where  $s_{r,n}$  is the  $n^{\text{th}}$  order dependent scaling factor of the cutoff radii  $R_0^{AB}$  for atom pair AB, which determines in which interatomic distance region the dispersion energy is decreasing (in absolute value) and eventually vanishing. The  $\alpha_n$  is the parameter describing the steepness of the function for small  $R_{AB}$ .

The three-body terms is expressed as follows:

$$E^{(3)} = \sum_A^{M-1} \sum_{B>A}^{M-1} \sum_{\substack{C>A \\ C>B}}^M \frac{C_9^{ABC} (3 \cos \theta_a \cos \theta_b \cos \theta_c + 1)}{(R_{AB} R_{BC} R_{AC})^3} f_{dmp,(3)}(\bar{r}_{ABC}) \quad (40)$$

The  $\theta_a$ ,  $\theta_b$ ,  $\theta_c$  terms are the internal angles of the triangle formed by the AB, BC and AC segments (corresponding to  $R_{AB}$ ,  $R_{BC}$  and  $R_{AC}$ ); the  $C_9^{ABC}$  term is the ninth-order dispersion coefficient and it is described as the geometrical average of the previously defined atom-pair dispersion coefficients:  $C_9^{ABC} \approx -\sqrt{C_6^{AB}C_6^{AC}C_6^{BC}}$ .

### 3.C. QM/MM

The previous sections have focused on quantum chemistry/mechanics (QM) methods. The molecular mechanics (MM) formalism does not explicitly treat movements of electrons according to the Schrödinger equation; instead, atoms are treated as balls and bonds as springs. The movements of atoms are described by classical Newton equations. The second Newton's law ( $F = ma$ ) allows introducing velocities to perform molecular dynamics (MD) simulations:

$$-\frac{dV}{dx_i} = m_i \frac{d^2x_i}{dt^2} \quad (41)$$

where the left-handed term is the force acting on atom  $i$  having mass  $m_i$  and moving along coordinate  $x_i$ . For a given geometry of the molecular system, forces are applied on each atom, which induce changes in atomic position and velocity, to reach another conformation at another time step. MD simulations are performed on many time steps and the output of MD simulations is a trajectory made of all geometries.

In MM, all interactions are parameterized in force fields (FFs), which consist of an equation to calculate the energy and a set of parameters for each type of bonded (bond, angle, dihedral angle) and non-bonded (electrostatic, van der Waals) interactions between each atom type. Many different FFs have been built, which are more or less specific of molecular systems, *i.e.*, some are better parameterized for proteins, other for lipids, or sugars, crystals *etc.*<sup>109–112</sup> MD simulations allow tackling conformational hypersurfaces (*e.g.*, using simulating annealing procedures) and studying the dynamical behavior of molecular systems (*e.g.*, insertion of xenobiotics in lipid bilayer membranes).

In QM/MM approaches, a regular MD simulation is first performed to sample the conformational space as thoroughly as possible. QM calculations are performed on several snapshots (geometries) from the trajectory. To account for solvent effect, two approaches can

be used: implicit or explicit solvent model. In the former, the solute is embedded in a shape-adapted cavity, which is surrounded by a dielectric continuum (implicitly describing the solvent) and which is characterized by a dielectric constant  $\epsilon$ . This approach loses the information about specific solute-solvent interactions, which are on the other hand taken into account within the explicit solvent model, where solvent molecules are explicitly added around the system. Based on a QM/MM approach, the polarizable embedding (PE) scheme has been proposed to explicitly account for electrostatic contributions of solvent molecules to molecular properties. Solvent molecules around a molecular QM core is defined as a center multipole expansion corresponding to the so-called electrostatic embedding potential. For readability sake, only the basic concepts concerning ground state PE are discussed here; for a detailed description, see refs. 113–117.

For example, the zero-order expansion is defined as a multicenter point charge distribution that is defined by given MM charges and polarizabilities at the solvent atomic nuclei positions. Therefore, solvent-molecular core interactions consist of electrostatic interactions between atomic charges of the QM core and solvent point charges ( $E_{es}$ ) as well as induction energy ( $E_{ind}$ ). The total energy of the system  $E_{PE}^{total}$  is given by:

$$E_{PE}^{total} = E_{QM} + E_{es} + E_{ind} \quad (42)$$

where  $E_{QM}$  is the energy of the isolated core fragment. In a multipole expansion (*i.e.*, including charge, dipole, quadrupole, *etc.*) the electrostatic interaction represents the interactions between the permanent multipoles (in the environment) and the nuclei and electrons in the QM core, following the classical response methods. For example, at the zeroth-order, *i.e.*, charge-charge electrostatic interactions can be defined as:

$$E_{es} = \sum_{s=1}^S \left( \sum_{m=1}^M \frac{Z_m}{r_{ms}} - \sum_{i=1}^N \frac{1}{r_{is}} \right) \mathbf{Q}_s^{(0)} \quad (43)$$

$S$  is the number of sites in the surrounding environment;  $M$  and  $N$  are the number of nuclei and electrons, respectively, in the QM core region;  $Z_m$  is the nuclei charge;  $r_{ms}$  and  $r_{is}$  are inter-nucleus and electron distances, respectively; and  $\mathbf{Q}_s^{(0)}$  is the zeroth-order multipole moment operator (*i.e.*, point atomic charge distribution). In other words, the first term in the parenthesis corresponds to the nuclear contribution, the second term is the electronic contribution.

The induction contribution is due to the polarization of the surrounding fragments by the molecular core:

$$E_{ind} = -\frac{1}{2}\boldsymbol{\mu}^{ind}(\mathbf{F}^{nuc} + \mathbf{F}^{elec} + \mathbf{F}^{es}) \quad (44)$$

$\boldsymbol{\mu}^{ind}$  is the set of induced dipole moments and  $\mathbf{F}^i$  are the electric field vectors containing the information about the electric fields from the nuclei and electrons in the central QM core but also to the permanent multipole moments from all the other fragments in the environment. In other words, in PE-approach, polarization of solvent is due to the molecular core as well as to the self-polarization. Within the DFT formalism, PE potential is derived by an effective KS potential  $\hat{v}_{PE}$ :

$$\hat{f}_{eff} = \hat{f}_{KS} + \hat{v}_{PE} \quad (45)$$

where the PE potential functional form corresponding to the zeroth-order is given as:

$$\hat{v}_{PE}^{(0)} = \sum_{s=1}^S \mathbf{q}_s^{(0)} \sum_{pq} \frac{\hat{E}_{pq}}{\mathbf{r}_{s,pq}} - \sum_{s=1}^S \mu_s^{ind}(\mathbf{F}[\rho]) \sum_{pq} \frac{\nabla \hat{E}_{pq}}{\mathbf{r}_{s,pq}} \quad (46)$$

$pq$  correspond to a matrix element of the corresponding operator in KS orbital bases, the  $\hat{E}_{pq}$  term is the so-called excitation operator. The first term in eq. 46 contains the electrostatic embedding potential introduced here in terms of a set of localized multipole moments, while the second term accounts for a polarization of the environment by the solute electron density. For each self-consistent field (SCF) iteration, the PE potential is determined by minimizing the total energy functional according to the electron density of the QM core. In other words, the QM core energy explicitly accounts for the electrostatic solvent interaction from the PE region that is in turn updated for each SCF iteration to account for the new electron density. This allows the resolution of a fully self-consistent treatment of polarization, *i.e.*, polarization of solute by solvent and *vice versa*.

## 4. HOW TO CALCULATE EXPERIMENTAL OBSERVABLES?

### 4.A. Sampling the conformational space

To properly study physical-chemical properties of molecular systems, a careful analysis of conformational space is required. This is particularly true when dealing with real-world derivatives of medium- to big- size, for which the number of degrees of freedom is large. For instance, when calculating *i*) redox properties with DFT, or even more important *ii*) optical properties with TD-DFT, a complete conformational sampling is mandatory to average these properties for all possible conformers existing in solution. For small molecules, a systematic evaluation of any conformational change can be achieved to describe the few existing conformers (publications **I – V**). With bigger molecules (*e.g.*, dimers, copigmentation complexes), as the number of degrees of freedom dramatically increases (publication **II**), a systematic DFT-based conformational search is precluded and MD simulations have to be considered. The MD-derived techniques allow obtain all possible molecular arrangements within a reasonable time scale. The all desired properties (*e.g.*, antioxidant and UV/Vis absorption properties) are calculated for all conformers and averaged to mimic experimental conditions as best as possible.

A potential energy (hyper)surface can be terribly complex for big molecular systems. The conformational sampling can thus be achieved by simulated annealing procedures<sup>76,118</sup>. Thanks to heating-cooling loops, molecules overcome energetic barriers, jumping from one to another local minimum, eventually reaching the global minimum, but also the relevant local minima. More precisely, the system is quickly heated to high temperature and then slowly cooled down. This procedure is performed several times (heating-cooling loops), which favors a complete sampling of all energetic minima. In principle, the molecule reaches a new local minimum at each loop. An alternative to simulated annealing is simple unbiased MD simulations on sufficiently long time to ensure sampling of conformational space. QM/MM calculations can then be performed on all snapshots along MD trajectories. For UV/Vis QM calculations, the system is split into a core region and surrounding fragments in the environment. Multipole moments and polarizabilities are calculated, which are used to build a PE potential, itself added to the vacuum KS operator.



## 4.B. Molecular spectroscopy: TD-DFT

### 4.B.a. Runge-Gross theorem

The evaluation of excited states within QM formalism requires solution of the time-dependent Schrödinger equation:

$$H(r, t) \Psi_i(r, t) = i\hbar \frac{\partial}{\partial t} \Psi_i(r, t) \quad (47)$$

where  $\hbar$  is the reduced Planck constant ( $\hbar = h/2\pi$ ).

TD-DFT method is based on the Runge and Gross theorem<sup>119–121</sup>, which is the time-dependent equivalent to the Hohenberg-Kohn first theorem. It proves that a particular density  $\rho(r, t)$  determines a particular external potential  $v_{ext}(r, t)$ . In other words, for two different external potentials varying by a time-dependent constant, the corresponding time-dependent densities are different. Once the density is determined, all observables can be obtained. The time-dependent wave function is written as:

$$\left( -\frac{1}{2}\nabla_i^2 - \underbrace{\left( v_{ext}(r, t) + \int \frac{\rho'(r', t)}{|r-r'|} dr' + v_{xc}(r, t) \right)}_{v_{KS}(r, t)} \right) \Psi_i(r, t) = i\hbar \frac{\partial}{\partial t} \Psi_i(r, t) \quad (48)$$

where  $v_{ext}(r, t)$  is the external potential,  $\int \frac{\rho'(r', t)}{|r-r'|} dr'$  is the classical electrostatic electron-electron interaction and  $v_{xc}(r, t)$  is the exchange-correlation potential.

The perturbation related to the excitation can be expressed as a perturbation of the KS potential ( $v_{KS}(r, t) = v_{KS}(r) + \delta v_{KS}(r, t)$ ) as well as changes in density over time ( $\rho(r, t) = \rho(r) + \delta\rho(r, t) + \dots$ ). The  $\delta\rho$  corresponds to the response of the system and it is related to the perturbation of the KS potential  $\delta v_{KS}$  as:

$$\delta\rho(r, t) = \int dt' \int \chi[\rho_{GS}](r, r', t - t') \delta v_{KS}(r', t') dr' \quad (49)$$

where  $\chi$  is the linear response of the ground state electron density at point  $r$  and time  $t$ , if the external potential is applied at position  $r'$  and time  $t'$ .

#### 4.B.b. Selection rules for absorption spectroscopy

As shortly mentioned, when a system is exposed to light, its response can be added to the classical Hamiltonian as a perturbation that is a time-dependent excitation. The wave function is written as a linear combination of the ground state (GS) and the excited state (ES) wave function depending on time and coordinates as follows:

$$\Psi(x, t) = \sum_{i=0} c_i \Psi_i(x, t) \quad (50)$$

When  $t = 0$ , no excitation has occurred yet and the system is described only by the wave function of the GS. At  $t > 0$ , *i.e.*, when electromagnetic excitation applied, the coefficients  $c_i$  change according to the perturbation as:

$$c_i(t) = \frac{1}{2\hbar i} \varepsilon_0 \left[ \frac{e^{i(\omega_{m0} + \omega)t} - 1}{\omega_{m0} + \omega} - \frac{e^{i(\omega_{m0} - \omega)t} - 1}{\omega_{m0} - \omega} \right] \langle \Phi_m | \hat{\mu} | \Phi_0 \rangle \quad (51)$$

where  $\omega_{m0} = \frac{E_m - E_0}{\hbar}$  and  $\omega = 2\pi\nu$ ;  $|c_i|^2$  corresponds to the probability of the transition between the  $m$  ( $\Phi_m$ ) and  $0$  ( $\Phi_0$ ) states;  $\hat{\mu}$  is the electric dipole moment operator;  $\nu$  is the frequency of the electric field; and  $\varepsilon_0$  is the amplitude of the electric field. When  $\omega_{m0}$  approaches  $\omega$ , the magnitude of  $c_m^2$  increases, *i.e.*, the energy difference between GS and ES approaches that of the photon that can be absorbed.

The term  $\langle \Phi_m | \hat{\mu} | \Phi_0 \rangle$  is the transition dipole moment between states  $m$  and  $0$ . The vertical transition is forbidden if this integral is zero. The dipole moment can be divided into the electron ( $\hat{\mu}_e$ ) and nucleus ( $\hat{\mu}_m$ ) components:

$$M_{m0} = \langle \Phi_m | \hat{\mu}_e + \hat{\mu}_m | \Phi_0 \rangle \quad (52)$$

Within the Born-Oppenheimer approximation and including spin parts, where  $e$ - and  $n$ - indices refer to the electron and nucleus wave functions, respectively,  $M_{m0}$  is re-written:

$$M_{m0} = \langle \varphi_{m,e} | \hat{\mu}_e | \varphi_{0,e} \rangle \langle \Phi_{m,n} | \Phi_{0,n} \rangle \langle S_m | S_0 \rangle \quad (53)$$

This equation leads to the selection rules for absorption<sup>122,123</sup>. The first term refers to the spatial distribution, *i.e.*, selection rules on spatial orbitals; it is maximum when the transition is allowed

(the integral is nonzero) and it equals zero when the transition is forbidden. Both symmetry and orbital overlap from GS to ES play a crucial role. This rule is equivalent to the fact that an electronic transition is orbitally-allowed if and only if the triple direct product of the dipole moment and the orbitals' irreducible representation  $[\Gamma(\varphi_{m,e}) \times \Gamma(\hat{\mu}_e) \times \Gamma(\varphi_{0,e})]$  contains the totally symmetric irreducible representation of the point group of the molecule. For a totally symmetric GS, the symmetry allowed transitions corresponds to ES that having similar symmetry, meaning that the transition dipole moment from GS orbital to ES orbital must include identity symmetry.

The second term in eq. 53 is the product of the Franck-Condon factor, which connects two vibrational states (*e.g.*, one of GS, another one of ES) of a vertical transition. The third term of eq. 53 is the spin selection rule and it states that a transition is allowed when the integral is different from zero and it is allowed only between two states having the same spin multiplicity (due to orthogonality).

If the transition is spin- and/or symmetry forbidden, the molar extinction coefficient ( $\varepsilon_m$ ) is zero. It becomes non-zero by spin-orbit coupling in the first place, and by Herzberg-Teller coupling<sup>124,125</sup> in the second place, giving  $\varepsilon_m$  generally between  $10^{-5} - 10^0 \text{ M}^{-1} \text{ cm}^{-1}$  (regardless the answer to the vibrational or orbital selection rules). If the transition is spin-allowed but orbitally forbidden,  $\varepsilon_m$  is in the range  $10^0 - 10^3 \text{ M}^{-1} \text{ cm}^{-1}$  (regardless the answer to the vibrational rules). If the integrals are nonzero, *i.e.*, spin and orbitally allowed,  $\varepsilon_m$  is in the range  $10^3 - 10^5 \text{ M}^{-1} \text{ cm}^{-1}$ .

The oscillator strength  $f$  is proportional to the square of the transition dipole moment and it is related to absorbance  $A$ : the higher the transition dipole moment, the higher  $f$  and the higher  $A$ . The  $f$  value of the main transition can be obtained (in a given solvent) from the molar extinction coefficient  $\varepsilon_m$  as obtained by Lambert-Beer's law ( $A = \varepsilon_m \cdot c \cdot d$ , where  $c$  is the molar concentration and  $d$  is the path length) by integration of the spectral band plotted in wavenumbers:

$$f = 4.319 \cdot 10^{-9} \text{ mol} \cdot \text{cm}^2 \cdot \text{dm}^{-3} \int \varepsilon_m(\nu) d\nu \quad (54)$$

### 4.B.c. Energies between ground and excited states

When light is absorbed by a molecule, the molecule reaches higher excited states, the absorption occurs as a vertical transition between the GS and ES (Franck-Condon principle), *i.e.*, nuclei do not have time to rearrange as conformational reorganizations are too slow compare to the fast absorption process. TD-DFT calculations provide the successive excited states, which are attributed to each successive UV/Vis absorption band. The excited states are described by different contributions of electronic transitions between the frontier molecular orbitals, *e.g.*, transition from the highest occupied molecular orbital (HOMO) to the lowest unoccupied molecular orbital (LUMO).

There are different approximations to calculate the different energetic transitions<sup>126–129</sup> between GS and ES:  $E^{abso}$ ,  $E^{fluor}$ ,  $E^{0-0}$  and  $E^{adia}$  (Figure 9). The vertical absorption corresponding to the energy difference between the ES and GS at the geometry of GS (written as  $R^{GS}$ ) is the most commonly calculated energy and is given as:

$$E^{abso} = E^{ES}(R^{GS}) - E^{GS}(R^{GS}) \quad (55)$$

This absorption energy from the bottom of the potential well of the GS is often compared, as a first approximation, to the experimental wavelength of maximum absorption ( $\lambda_{max}$ ).

The same energy difference calculated with the geometry of ES corresponds to the fluorescence from a singlet excited state (or to phosphorescence from a triplet excited state):

$$E^{fluor} = E^{ES}(R^{ES}) - E^{GS}(R^{ES}) \quad (56)$$

The energy difference between ES and GS at their minimum is called the adiabatic contribution and it is given by:

$$E^{adia} = E^{ES}(R^{ES}) - E^{GS}(R^{GS}) \quad (57)$$

The 0-0 energy (when the molecule goes from vibrational state 0 of GS to vibrational state 0 of ES) is the adiabatic energy corrected for the difference of zero-point vibrational energy (ZPVE) between the GS and ES:

$$E^{0-0} = E^{adia} - \Delta E^{ZPVE} \quad (58)$$

where

$$\Delta E^{ZPVE} = E^{ZPVE}(R^{ES}) - E^{ZPVE}(R^{GS}) \quad (59)$$

Environmental effects might be a challenge in determining of the  $E^{0-0}$  energy. Differences between ES and GS are generally associated with important Stokes shifts, which are known as the difference between vertical emission and absorption energies.

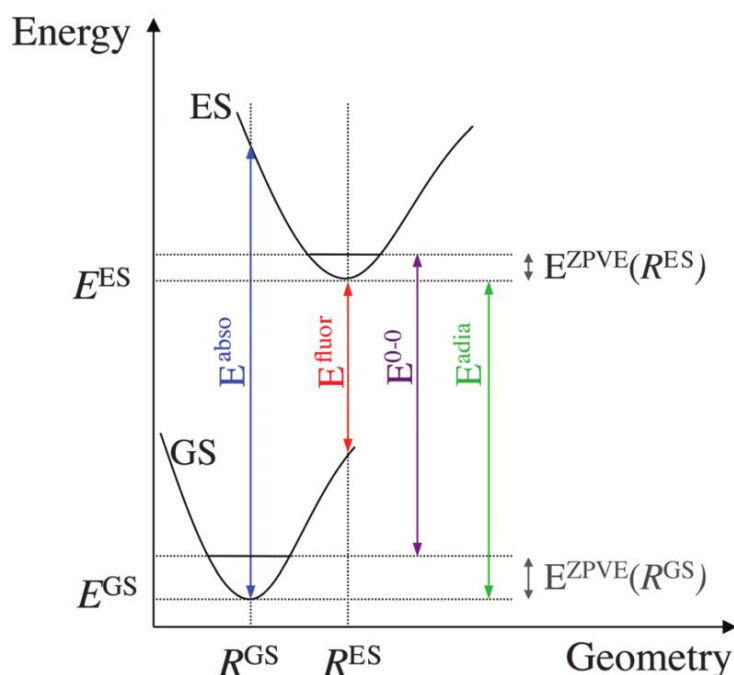


**Figure 9.** Franck-Condon diagram showing only two states (GS and ES) and different energies.

Modified from ref. <sup>127</sup>.

#### 4.B.d. Different methods for evaluation of the excited states

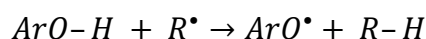
TD-DFT methods have become very popular to predict optical spectra. Nevertheless, the ZINDO and CASP models have also been introduced allowing a description of UV/Vis spectra.<sup>127,128</sup> The ZINDO model (Zerner's intermediate neglect of differential overlap) is a semi-empirical method based on the wave function, in which several integrals are estimated empirically. These calculations are fast and can be used to treat big molecules or large series of compounds. Among other methods, let us name CAS-PT2 (complete-active-space second-order

perturbation theory), CI (CIS – configuration interaction singles, MR-CI – multi-reference CI, SAC-CI – symmetry adapted cluster CI) *etc.* or coupled cluster (CC2) methods. These methods are based on the wave function and they are very accurate and robust, however limited to small systems because they are computational time-demanding.

#### 4.C. Reactivity of –OH groups

Antioxidants are molecules that protect cells against damaging effects produced by ROS. The imbalance between protective effects of antioxidants (*e.g.*, inhibition of free radical production, radical scavenging) and production of ROS results in oxidative stress in the organism. Many polyphenols exhibit antioxidant activity, namely they are *i*) inhibitors of certain enzymes involved in oxidative stress<sup>11</sup>; *ii*) lipid peroxidation inhibitors; *iii*) chelators of metals, which serve as mediators of ROS production; or *iv*) direct scavengers of free radicals. There exist various antioxidant assays, among which DPPH assay measures scavenging capacity as the ability of the substances to reduce 1,1-diphenyl-2-picrylhydrazyl (DPPH) radicals; ABTS assay is based on the ability of the compounds to scavenge the [2,2'-azinobis-(3-ethylbenzothiazoline-6-sulfonic acid)] radical cation (ABTS<sup>+</sup>); and FCR assay (measuring Folin-Ciocalteu reagent (FCR) reduction) or it can be evaluated theoretically. Other approaches to measure antioxidant activity can be found in refs. <sup>130</sup> and <sup>131</sup>. QM calculations and MD simulations allow an accurate prediction of the free radical scavenging capacity; different descriptors have been identified to correlate to the antioxidant capacity obtained experimentally. Antioxidants (*ArO-H*) may scavenge free radicals (*R•*) by H atom transfer through several mechanisms which exhibit the same thermodynamic balance ( $\Delta G^{PCET} = \Delta G^{ET-PT} = \Delta G^{SPLET} = \Delta G^{AF}$ ) since reactants and products are the same<sup>9,132,133</sup>:

- i) HAT (hydrogen atom transfer) and PCET (proton-coupled electron transfer)



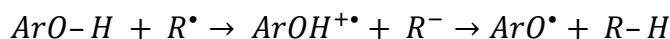
This is the direct HAT, where the free radical is reduced by the transfer from the antioxidant to the free radical. It is governed by the homolytic bond dissociation enthalpy (BDE) of the active OH groups; the O-H BDE is calculated as follows:

$$BDE = H_{298K}^0(ArO^{\bullet}) + H_{298K}^0(H^{\bullet}) - H_{298K}^0(ArOH) \quad (60)$$

where  $ArOH$  is the neutral form of a compound,  $ArO^\bullet$  is the aryloxy (phenoxy) radical formed when hydrogen atom is abstract from  $ArOH$ : the lower the BDE, the more delocalized radical spin density, the easier radical is formed and the higher antioxidant capacity (the more important role) of the corresponding OH group.

In HAT, a proton and an electron of the H-atom are transferred to the same atomic orbital in the free radical. PCET is distinguished from the pure HAT as it involves several molecular orbitals in H-bonding pre-reaction complex. This proton transfer is coupled with the electron transfer that occurs from a lone pair of the antioxidant to the single occupied molecular orbital of the free radical.

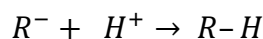
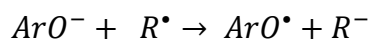
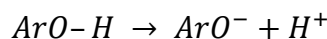
- ii) ET-PT (electron transfer – proton transfer) or SET-PT (sequential ET-PT)



The first step of this reaction is yielding the radical cation ( $ArOH^{+\bullet}$ ), which is obtained after electron transfer (electron loss, ET) from the neutral form of polyphenols. It easily undergoes heterolytic O–H bond dissociation (*e.g.*, proton loss, proton transfer, PT) leading to the same final products as PCET. The first step is mainly governed by the ionization potential (IP) of antioxidants. The energy related to electron abstraction is given as follows:

$$IP = H_{298K}^0(ArO^{+\bullet}) - H_{298K}^0(ArOH) \quad (61)$$

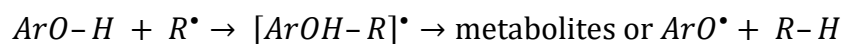
- iii) SPLET (sequential proton-loss-electron-transfer)



In this mechanism, a proton is lost prior to electron transfer, which thus occurs from the subsequent  $ArO^-$  anion to the free radical leading to the same products as PCET and ET-PT. SPLET is strongly enhanced under alkaline conditions, which may favor proton loss. Electron transfer enthalpy (ETE) (energy required to transfer an electron from the deprotonated form of polyphenols) is used to evaluate this process:

$$ETE = H_{298K}^0(ArO^\bullet) - H_{298K}^0(ArO^-) \quad (62)$$

iv) AF (adduct formation)



This mechanism has been observed in radiolytic solutions and it is relatively specific to  $^\bullet OH$  free radicals. AF is favored with carbon-centered radicals and for antioxidants bearing double bonds or hydroxyl radical and aromatic rings.

QM calculations (mainly DFT) have appeared efficient to evaluate BDE, IP and ETE values (publication **I** and **II**). Moreover, relative Gibbs energies of deprotonation from the different –OH groups within the molecule may help to evaluate the acid-base transitions, as the lowest relative Gibbs energy corresponds to the –OH group, which is deprotonated first (publication **III**).



## 5. RESULTS AND DISCUSSION

In this chapter, the different publications related to this PhD work are summarized in three main sections. The first section is describing redox properties of flavonolignans (publication **I**) and other conjugates (publication **II**). My contribution to these articles consisted in calculating and analyzing conformers and the main antioxidant descriptors. The second section deals with optical properties of flavonolignans (publication **III**) and pyranoanthocyanins (publication **IV**) and their pH dependence. In the former subsection, my contribution consisted of performing both the experimental part (measurement of pH-dependent absorption properties) and the theoretical part (calculations of theoretical absorption spectra and corresponding molecular orbital pictures). In the latter subsection, my contribution was limited to the theoretical part; precisely, calculations of geometries and optical properties of the copigmentation complexes and separated fragments. The third section deals with interactions of flavonolignans with the lipid membrane (publication **II**) and Na<sup>+</sup>/K<sup>+</sup>-ATPase (NKA) pump (publication **V**).

Each section will provide only a short overview of each publication. Full-texts and detailed results and discussion of all publications **I** – **V** are attached into the Appendix.

It is important to mention in this point that all the flavonolignans were either prepared in the laboratory of Prof. Křen (Institute of Microbiology, Laboratory of Biotransformation, Czech Academy of Science) or were commercial available. Pyranoanthocyanins were prepared in the partner laboratory in Montpellier, France.

## 5.A. Redox properties of polyphenols

The main aim of publications **I** and **II** was to explore electron-donor properties of flavonolignan derivatives using both experimental and computational approaches, in order to better understand their mechanism of action and to rationalize their antioxidant properties. The following subsections provide only a short overview.

### 5.A.a. Flavonolignans and their 2,3-dehydroderivatives

In publication **I**, electron-donor properties were investigated experimentally and theoretically within the DFT formalism for three (dehydro)flavonolignans, namely, (DH)SB, (DH)SCH and (DH)SD. The hybrid functional B3P86 was used as it is particularly adapted to rationalize the structure-antioxidant activity relationship of many compounds<sup>41,134</sup>. Solvent effects were taken implicitly using the PCM model, where dielectric constant is introduced allowing molecule to be polarized. The choice of the solvent was driven by the solvent used experimentally. The antioxidant capacity was assessed by several assays: FCR, DPPH scavenging and ABTS<sup>+</sup>• scavenging assays and the hierarchy in terms of the most active compound was established. The assays are based on different reactions; hence they reflect different radical scavenging mechanisms. The FCR method is also known as total phenol analysis, and it is based on measurements of reduction capacity, somehow reflecting the overall antioxidant status. It provided the following hierarchy: SCH > DHSCH > DHSB ~ SD ~ DHSD > SB, with SCH being the most active compound. The DPPH scavenging may occur either by electron- or H-atom transfer from the antioxidant and here the observed hierarchy was: DHSCH > DHSB > DHSD > SCH >> SD >> SB. The ABTS<sup>+</sup>• scavenging occurs mainly by electron transfer; in this case, the observed hierarchy was: SD ~ DHSD > SCH > DHSCH ~ DHSB ~ SB.

Computationally, the antioxidant properties were evaluated in terms of BDE values. The values for individual -OH groups of each of the analyzed compounds are given in Table 2. The capacity to oxidation attack was evaluated from the BDEs, and it was consistent with the results of the DPPH scavenging activity measurements.

**Table 2.** The O-H BDE values (kcal/mol) for the different OH groups of the flavonolignans. Numbering of (DH)SB is shown in Figure 10. The numbering is similar to both (DH)SCH and (DH)SD, see publication I.

	C-3	C-5	C-7	C-12a	C-15	C-19	C-20
SB	108.9	98.1	95.6				87.9
DHSB	82.8	96.2	91.1				88.0
SCH	108.8	98.1	95.5		84.3	84.2	
DHSCH	82.0	95.7	90.4		84.6	84.3	
SD	108.8	97.9	95.6	98.5			85.8
DHSD	83.0	96.6	92.3	98.5			84.1

Next analyses were aimed at elucidation of the observed antioxidant behavior on the structural basis. Experimentally, the flavonolignans were analyzed using square-wave voltammetry (SWV). According to the electrochemical data at low pH, SB displayed two oxidation peaks (Figure 10). The first peak was successfully assigned to oxidation involving the C-20 OH group, which was confirmed by the lowest BDE value for this OH group. The other three -OH groups exhibited rather high BDE values, which was in agreement with oxidation potential of the second peak (Figure 10), and which was attributed to the oxidation of -OH groups localized in the A-ring. These results were also in agreement with the computed results of HOMO topology, which revealed that electron transfer was mainly attributed to the E-ring of SB. Similarly, we rationalized the redox behavior of SD. Redox properties of SCH exhibited a different pattern than SB and SD.

Based on the experiments with methylated analogs, we were able to assign each oxidation peak to an OH group of SCH. Both C-15 OH and C-19 OH groups exhibited rather low BDEs, confirmed by the HOMO distribution as it is delocalized over the rings, where the C-15 OH and C-19 OH groups are located (Figure 11), and as displayed by broader oxidation peaks.

For DHSB, two oxidation peaks 1 and 2 (Figure 10) were observed as well, which were assigned to the same -OH groups of DHSB as it was for SB. A third peak was observed (1') even with a lower potential than peaks 1 and 2 and assigned to the C-3 OH related oxidation. Due to the presence of 2,3-double bond in both DHSB and DHSCH, the HOMO is strongly modified allowing electron delocalization across the whole structure (Figure 11). This was also observed for DHSD but with less extended delocalization. This caused a decrease in C-3 OH BDE of all

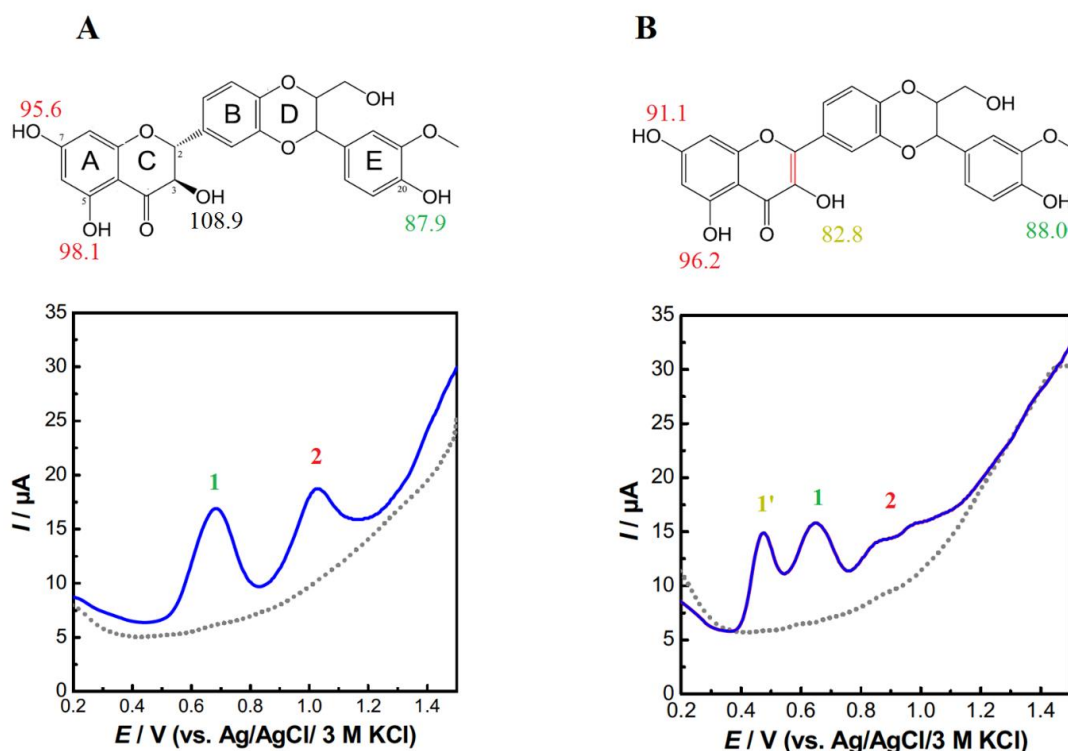


**Figure 10.** Voltammograms and structures of (A) SB and (B) DHSB as performed in the laboratory of Doc. Vacek (Department of Medical Chemistry and Biochemistry, Faculty of Medicine and Dentistry, Palacký University). The BDE values of each OH group are expressed in kcal/mol next to the OH groups. The color of the value corresponds to the color of the oxidation peak's number.

three dehydroderivatives, which now becomes very active. Slight differences in the BDEs for C-3 OH of DHSB and DHSCH were rationalized from spin density distribution, which was slightly more delocalized in DHSCH radical than DHSB radical (Figure 12), leading to slightly lower BDE (Table 2). Thus, the 2,3-dehydroderivatives are much more easily oxidized than their parent flavonolignans.

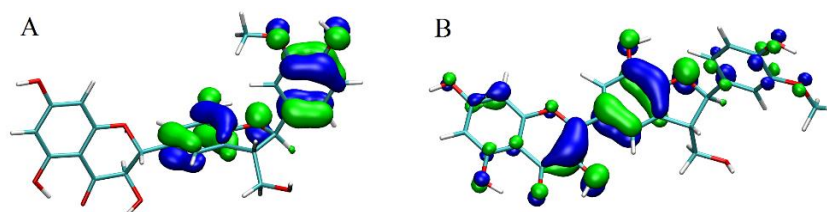


**Figure 11.** The HOMO of (A) SCH and (B) DHSCH.

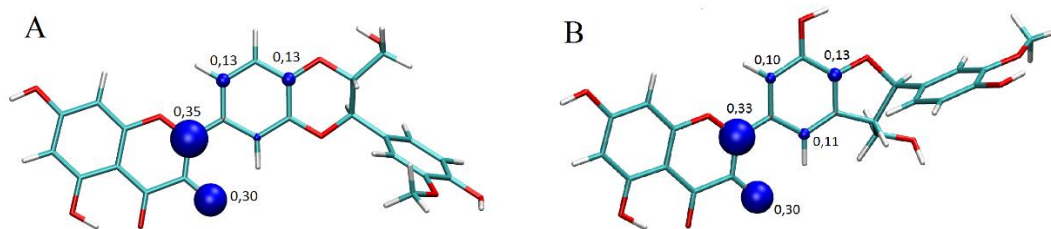


**Figure 12.** Spin density distribution of the radical formed after hydrogen atom abstraction from the C3-OH group of (A) DHSB and (B) DHSCH.

### 5.A.b. Novel flavonolignan hybrid antioxidants

The chemical conjugation of several (at least two) derivatives bearing antioxidant activities may potentiate activities; addition or even supra-addition (synergism) of the effects from each constitutive component is expected. We explored this issue in publication **II**, in which SB was conjugated to L-ascorbic acid (AA), trolox alcohol or tyrosol via C<sub>12</sub> hydrophobic aliphatic linker. The experiments revealed that the SB-C<sub>12</sub>-AA conjugate (Figure 13) was an excellent electron-donor and it was the best lipid peroxidation inhibitor compared to the other compounds studied.

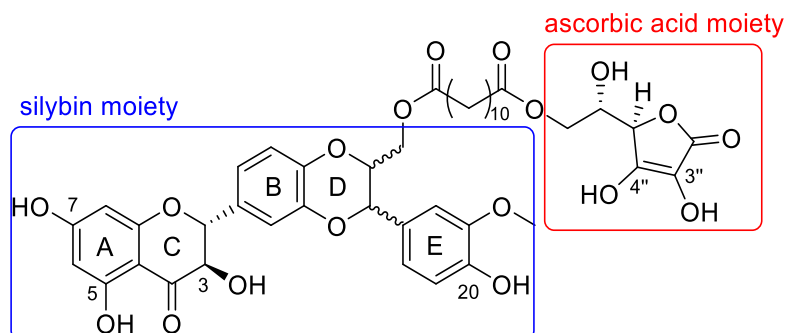


**Figure 13.** Chemical structure of the SB-C<sub>12</sub>-AA conjugate.

To evaluate and to calculate physico-chemical properties, a careful conformational analysis had to be done as SB-C<sub>12</sub>-AA exhibits more degrees of freedom than SB and AA themselves. To do so, we performed MD simulations in water to efficiently explore the potential energy surface. We identified several conformers and we re-optimized them at the DFT-D level to account for possible dispersion interactions (the  $\omega$ B97X-D functional was used as it is well adapted to describe dispersion forces, which may influence certain geometries). We identified several folded and linear conformers, highlighting the main stabilizing forces between the different moieties of SB-C<sub>12</sub>-AA. Although the most stable conformer (Figure 14) was identified as one

of the folded forms, the calculated differences in ETEs or BDEs were negligible between all unfolded and folded conformations (Table 3). ETE and BDE values were calculated by both  $\omega$ B97X-D (to keep the consistency with the functional used for optimization) and B3P86 (as it appeared well adapted to evaluate redox properties) functionals. Only values for the latter were reported in the publication, since both functionals gave the same trends.

The descriptors for hydrogen atom and electron transfer capacities were calculated for SB, AA, SB-C<sub>12</sub>-AA and AA-C<sub>12</sub> to rationalize the redox properties of the conjugate. Nevertheless, there were no significant differences in terms of BDE between the conjugate and the constitutive components. The data were in agreement with the fact that AA is more easily oxidized than SB, and the lowest BDE value of the conjugate was obtained for -OH group at the AA moiety (around 77 and 79 kcal/mol; Table 3).

Again, BDE values agreed with DPPH scavenging capacity. AA was almost 100 times more active than SB in DPPH assay (Table 3). The combination of AA and SB led to a decrease in DPPH scavenging activity by about 10 times. The calculated ETE values were in agreement with the ABTS scavenging test, where SB was more active than AA. After conjugation of both SB and AA moieties, the activity of the resulting compound was enhanced in an additive way, confirming that the conjugate was better antioxidant than its separate constituents (Table 3).

**Table 3.** BDE and ETE values for SB-C<sub>12</sub>-AA and its constitutive components with their antioxidant activities. All energetic values are given in kcal/mol.

Compounds	SB	AA	SB-C <sub>12</sub> -AA folded	SB-C <sub>12</sub> -AA linear	AA-C <sub>12</sub>
ETE	C-7 OH	131.7	136.6	134.0	
	C-20 OH	112.1	115.0	117.2	
	C-3" OH		124.5	123.8	122.4
	C-4" OH		116.8	116.7	115.5
BDE	C-7 OH	91.4	92.9	93.3	
	C-20 OH	82.5	83.5	84.7	
	C-3" OH		76.9	76.5	77.1
	C-4" OH		79.4	79.4	79.3
DPPH (IC <sub>50</sub> (μM))	244 ± 10	2.76 ± 0.17	20.6 ± 0.5	34.5 ± 1.0	
ABTS (TEAC)	0.78 ± 0.06	0.57 ± 0.03	1.32 ± 0.04	0.77	0.08

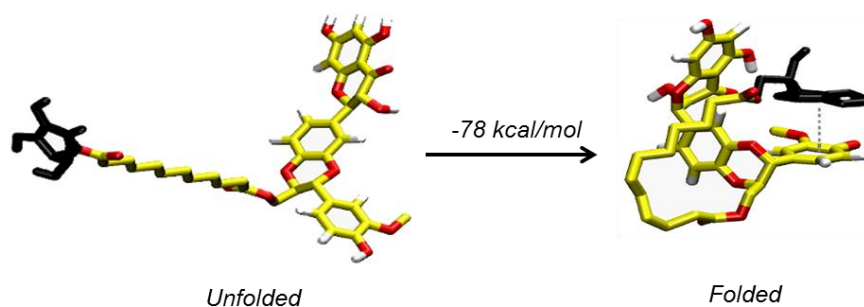


**Figure 14.** Representative linear and folded conformers of the SB-C<sub>12</sub>-AA conjugate. The AA moiety is in black.

## 5.B. UV/Vis absorption properties of polyphenols

This section is devoted to UV/Vis absorption properties of flavonolignans and pyranoanthocyanins. We theoretically studied excited states and electronic transitions within the TD-DFT formalism; papers **III** and **IV** will be discussed here.

### 5.B.a. Tunable optical properties of silymarin flavonolignans

Skin exposure to UV radiation induces a number of skin disorders (sunburn, erythema, DNA damage, photoaging, skin cancers, immune suppression ...). Both UVB and UVA radiations induce ROS, which create oxidative stress in skin cells and play a role in the initiation, promotion and progression of skin aging and carcinogenesis. Silymarin components absorb light in UV/Vis range and it can be used in sunscreen preparations. It has been shown to exhibit preventive effects against photocarcinogenesis in various animal tumor models<sup>44</sup> and UVB-exposed skin cells<sup>56</sup>.

Our article (publication **III**) described the pH-dependence of UV/Vis absorption properties of (DH)SB, (DH)SCH and (DH)SD. We used both B3P86 and CAM-B3LYP functionals with implicit solvent description, where solvents are described only by their dielectric constants and where specific solute-solvent interactions are neglected (more about solvent effects can be found at the end of this subsection and in Section 6), to compute the UV/Vis absorption properties. After comparison to experimental data, B3P86 appeared to describe correctly the neutral forms of flavonolignans, but it failed in describing the deprotonated forms (Figure 15).

Therefore, we decided to describe the absorption properties with the CAM-B3LYP, as this functional succeeded at evaluating spectral shifts from the neutral to the charged form of the flavonolignans, even though the predicted wavelengths of absorption peaks were underestimated for both the neutral and deprotonated forms. Based on the comparison to experimental data (Figure 16), a correcting factor of 1.12 was applied on the calculated transition energies.

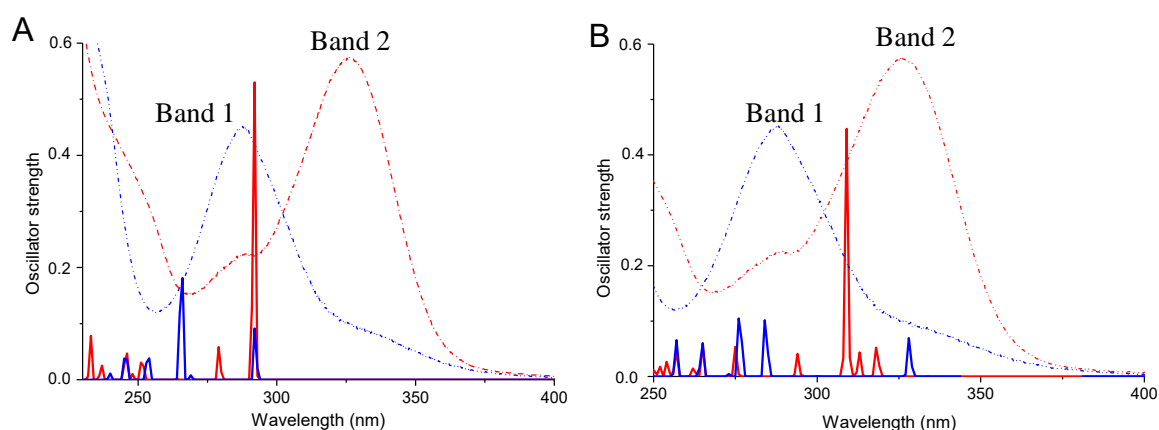


**Figure 15.** Theoretical spectra of the fully protonated (in blue) and the C7-OH deprotonated form (in red) of SCH with A) CAM-B3LYP and B) B3P86 functionals. The theoretical and experimental spectra are superimposed. Solid lines correspond to the theoretical spectra, whereas dashed lines to the experimental spectra.

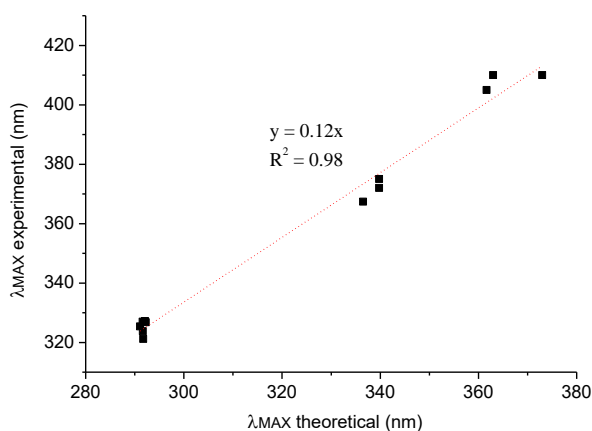


**Figure 16.** Correlation between theoretical and experimental wavelength values of absorption peaks.



The most acidic group of all flavonolignans was C7-OH (Table 4), therefore, we deprotonated this group to study basic environment (pH higher than pKa). Under acidic conditions (lower pH than pKa), SB, SCH and SD exhibited a major peak in the UVB region (at around 288 nm – referred to as Band 1), whereas a band in the UVA region (at around 330 nm – Band 2) was observed only as a shoulder (Figure 17). When pH increases, strong hyperchromic and hypochromic effects were observed for Band 1 and 2, respectively. When deprotonating at C7-OH, the HOMO was strongly modified (Figure 17), which made the HOMO → LUMO electronic transition (Band 2) likely and efficient. It was not the case for the neutral form, where this electronic transition was unlikely due to complete spatial separation. At high pH value, Band 1 appeared as a shoulder with low oscillator strength. TD-DFT calculations fully rationalized this behavior by observed electronic transitions and the corresponding molecular orbital description. Thus, under pH variation around pKa, SB, SCH and SD could reversibly change from UVB protective to UVA protective.

**Table 4.** Relative Gibbs energy (kcal/mol) of deprotonation for different OH groups of (DH)SB, (DH)SCH and (DH)SD.

Deprotonation site	SB	SCH	SD	DHSB	DHSCH	DHSD
C3-OH	20.9	20.5	19.2	4.6	4.2	2.1
C5-OH	9.2	9.2	8.9	8.7	8.2	8.4
C7-OH	0.0	0.0	0.0	0.0	0.0	0.0
C15-OH		9.3			5.6	
C12a-OH			13.7			12.2
C19-OH		12.1			9.1	
C20-OH	11.6		13.2	9.9		11.6

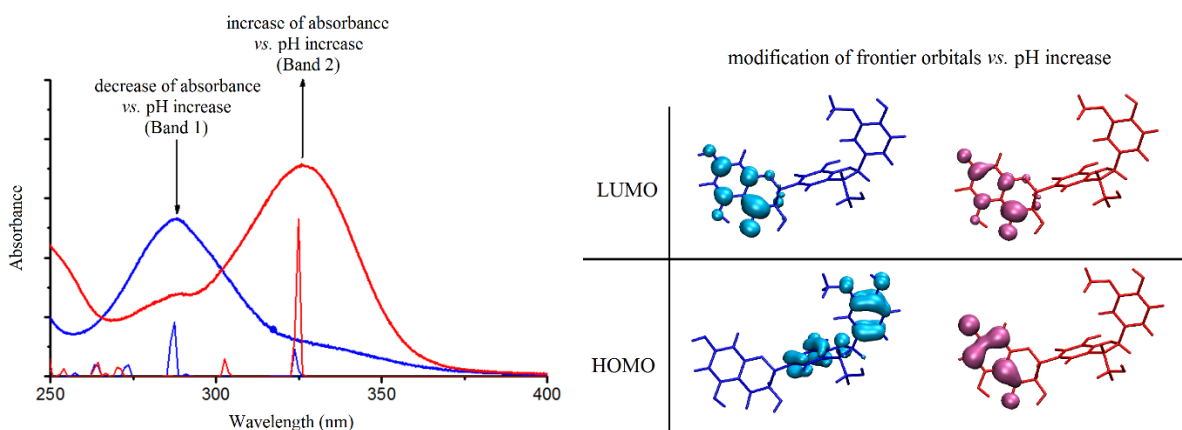


**Figure 17.** Superimposed theoretical and experimental absorption spectra of SCH vs. pH (on the left) and MO description of the neutral and C7-OH deprotonated form in the first and second column, respectively, on the right. The blue color corresponds to the neutral form; the red color corresponds to the C7-OH deprotonated form.

The dehydroderivatives exhibited a different pH behavior than their corresponding parent flavonolignans. The 2,3-double bond resulted in  $\pi$ -conjugation over the flavonoid moiety. At low pH values, the predominant peak was in the UVA region, which was bathochromically shifted by *ca* 1.2 eV compared to corresponding flavonolignans, as explained by the modifications observed in the MO diagram. When these compounds were deprotonated, a clear shift of the maximum absorption wavelength to the higher wavelengths (towards the visible part of the spectrum) by *ca* 0.4 eV was observed (Figure 18). The LUMO was somewhat similar in terms of orbital energies and electron delocalization for both the neutral and deprotonated forms. Besides, the HOMO was destabilized in the deprotonated form. Again, all changes were perfectly described by TD-DFT. Here deprotonation turned the dehydro-derivatives from a potential UVA-protector to a dye.

As already mentioned, in our calculations, we used an implicit polarizable continuum solvent model (PCM). Limitations of such models is that all the site-specific solute-solvent interactions, *e.g.* hydrogen-bonding, are neglected (see Section 6 for further computational results on explicit description of solvent molecules). Experimentally, we evaluated the effect of polarity and intermolecular hydrogen bonding interactions in selected series of solvents. They are characterized by tabulated empirical parameters, and a multi-linear parametric analysis reveals influence of various solute interactions with its environment on the absorption spectra. This analysis showed that the absorption spectra of fully protonated forms were rather insensitive to

the interaction with surrounding molecules, whereas deprotonated forms exhibited much higher sensitivity to solvent effects. For most of the compounds, the contribution of polarity effects was lower than those of intermolecular hydrogen bonding. However, spectral shifts due to hydrogen bonding were significantly lower compared to the effects caused by (de)protonation.

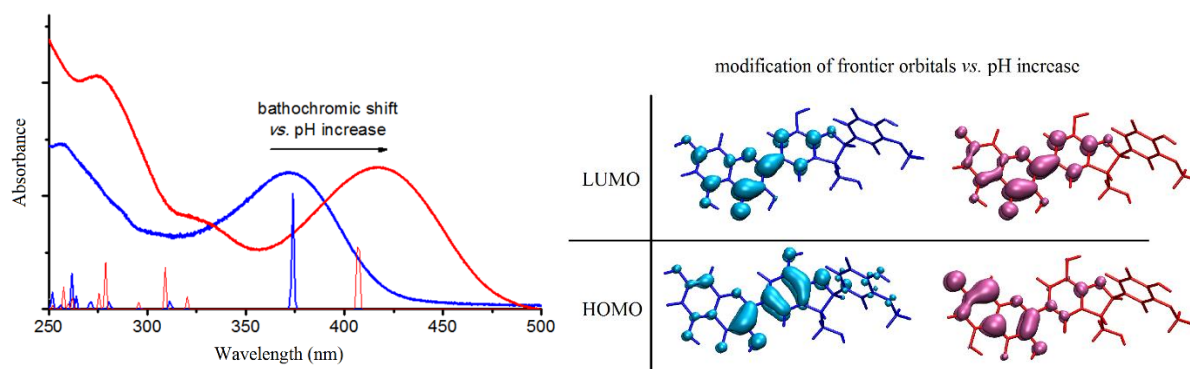


**Figure 18.** Superimposed theoretical and experimental absorption spectra of DHSCH vs. pH (on the left) and MOs description of the neutral and C7-OH deprotonated form in the first and second column, respectively, on the right. The blue color (spectrum on the left and MOs on the right) corresponds to the neutral form; the red color corresponds to the C7-OH deprotonated form.

### 5.B.b. p-Hydroxyphenyl-pyranoanthocyanins – acid-base properties and molecular interactions

Publication **IV** is dealing with the wine pigments pyranoanthocyanins and their physicochemical properties with an emphasis on proton transfer, copigmentation and self-association processes. To theoretically investigate UV/Vis properties of single compounds, the hybrid functional B3P86 was used as it has appeared well adapted for thermodynamic and UV/Vis absorption properties of polyphenols. To study copigmentation and self-association complexes, using DFT-D methods (namely here B3P86-D2) appears crucial to take noncovalent interactions in the complexes into account. The obtained geometries were used to calculate theoretical absorption spectra with the  $\omega$ B97X-D functional, which correctly accounts for possible charge transfer in the excited state.

Catechyl-pyranomalvidin-3-*O*-glucoside (PA1) was one of the studied compounds here (Figure 19). The neutral deprotonated form of PA1 was hypsochromically shifted by more than 20 nm with respect to the cation form. This experimentally observed shift to the shorter wavelength was uncommon, namely bathochromical shift was expected.

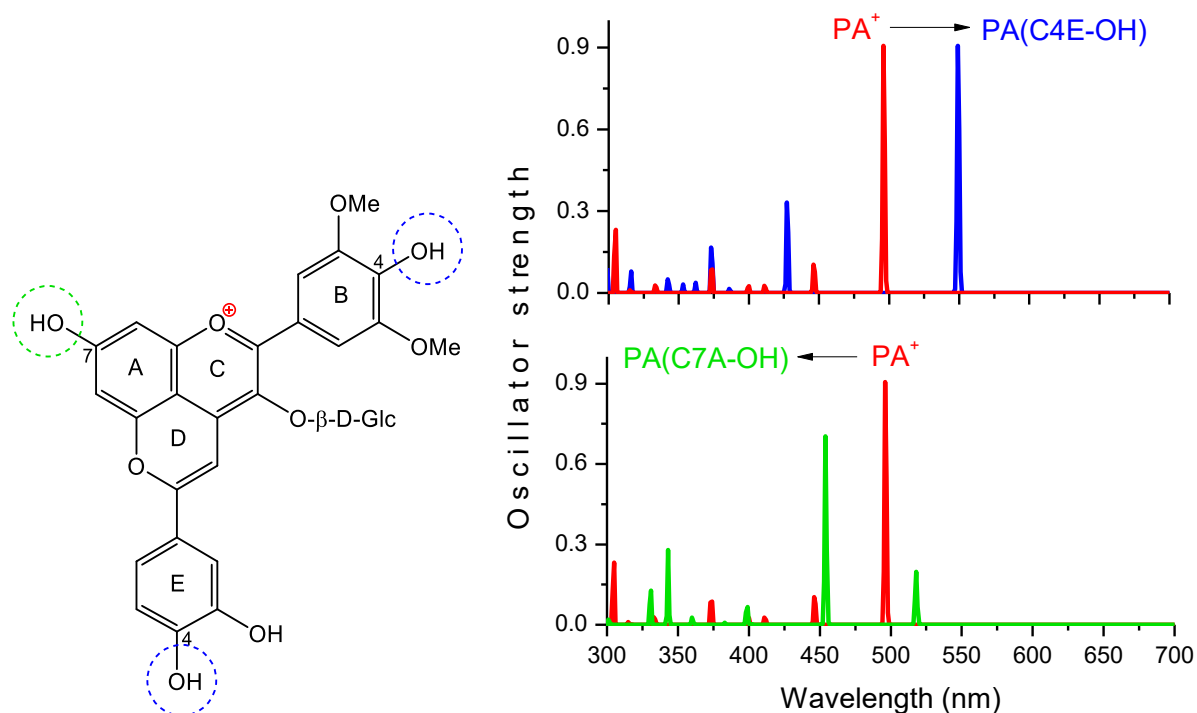


**Figure 19.** PA1 structure (on the left) and theoretical absorption spectra (on the right). The C7A, C4B and C4E groups are prone to deprotonation. The cation form is in red, C4E-OH and C7A-OH deprotonations shown in blue and green, respectively. The deprotonation at C4B is similar to that at C4E (see Publication IV).

TD-DFT calculations well predicted the behavior of the cation form of PA1 and the corresponding HOMO and LUMO were delocalized along an extended conjugated path. To study the excited states of deprotonated forms at higher pH values, three possible neutral bases were investigated (as shown by the green and blue circles in Figure 19). The HOMOs of each deprotonated forms were strongly modified according to the site of deprotonation (Figure 20). The deprotonation at C4E-OH and C4B-OH (Figure 19) resulted in a clear bathochromic shift caused by a decrease in the energy gap between HOMO and LUMO, compared to the cation

form (the energy gap being 2.84 eV for the cation form and 2.40 eV and 2.30 eV for C4E-OH and C4B-OH deprotonation, respectively). The agreement between the experimental and theoretical spectra was seen only for C7A-OH deprotonation, supporting the presence of only one neutral quinonoid base and corresponding to proton loss from this group. The HOMO was displaced toward the A-ring, decreasing the overlap with the LUMO (LUMO for C7A-OH was similar to that for cation form, see publication **IV**) and resulting in relatively low oscillator strength. Based on MO rationalization, we deduced that the observed hypsochromic shift was not an actual shift, but it was an inversion between the first and second excited states.

Three possible self-association systems were studied, namely  $AH^+ \cdots AH^+$ ,  $AH^+ \cdots A$  and  $A \cdots A$ , where  $AH^+$  stands for the cation form and  $A$  for C7A-OH deprotonated form. Three types of conformers could be distinguished according to the interactions among certain parts of PA1 (Figure 21; for clarity, one PA1 partner is in blue, the other is in red and the sugar moiety is in green). The  $\pi$ - $\pi$  stacking was the main driving force of self-association, H-bonding and electrostatic interactions influencing orientation of both units of PA1 with respect to each other. As suggested by experimental data, self-association occurred mainly with the neutral quinonoid base. The DFT-D calculations confirmed this observation and the corresponding association energies were calculated for each conformer, confirming that  $A \cdots A$  association was favored. Indeed the most stable  $A \cdots A$  conformer was more stable than the most stable  $AH^+ \cdots AH^+$  and  $AH^+ \cdots A$  conformers by *ca* 3 kcal/mol.

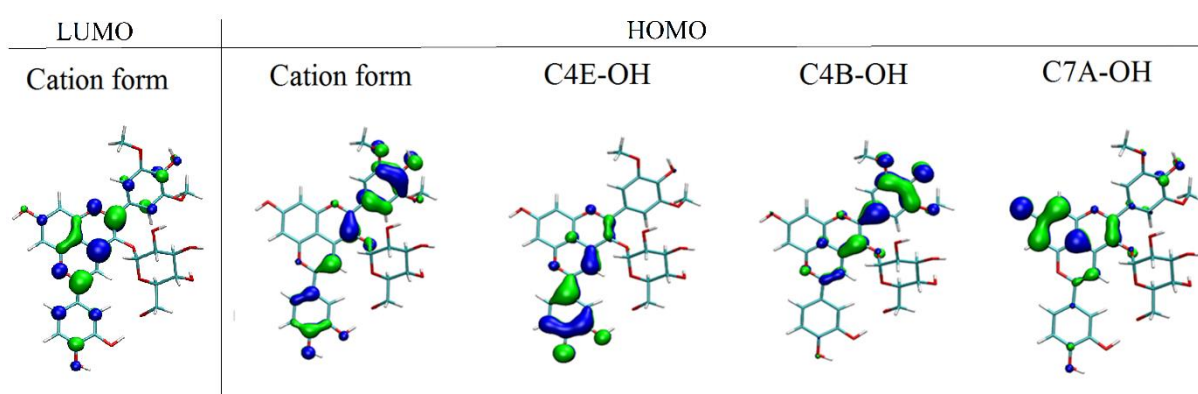


**Figure 20.** Molecular orbitals of the cation form and deprotonated forms (at C4E-OH, C4B-OH and C7A-OH position) of PA1. Full MO diagrams are part of publication **IV**.

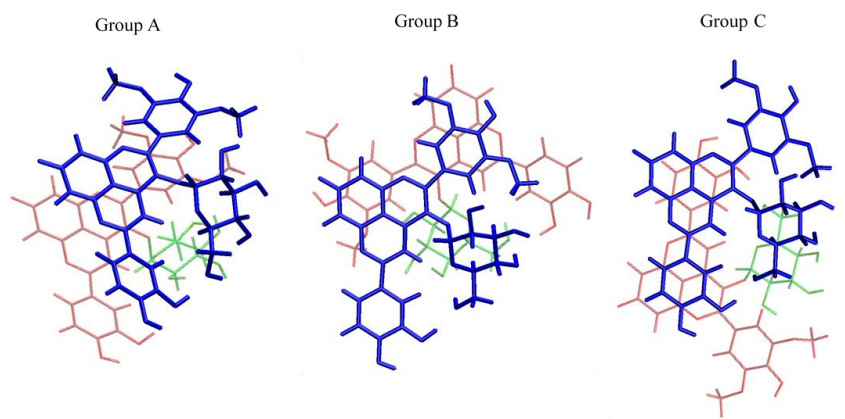


**Figure 21.** Three representative conformers of PA1...PA1 dimers. Group A: interactions between A-, C-, D- rings of both PA1 fragments; Group B: interactions between A-, C-, D- rings of one PA1 and the B ring of the other PA1 and Group C: interactions between A-, C-, D- rings of one PA1 with the E ring of the other PA1.

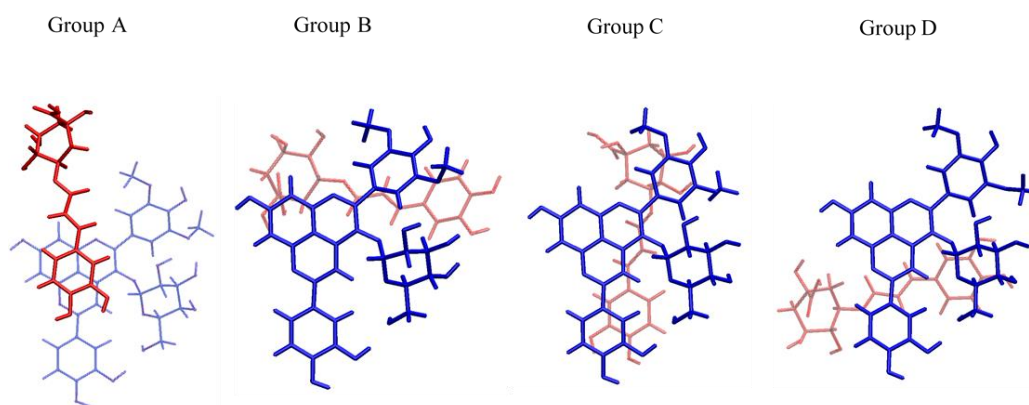


**Figure 22.** Four representative conformers of copigmentation complexes between PA1 (blue) and chlorogenic acid (red). The catechol moiety of chlorogenic acid is in interaction with the following moieties of PA1: A-, C- and D-rings (Group A); B-ring (Group B); E-ring (Group C) and glucose (Group D).

Copigmentation of PA1 with chlorogenic acid resulted in bathochromic shifts of the maximum absorption wavelength by *ca* 10 nm. This is typical for copigmentation processes and it was fully rationalized by TD-DFT, where the spectral behavior strongly depended on the conformer (for some conformers, the charge transfer character was strong, for others it was weak). Four groups of conformers (Figure 22) were distinguished according to possible orientations of chlorogenic acid with respect to the pigment. A complex mixture of  $\pi$ - $\pi$  stacking and/or

intermolecular electrostatic and H-bonding interactions was driving stabilization. Copigmentation appeared less favorable than self-association. This was consistent with the observation that chlorogenic acid had to be used in large excess to prevent aggregation.

### **5.C. Interaction with biomolecules**

In this section, we briefly discuss the interactions of flavonolignans with biomolecules (lipid bilayer membrane or NKA pump).

#### **5.C.a. Novel flavonolignan hybrid antioxidants in lipid bilayers**

In the preceding section, we described the conformational analysis and redox properties of the SB-C<sub>12</sub>-AA conjugate. The conjugate was found to have a protective effect against lipid peroxidation (Lpx). To efficiently inhibit Lpx, the compound should be sufficiently embedded in the lipid bilayer to be in contact with the lipid chains where oxidation occurs. We performed MD simulations and we studied the interaction of this conjugate with a lipid bilayer (publication **II**). A 43A1-S3 force field for simulation of membranes was used as implemented in GROMACS simulation package. The bilayer model consisted of DOPC molecules surrounded by water molecules. A global picture of drug membrane penetration over hundreds of nanoseconds for each molecule in different protonated states with different starting points were calculated and evaluated. Representative equilibrated location of SB-C<sub>12</sub>-AA in lipid bilayer is shown in Figure 23. The center of mass of the SB moiety of the conjugate was embedded deeper in the bilayer than the center of mass of the AA moiety. Moreover, the SB moiety was oriented towards the polar head group region, however the most active free radical scavenger group of SB moiety (namely, C-20 OH in E-ring) was embedded deeper in the lipid bilayer than SB alone. This results in efficient inhibition of the propagation stage of Lpx. The global pulling of the conjugate deeper into lipid bilayers confirmed its better capacity to inhibit the propagation stage of Lpx, with respect to SB and even more to AA, which was not active.

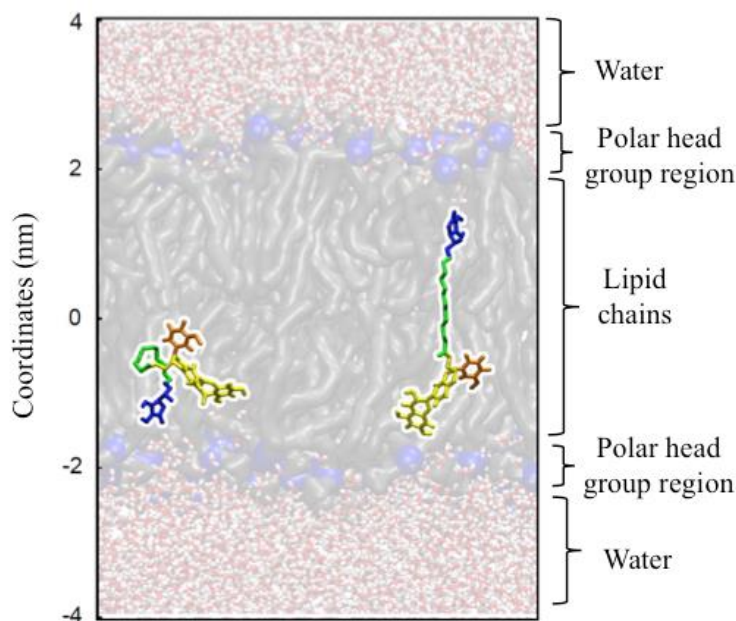


**Figure 23.** Representative equilibrated location of SB-C<sub>12</sub>-AA in lipid bilayer. Averaged location of a folded (left side) and a linear (right side) conformer over the last 100 ns of 500 ns long MD simulation. AA in blue, linker in green, E-ring of SB in orange and the rest of SB in yellow.

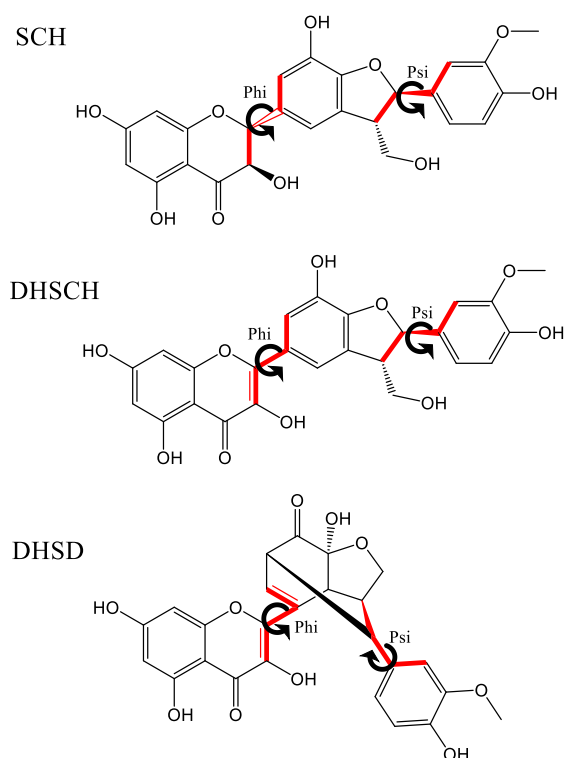
### 5.C.b. Flavonolignans as a novel class of sodium pump inhibitors

NKA pump is an enzyme of major importance for all animal cells and it determines concentrations of cytoplasmic Na<sup>+</sup> and K<sup>+</sup> and the resting plasma membrane potential. During one catalytic cycle, the enzyme translocates three sodium ions out of the cell and two potassium ions in opposite direction. The active transport is catalyzed by ATP hydrolysis and the enzyme is transiently auto-phosphorylated. The high-resolution structure of the enzyme has been determined using X-ray crystallography. It revealed two major enzyme conformations. In the conformation with bound sodium, the three cytoplasmic domains form a compact assembly, while in the potassium-bound state, the cytoplasmic headpiece is open. The structural changes are reflected also in the transmembrane domain, where the cation-binding sites are located.



**Table 5.** Structural parameters of the most stable conformers for (DH)SCH and DHSD used for docking.

Species	Conformer	Phi (°)	Psi (°)	Relative Gibbs energy (kcal/mol)
SCH	1	81	-71	0
	2	82	98	0.9
	3	-105	52	0.1
	4	-97	-141	0.7
DHSCH	1	174	-52	0
	2	175	87	0.2
	3	9	97	0.1
	4	7	-55	1.6
DHSD	1	1	-45	0
	2	1	142	0.3
	3	166	-40	0.2
	4	166	145	0.8



The image shows three chemical structures: SCH, DHSCH, and DHSD. Each structure is a flavonolignan derivative with a central chromane ring system. The SCH structure has a hydroxyl group at the 7-position and a methoxy group at the 8-position. The DHSCH structure has a hydroxyl group at the 7-position and a methoxy group at the 8-position. The DHSD structure has a hydroxyl group at the 7-position and a methoxy group at the 8-position. The structures are shown in their most stable conformations, with the torsion angles Phi and Psi indicated by red arrows and labels. The Phi angle is between the C and B rings, and the Psi angle is between the D and E rings.

The extracts of cardiac glycosides, which are very specific NKA inhibitors, are, in low concentrations, used to control heart tonics. On the other hand, an uncontrolled inhibition of NKA can lead to severe diseases or even death. Here, we examined the inhibitory effect and interactions of the (dehydro)flavonolignans with NKA and we identified several possible binding sites for these molecules on NKA using molecular docking. Within the DFT formalism, geometry optimizations of all structures were performed by the hybrid functional B3P86. Our calculations revealed that all (dehydro)flavonolignans can adopt several stable conformations depending mainly on the torsion angles between the C and B rings, and D and E rings (Table 5). Differences between the conformers may play no important role in *e.g.*, redox properties, but they may play a crucial role in the interaction with enzymes or other biomolecules. SCH, DHSCH and DHSD showed substantial inhibition on NKA, therefore their four most stable conformers were chosen to be docked into the opened and closed structures of NKA (Figure 24). Multiple binding sites were identified, more precisely, there are five major binding sites (one extracellular and four in the cytoplasmic segment of the protein) – three of them common for both the opened and closed forms of NKA, one exclusively observed for the opened conformation and another one exclusively for the closed state. By far, the most frequently

occupied site was the cleft between cytoplasmic domains N and P, near the phosphorylation site. Binding of the large flavonolignan molecule into this site likely results in allosteric inhibition of the enzyme by effective hindering of the cytoplasmic domains movements. Extracellular- and C-terminal binding sites were occupied with lower frequency. Flavonolignan binding to these sites would block the pathways toward the cation-binding sites in the transmembrane domain. Identification of the precise NKA inhibitory mechanism by flavonolignans requires further research, and the data from molecular modeling provide good basis for design of proper experiments.

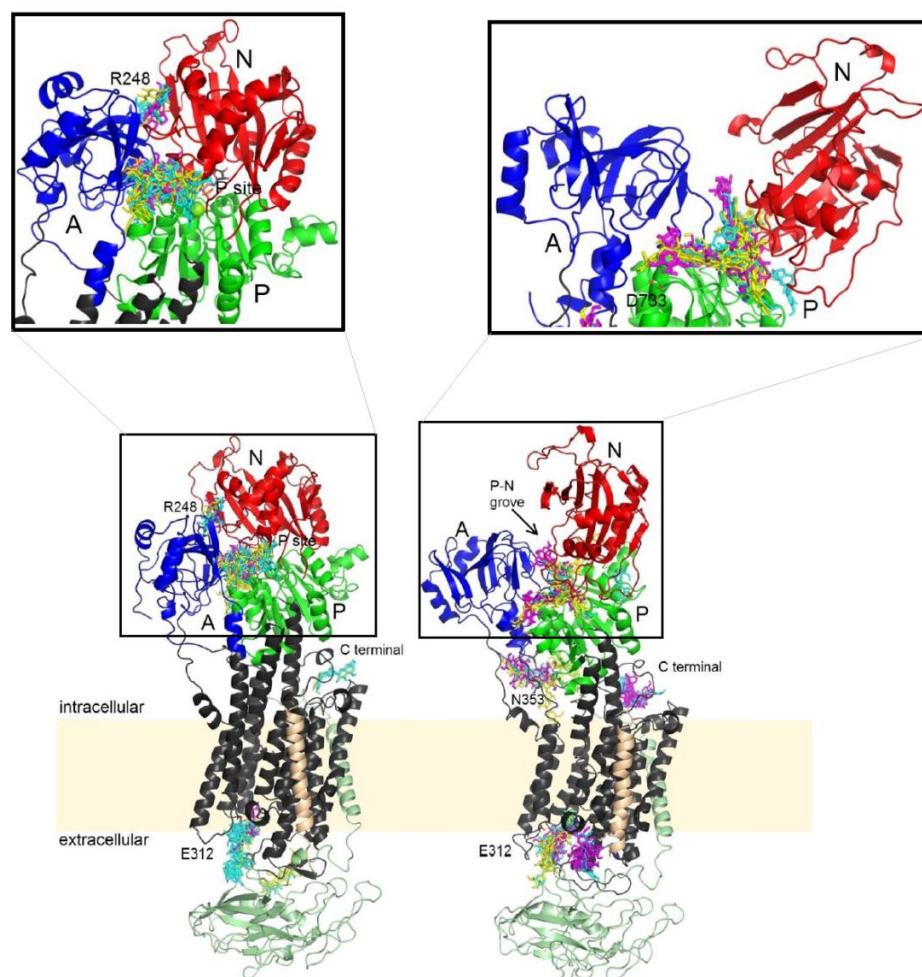


**Figure 24.** Binding sites and zoom on the binding site on cytoplasmic loops for SCH (yellow), DHSCH (cyan) and DHSD (magenta) in the closed (left) and opened (right) structure of NKA. Beta subunit of NKA is in light green; the FXYD protein in light orange; A, N and P domains in blue, red and green respectively.

## 6. ONGOING PROJECT - SAMPLING CONFORMATIONAL FEATURES OF COPIGMENTATION COMPLEXES

### 6.A. Introduction

Copigmentation is a process in which a pigment and a copigment stack together by noncovalent interactions. Within these noncovalent complexes, the pigment is stabilized (*i.e.*, shift of its pKa; see the Copigmentation section 2.G.). This process has only been described for natural anthocyanin derivatives, usually combined with other uncolored polyphenols (flavonoids or phenolic acids). This phenomenon attracted much interest in food industry, as it may stabilize specific hues by a natural or at least bioinspired process, *i.e.*, just by adding copigment compounds. There exist a subtle selectivity for a pigment/copigment couple to efficiently associate. The Gibbs energies of association are usually relatively low, and the balance between negative and positive values depends on a complex combination of dispersion forces, hydrophobic effects and hydrogen bonding.<sup>76</sup> For a given pigment, several copigments can be used with more or less efficacy. To establish complete structure-property relationship, it is crucial to predict the capacity of any pigment/copigment couple to form stable copigmentation complexes.

Theoretical chemistry has recently proved remarkable efficiency at describing copigmentation complexes. By using dispersion-corrected density functionals, various noncovalent complexes of prototypical pigment/copigment systems were fully characterized, namely geometrical features of the supramolecular arrangements, Gibbs energy of association and related optical properties (in which the bathochromic shifts were partially attributed to the occurrence of charge transfer excited states). These theoretical evaluations have shown remarkable accuracy with respect to experimental data, when available.<sup>135,136</sup>

This work aims at a further usage of theoretical chemistry method to establish structure-copigmentation relationships. However a revisited and well-chosen methodology is required. Indeed, the previous calculations were purely performed by QM methods, in which the solvent was taken into account implicitly, namely using PCM models. Although this strategy was sufficient for prototypical pigment/copigment systems, real world systems bear much more degrees of freedom and a more complex surface accessible to solvent (*e.g.*, larger compounds, presence of sugar moieties). In this case, the solvent should be systematically taken into account

explicitly. Moreover a complete conformational sampling has repeatedly been shown as mandatory. Only sufficiently long molecular dynamic simulations can achieve these two main key issues in copigmentation description (explicit solvent and conformational sampling). As Gibbs energies of association and (so characteristic of copigmentation) visible absorption properties can only be achieved by QM methods, a QM/MM approach is required, and its robustness will be achieved in this work on a series of real world pigment/copigment systems, for which experimental data are available and which are representative of this phenomenon.

## **6.B. Methodology**

### Computational details

All studied solutes were optimized within the DFT formalism using the Gaussian software package and Ante\_R.E.D. program (B3LYP/cc-pVDZ in diethylether using an implicit PCM). From the optimized structures, ESP charges were obtained by Duan model with RESP-A1 method. From these geometries and charges, all MD simulations were carried out using the AMBER 14 force field. Topology and coordinate files for the complexes (pigment···copigment) were generated using the GAFF force field. The ff12SB force field was used to account for other ions (Cl<sup>-</sup>) to ensure electroneutrality due to the presence of one flavylum cation in the system. A square box of 12 Å wide was used, in which solvent molecules (water, TIP3PBOX) was added.

After initial temperature and density minimization, 100 ns MD simulations were performed with a 2 fs time step. We used periodic boundary with a constant pressure of 1 atm. Isotropic position scaling was used to maintain this pressure, and a relaxation time of 2 ps was used. A 12 Å cutoff was used for van der Waals and electrostatic forces; no position restrain was applied. The Shake algorithm was turned on, and bonds involving hydrogen were constrained. The entire system was heated up to 300 K. The Langevin dynamics was used to control temperature using a collision frequency of 1 ps<sup>-1</sup>.

MD simulations of 16 different combinations of pigments (Figure 25) and copigments (Figure 26) were performed. The choice of pigment···copigment systems was driven by available experimental data, mainly concerning association energies. To assess robustness of the MD procedure to sample the conformational space, three independent 100 ns MD simulations were

performed for the cyanidin-3-*O*-glucoside...quercetin prototypical system, from three different guess geometries (Figure 27). The presence of the sugar moiety has made conformational sampling complex, which has highlighted importance to run three different MD simulations from three different initial geometries for each system. All analyses were performed on single merged 300 ns long trajectory.

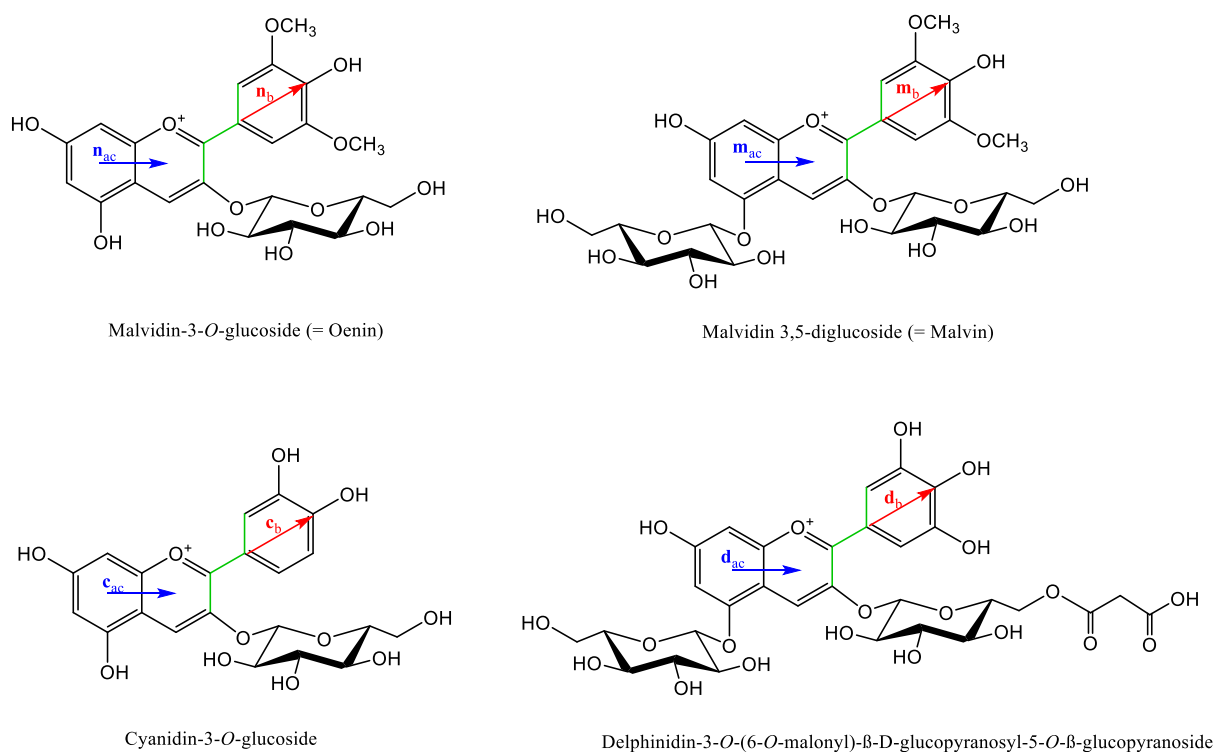


**Figure 25.** Structures of the pigments. For detailed description of pigment...copigment systems, vectors, as described in the main text, were used within the A-, C- rings and B ring as highlighted in blue and red color, respectively. Dihedral angles are in green.

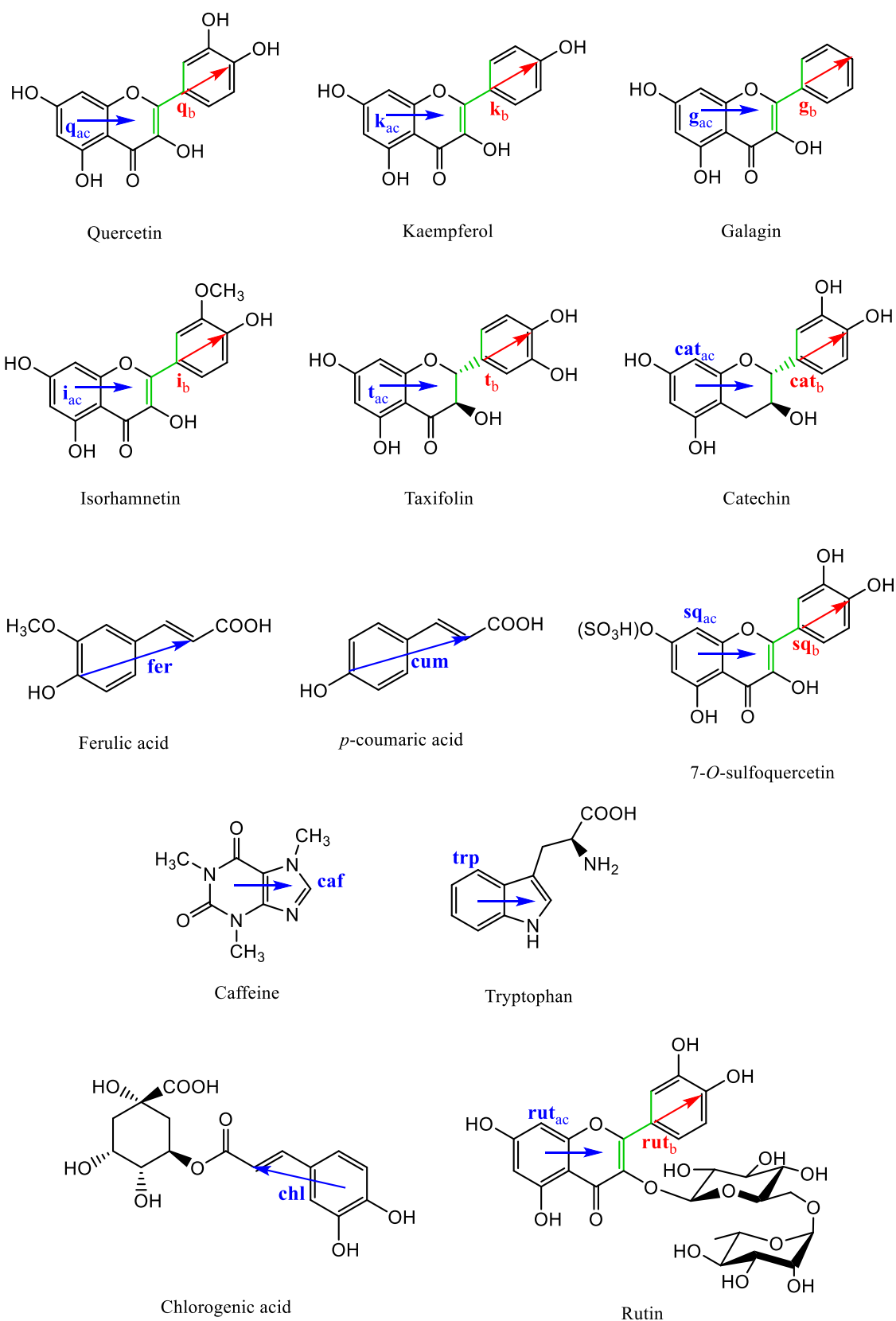


**Figure 26.** Structures of the copigments. For detailed description of pigment···copigment systems, vectors, as described in the main text, were used within the A-, C- rings (or A ring and a carbonyl atom for ferulic acid, *p*-coumaric acid and chlorogenic acid) and within the B ring as highlighted in blue and red color, respectively. Dihedral angles are in green.

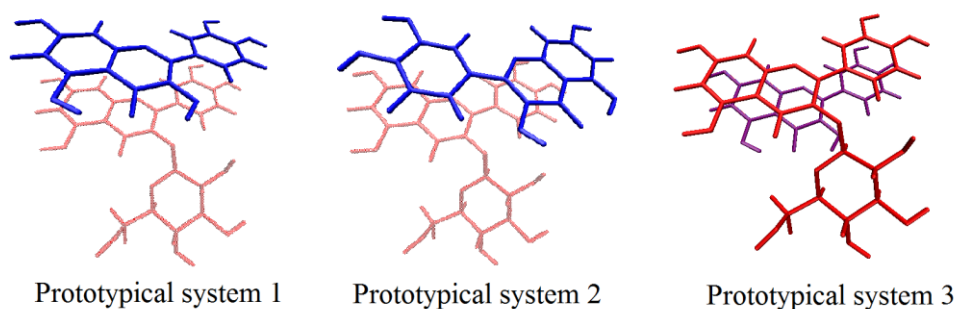


**Figure 27.** Three different guess geometries of cyanidin-3-O-glucoside (red) ··· quercetin (blue) prototypical systems.

### MM/PBSA and MM/GBSA

Molecular mechanics/Poisson-Boltzmann surface area (MM/PBSA) and its complementary molecular mechanics/generalized Born surface area (MM/GBSA) are two methods<sup>137–139</sup> implemented in AMBER and they are often used to calculate binding Gibbs energy ( $\Delta G_{binding,solv}$ ) of solvated pigment···copigment system as follows (Scheme 1):

$$\Delta G_{binding,solv} = \Delta G_{complex,solv} - (\Delta G_{pigment,solv} - \Delta G_{copigment,solv}) \quad (63)$$

or:

$$\Delta G_{binding,solv} = \Delta G_{binding,vacuum} + \Delta G_{complex,solv} - (\Delta G_{copigment,solv} + \Delta G_{pigment,solv}) \quad (64)$$

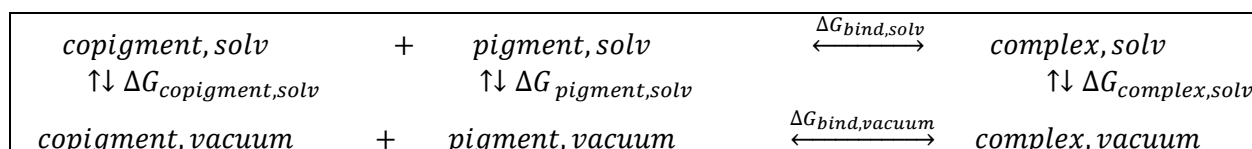
The  $\Delta G$  values for each system (pigment, copigment and complex) are obtained from sufficiently long MD simulations. The binding  $\Delta G$  is obtained as the difference between that of the complex and those of the free pigment and copigment. Then, the Gibbs energy change  $\Delta G$  of each of the three systems on the right side of eq. 63 is estimated as follows:

$$\Delta G = \Delta H - T\Delta S \approx \underbrace{\Delta E_{internal} + \Delta E_{electrostatic} + \Delta E_{vdW}}_{\Delta E_{MM}} + \underbrace{\Delta G_{PB} + \Delta G_{SA}}_{\Delta G_{solv}} - T\Delta S \quad (65)$$

where  $\Delta E_{MM}$  is the gas-phase MM energy and it includes bond, angle and dihedral energies (first term), electrostatic energy (middle term) and van der Waals energy (third term), the Gibbs energy of solvation  $\Delta G_{solv}$  is further decomposed as the sum of electrostatic solvation energy

$\Delta G_{PB/GB}$  (polar contribution; calculated by either the Poisson Boltzmann, PB, or Generalized Born, GB, model) and non-electrostatic solvation component  $\Delta G_{SA}$  (non-polar contribution; calculated by solvent accessible surface area),  $-T\Delta S$  is the conformational entropy change.

**Scheme 1** Thermodynamic cycle of pigment···copigment interaction.



### QM/MM

To calculate UV/Vis absorption properties with explicit solvent model, QM/MM calculations were used. They were carried out within the DFT formalism (CAM-B3LYP/aug-cc-pVDZ) as implemented in the Dalton package<sup>140</sup>. As the size of solvation shell around the system delimits accuracy and computation time, we benchmarked calculations with 5, 10, 15 and 20 nm shell size for cyanidin-3-*O*-glucoside···quercetin as a prototypical system. The theoretical absorption maximum wavelength was already converged with a 10 nm shell size (Figure 28), which was used for all systems.

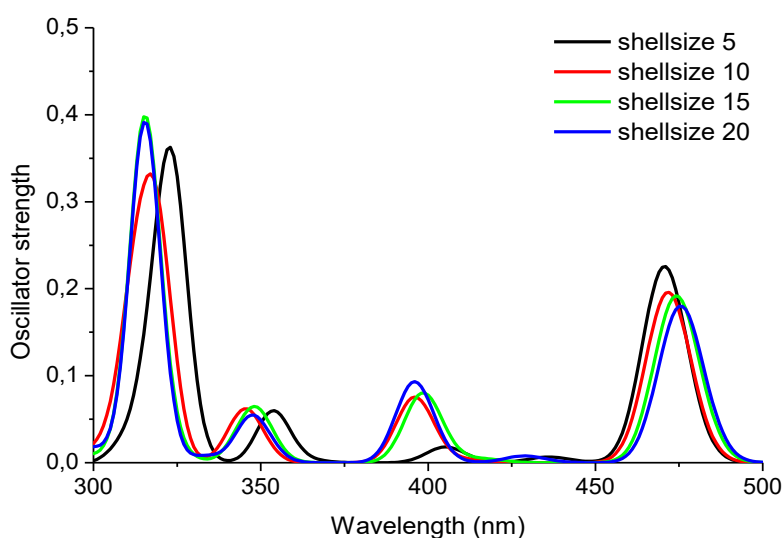




**Figure 28.** Theoretical absorption spectra of cyanidin-3-*O*-glucoside...quercetin with four different size of solvation.

Abecedarium for analysis

To thoroughly analyze conformational features over the 300 ns MD simulations, a set of geometrical parameters (distances, angles, dihedral angles) was defined:

$d_1$  = distance between center-of-mass (COM) of both the anthocyanidin and flavonoid moieties

$d_2$  = distance between COM of A,B,C-rings of both the anthocyanidin and flavonoid moieties (*i.e.*, omitting the sugar moiety)

$d_3$  = distance between COM of A,C-rings of both the anthocyanidin and flavonoid moieties

$d_4$  = distance between COM of A,C-rings of anthocyanidin and B-ring of flavonoid

$d_5$  = distance between COM of B-ring of anthocyanidin and A,C-rings of flavonoid

$d_6$  = distance between COM of B-ring of both the anthocyanidin and flavonoid moieties

$d_7$  = distance between COM of sugar moiety of the anthocyanidin and A,C-rings of flavonoid

$d_8$  = distance between COM of sugar moiety of the anthocyanidin and B-ring of flavonoid

$d_9$  = distance between COM of A,C-rings of anthocyanidin and the aromatic ring of phenolic acid

$d_{10}$  = distance between COM of B-ring of anthocyanidin and the aromatic ring of phenolic acid

$d_{11}$  = distance between COM of sugar moiety of the anthocyanidin and the aromatic ring of phenolic acid

Two vectors in the pigment, and two vectors in the copigment define angles. The two vectors are along the longest axis of A,C-rings (depicted in blue in Figures 25 and 26) and the longest axis of B-ring (depicted in red in Figures 25 and 26). For instance for cyanidin-3-*O*-glucoside...quercetin, four angles can be defined, as quoted:

$$\alpha_1 = \alpha[\text{cya}_{AC}\text{-que}_{AC}]$$

$$\alpha_2 = \alpha[\text{cya}_{AC}\text{-que}_B]$$

$$\alpha_3 = \alpha[\text{cya}_B\text{-que}_{AC}]$$

$$\alpha_4 = \alpha[\text{cya}_B\text{-que}_B]$$

According to this definition, angles around  $0^\circ$  and  $180^\circ$  correspond to parallel and antiparallel orientations, respectively, *e.g.*, with respect to A,C-rings of both pigment and copigment for  $\alpha_1$ . Interestingly,  $\alpha_2$  and  $\alpha_3$  around  $45^\circ$  and  $135^\circ$  could as well represent parallel and antiparallel orientations, respectively. Additionally, the vectors normal to the plane defined by A,C-rings and B-ring define angles characteristic of stacking. Angles equal to  $0^\circ/180^\circ$  or  $90^\circ$  mean (anti)parallel or perpendicular orientation is preferred, respectively.

Dihedral angles are shown in green in Figures 25 and 26. Dihedral angles involving sugars moieties are not shown.

## 6.C. Results and Discussion

### Conformational featuring of malvidin...copigment complexes

Regardless the starting geometry, the MD simulations were sufficiently long to correctly sample the conformational space. Parallel and antiparallel situations were explored several times within the time scale of the MD simulations. Also proper sampling of interchanges from Re/Si to Si/Re and *vice et versa* was obtained (Figure 29). The distributions of  $\alpha_{1-4}$  angles clearly show specific populations, *i.e.*, corresponding to specific orientations of the pigment with respect to the copigment. Precisely, the well-distinguished two populations of  $\alpha_2$  and  $\alpha_3$  (at around  $45^\circ$  and  $135^\circ$ , respectively) correspond to parallel and antiparallel orientations, respectively. However,

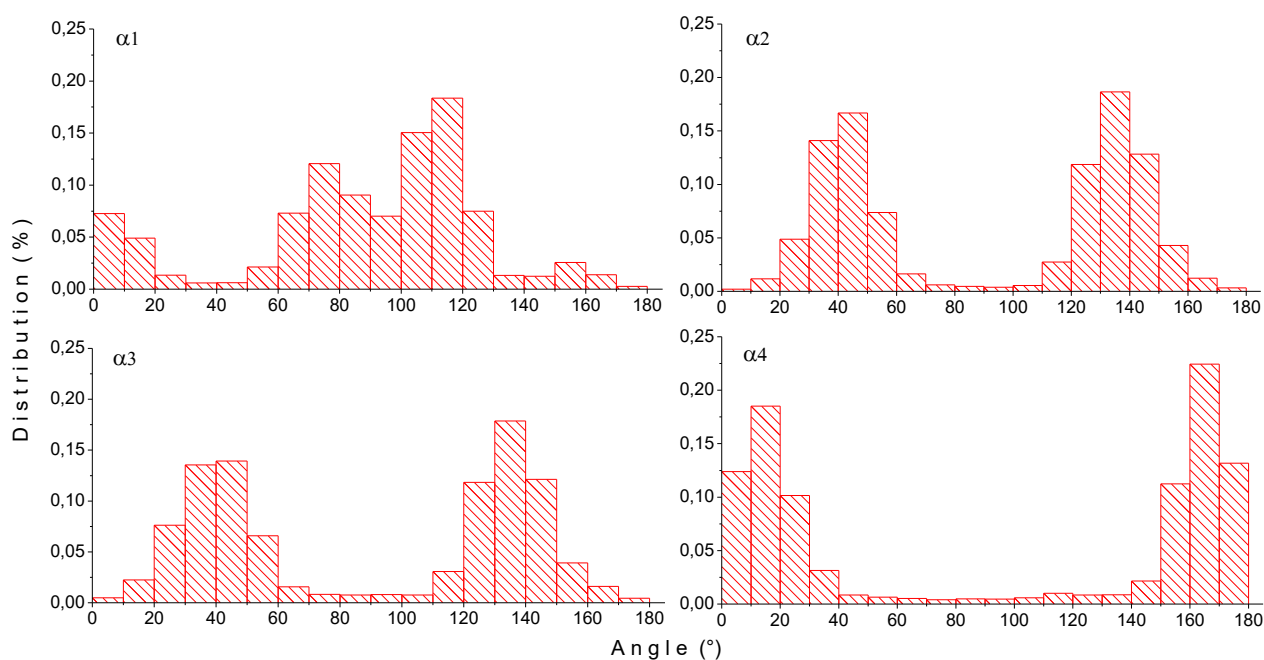


**Figure 29.** Angles' distribution of malvidin-3-*O*-glucoside...quercetin system.

distributions of  $\alpha_1$  highlight more than two different populations (at around  $0^\circ$ ,  $80^\circ$ ,  $110^\circ$ ,  $160^\circ$ ), which reflect flexibility and non-perfect parallel (or antiparallel) alignments. As already observed,  $\pi$ - $\pi$  stacking interactions drive the organization in copigmentation complexes<sup>76,141</sup>, however with more flexibility than ideal stacking, *e.g.*, as observed in material science<sup>142,143</sup>. These  $\pi$ - $\pi$  stacking arrangements are confirmed by the occurrence of a population at  $3.5 \text{ \AA}$  in  $d_{1-6}$  distributions, a distance that is typical of  $\pi$ - $\pi$  stacking interactions (Figure 30). The distance  $d_6$  exhibits a slightly lower density at around  $3.5 \text{ \AA}$  with respect to  $d_{3-5}$ , suggesting that pure B-ring...B-ring were slightly less common than those involving A,C-rings. The second (relatively large) population observed (from  $5$  to  $8 \text{ \AA}$ ) mainly corresponds to antiparallel orientation, in which the A,C rings interact with the B-ring. No short distances were observed for  $d_7$  and  $d_8$  along the MD simulations (Figure 30), confirming that the sugar moieties only rarely participate in the association forces.

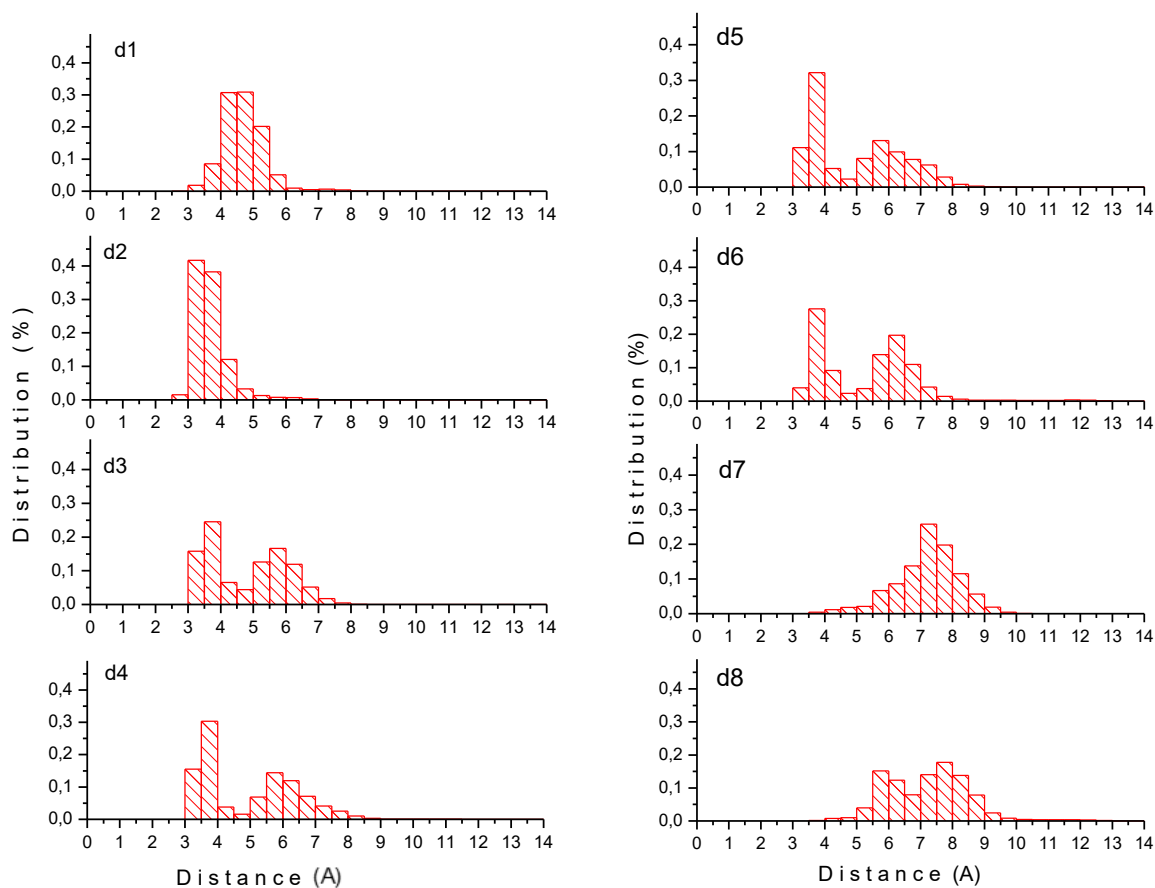


**Figure 30.** Distribution of distance for malvidin-3-*O*-glucoside...quercetin system.

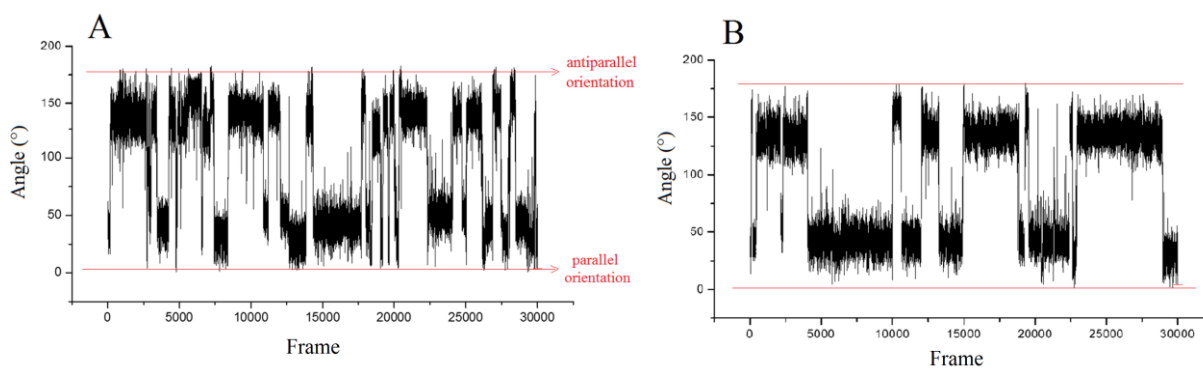


**Figure 31.** Changes between parallel ( $0^\circ$ ) and antiparallel ( $180^\circ$ ) orientations of A) cyanidin-3-*O*-glucoside: quercetin ( $\alpha_2$ ) and B) malvidin-3-*O*-glucoside: quercetin ( $\alpha_2$ ) within 300 ns MD simulation (1 frame corresponds to 10 ps).

It must be noted that, cyanidin-3-*O*-glucoside...quercetin and malvidin-3-*O*-glucoside...quercetin exhibit similar conformational features. They differ in the dynamic of the

switch from parallel to antiparallel orientations and *vice et versa*. The frequency of the conformational changes is higher in the former than in the latter system (Figure 31).

Based on  $\alpha_2$ -distribution, the antiparallel orientation is seen to occur more than three times less than the parallel one with isorhamnetin (characterized by one OCH<sub>3</sub> group at C4') than with quercetin. The occurrence of antiparallel orientation is even lower for galangin (substitution neither at C3' nor at C4'). The frequency of interchange from parallel to antiparallel orientation is as follows: galangin > kaempferol > isorhamnetin ~ quercetin (Figure 32). This suggests that the higher the degree of substitution in the B-ring, the stronger the stabilization in a given orientation. Here it must be stressed that the occurrence of H-bonding between pigment and copigment is weak. As already suggested, this is rationalized by the strong inter H-bonding network with surrounding water molecules, which dramatically weaken intra H-bonding in the copigmentation complex. This means that substitution modify the electron density distribution of the  $\pi$ -conjugated system in both pigment and copigment, enhancing the strength of  $\pi$ - $\pi$  stacking interactions between both partners.

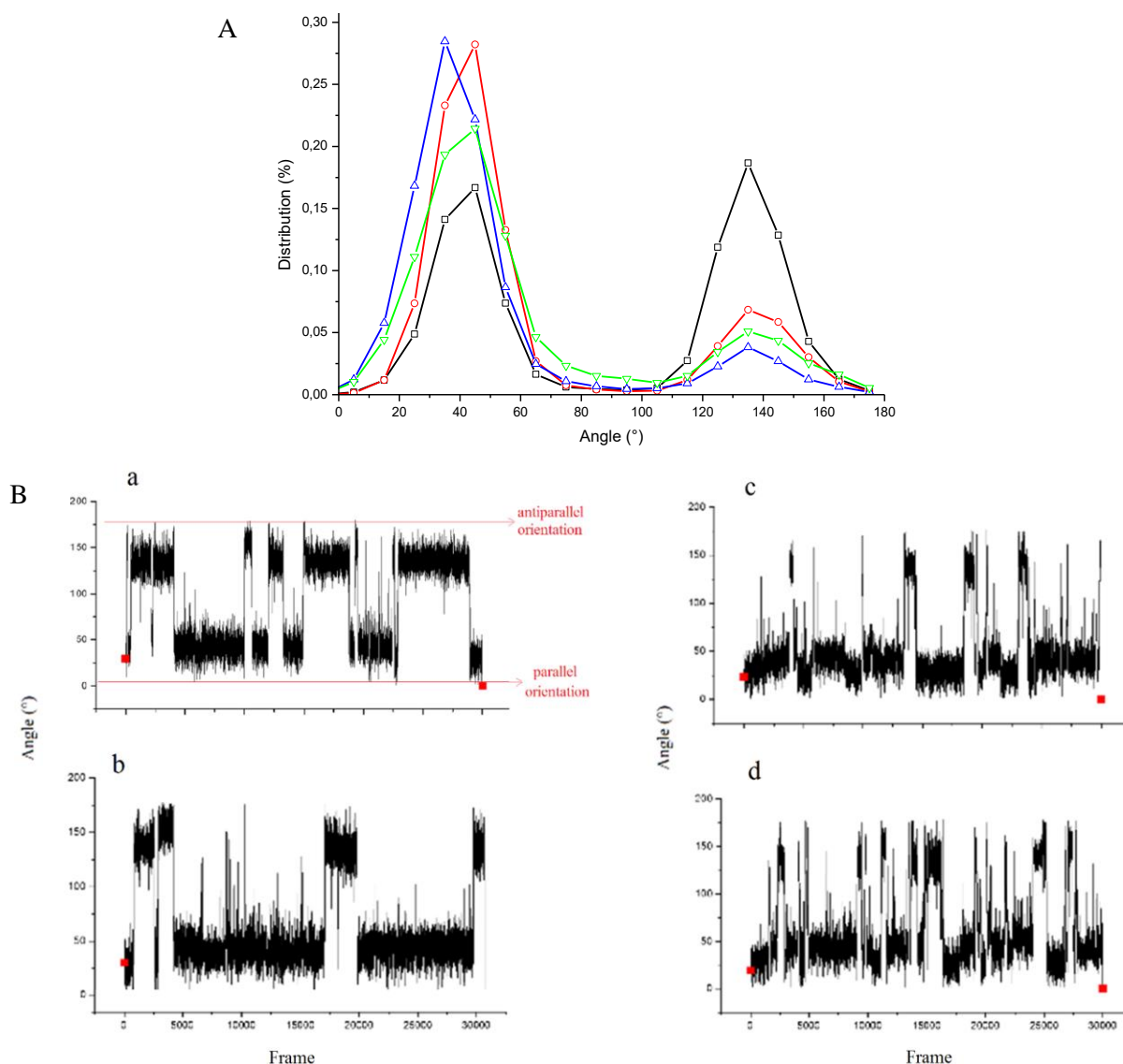


**Figure 32.** A)  $\alpha_2$ -distribution of malvidin-3-*O*-glucoside and quercetin (black), isorhamnetin (red), kaempferol (blue) and galangin (green). B) Changes between parallel and antiparallel orientations between malvidin-3-*O*-glucoside and: a) quercetin, b) isorhamnetin, c) kaempferol, c) galangin within 300 ns MD simulation (1 frame corresponds to 10 ps).

In case of taxifolin, characterized by the absence of the C2,C3 double bond, the B-ring is almost perpendicular with respect to the A,C rings, *i.e.*, two clear distributions centered at *ca.*  $-100^\circ$  and  $80^\circ$  (Figure 33A). With the flavonol derivatives, the structures were more planar, with however a slight twist of *ca.*  $+130^\circ$ ;  $-130^\circ$ ;  $+50^\circ$  and  $-50^\circ$  (Figure 33B). In the case of taxifolin this strong twisting precludes interaction between A,C rings and B-ring. This characteristic also lower the distribution of both parallel and antiparallel orientations with respect to flavonols, nevertheless the parallel orientation is dominant with taxifolin (not shown).

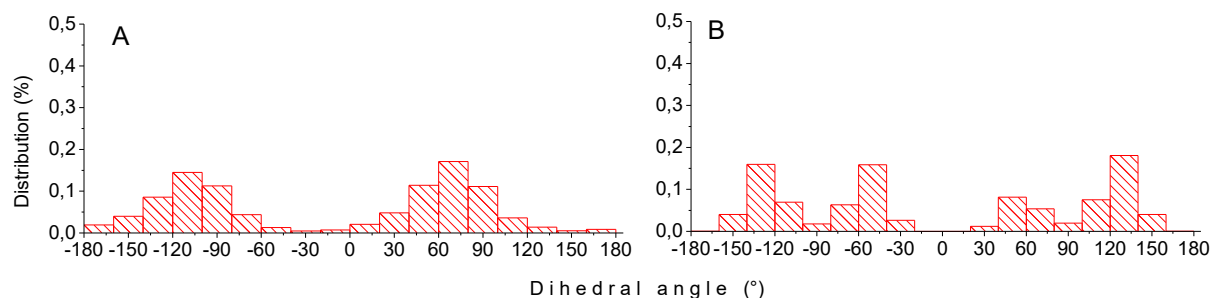


**Figure 33.** Dihedral angles of A) taxifolin and B) quercetin.

### Conformational featuring of malvin...copigment complexes

Malvin bears two sugar moieties, making the pigment more bulky than malvidin. This feature does not prevent  $\pi$ - $\pi$  stacking interactions. Conversely to what can be obtained from pure QM calculations with implicit solvent description, no extra H-bonding is observed in the presence of extra sugar moieties. Therefore, no specific stabilization is expected in malvin copigmentation complexes with respect to malvidin copigmentation complexes. The presence of a more bulky sugar substituent causes that a given orientation remains longer time prior switching to another one (Figure 34  $\alpha_2$ , inset), which is particularly the case for the switching process from parallel and antiparallel orientations. The presence of an extra sugar group in malvin compare to malvidin reinforces the populations of some specific conformations. For instance, with delphinidin...rutin, in which both pigment and copigment have a di-saccharide moiety, two major populations in  $\alpha_1$ -distribution were observed: *i*) 50% of parallel orientation, at 0 - 20°, also confirmed by  $d_3$ , the distance between those two moieties, as being 3 - 4 Å; and *ii*) 20 % of antiparallel orientation, at 140 - 160° (Figure 34  $\alpha_1$ ). A less populated distribution at *ca* 80° highlights a low-occurrence of a perpendicular orientation. As for malvidin, the whole chromophore (flavonoid moiety) is not fully planar, B-ring being twisted with respect to the A,C-rings. The different orientations correspond to interaction between A,C-rings and B-ring of both pigments and copigments, but also interaction of A,C-rings from one partner and B-ring from the other partner. The sugar moiety of delphinidin is relatively distant from the other part of the copigment (distance higher than 4.5 Å) and it is even higher with respect to sugar (of rutin), being higher than 5.5 Å.

In terms of angles, malvin···sulfoquercetin system exhibits similar conformational features as malvidin-3-*O*-glucoside···quercetin. In terms of inter-fragment distances, aromatic rings are less prone to close contact in the former than in the latter copigmentation complexes. Indeed the close-distance population is lower in the former than in the latter system (Figure 35).

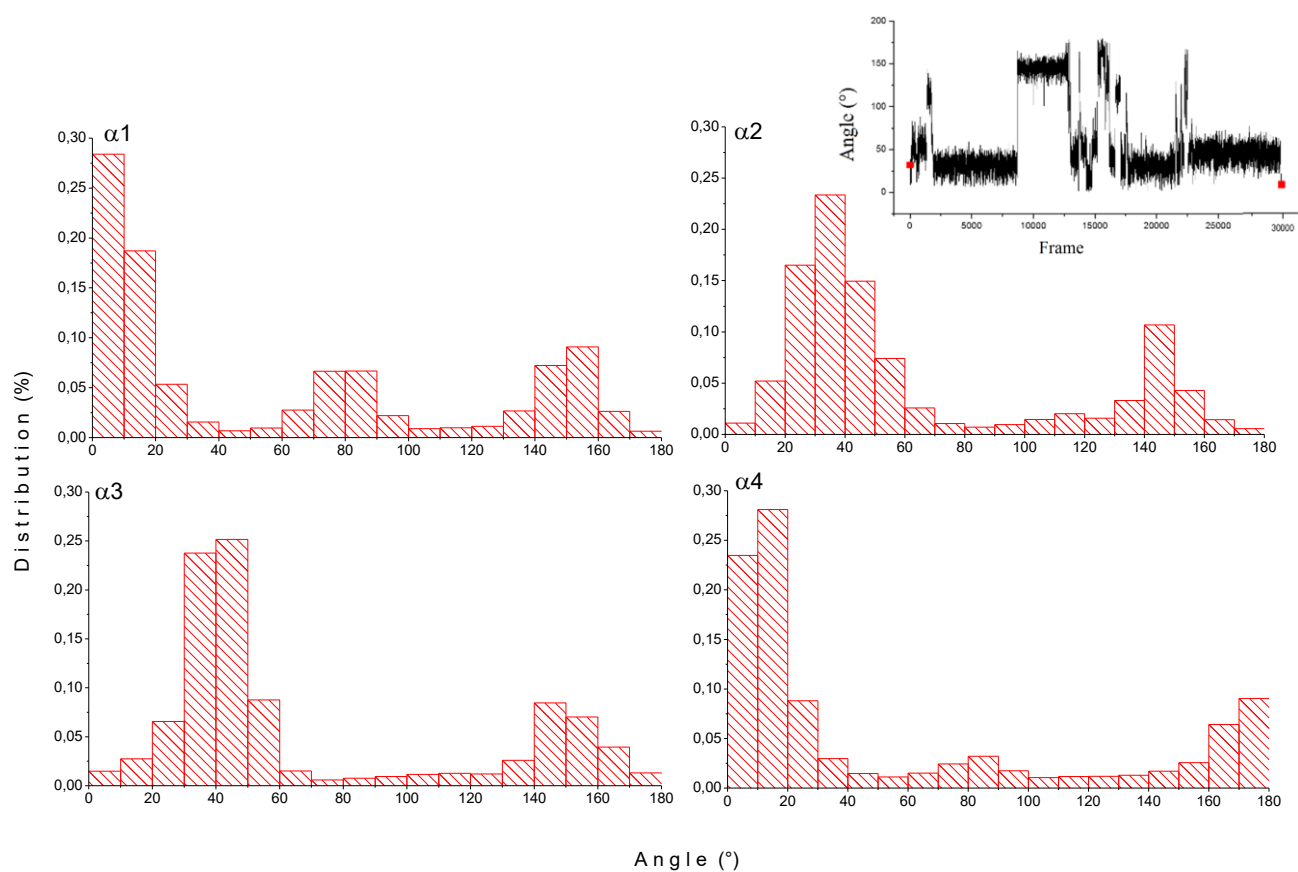


**Figure 34.**  $\alpha_1 - \alpha_4$  of delphinidin···rutin system. Inset: Frequency of the conformational changes between parallel and antiparallel orientations.



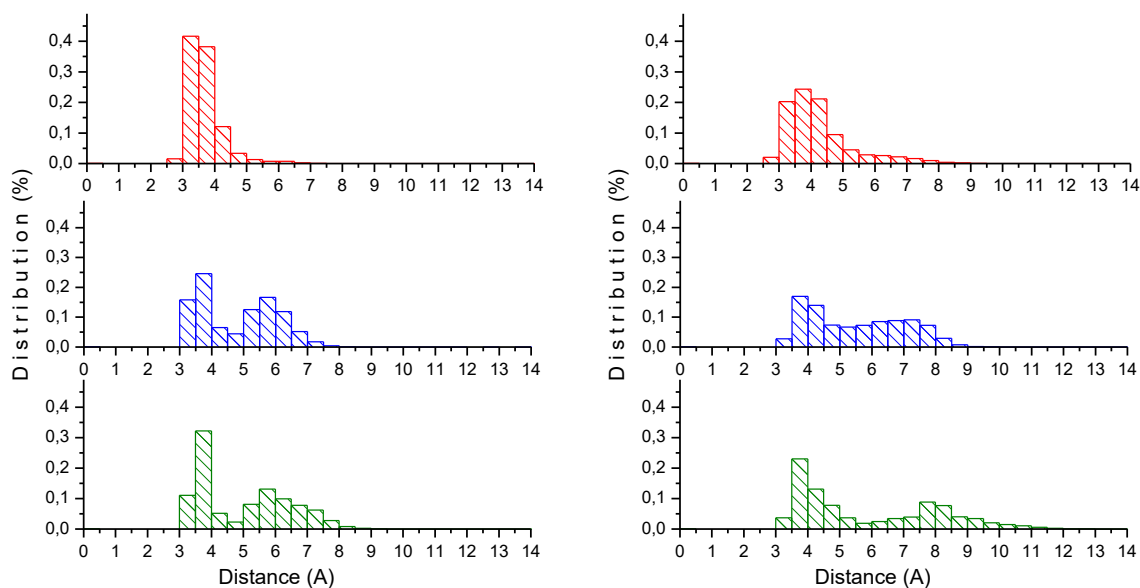


**Figure 35.**  $d_2$  (red),  $d_3$  (blue) and  $d_5$  (green) distances of malvidin-3-*O*-glucoside...quercetin (left) and malvin...sulfoquercetin (right).

### Conformational featuring of pigment...phenolic acid complexes

The case of phenolic acid as copigment was considered so far as a similar case than other copigments (flavonoids). Here we show that phenolic (ferulic or coumaric) acids behave as a particular case. Indeed, in all pigment...phenolic acid copigmentation complexes, no specific orientation of the two partners with respect to each other were observed (Figure 36A). Conversely, the copigment freely rotates around the normal to the aromatic plane. A clear low-distance population was observed for both the  $d_9$  and  $d_{10}$  distances, with coplanar orientation (Figure 36B). This confirms  $\pi$ - $\pi$  stacking of the aromatic ring of the phenolic acid with both A,C rings and B-ring of the pigment. No specific intra-complex H-bonding and no interaction between the phenolic acid and the sugar moiety of the pigment was observed (Figure 36B), again confirming that dispersion forces are the driving force of copigmentation with phenolic acid. However, having in mind that the copigment freely rotates around the normal to the aromatic plane, on top of the pigment, entropic effects are most probably strong contributor to pigment-copigment association. Interestingly, as a copigment, chlorogenic acid is slightly anchored to the pigment. It means that there exist slightly populated distributions at specific  $\alpha_1$  angles, *i.e.*, 0-20°, 60-70° and 120-160°. This is attributed to the presence of the sugar moiety, which slightly maintains the copigment in certain orientations. However, the distribution is still

flat (Figure 37), reflecting very low energetic barriers in the potential energy curve along the rotation around the normal to the aromatic ring.

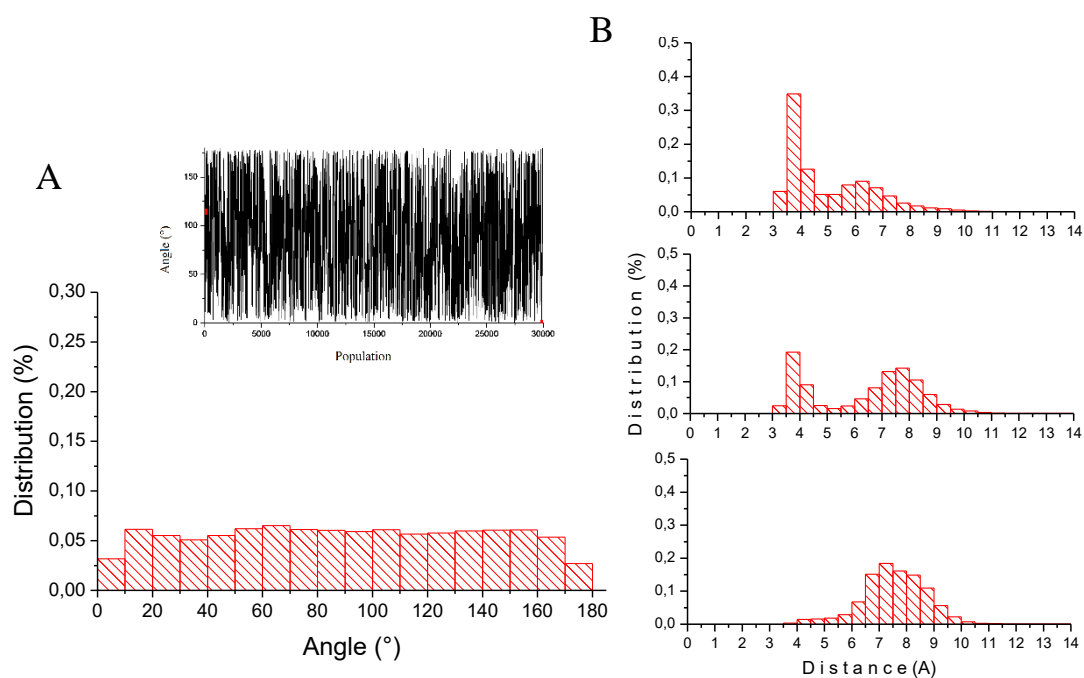


**Figure 36.** Malvidin-3-*O*-glucoside...caffeine system. A)  $\alpha_1$  angle. Inset: Frequency of the switch between parallel and antiparallel orientations. B)  $d_9$  (top),  $d_{10}$  (middle), and  $d_{11}$  (bottom) distances.

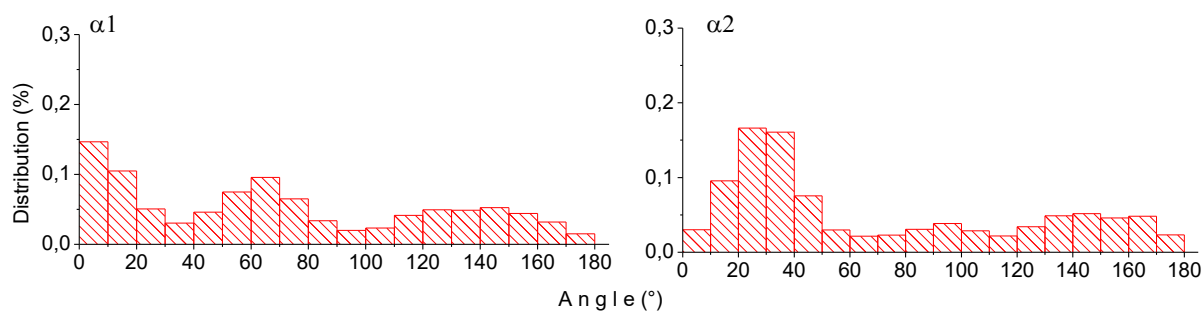


**Figure 37.**  $\alpha_{1,2}$  angle of malvidin-3-*O*-glucoside...chlorogenic acid.

### Association energies

Association energies were calculated by using different methods (MM/PBSA and MM/GBSA). With the no-entropy methods, the Gibbs energy of association was negative for all copigmentation complexes, with relatively slight differences between the different complexes.

These differences were however in agreement with the structure property relationship of the copigment efficacy.<sup>76</sup> For instance, for malvidin the following ranking is obtained from  $\Delta G_{association}^{MM/PBSA}$ : isorhamnetin > quercetin ~ kaempferol > galangin > taxifolin. This confirms the positive role of methoxy groups in copigment efficacy; this also confirms that flavonols (*e.g.*, quercetin) are better copigments than dehydroflavonols (*e.g.*, taxifolin). Although the quantitative description does not agree with the experimental data, the qualitative description does agree. Indeed the  $\Delta G_{association}^{MM/PBSA}$  correlates with  $\Delta G_{association}^{exp}$  with a regression coefficient of 0.85 (Figure 38). One should mention that this regression coefficient was obtained by precluding ferulic acid from the series.

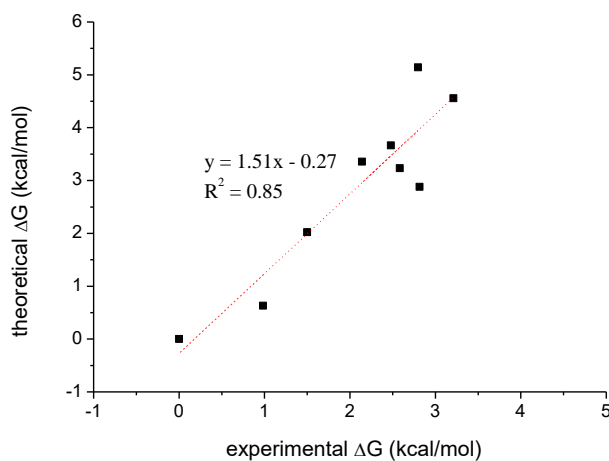


**Figure 38.** Correlation of theoretical Gibbs energy of association ( $\Delta G_{association}^{MM/PBSA}$ ) vs. experimental energy  $\Delta G_{association}^{exp}$ .

### UV/Vis properties

As it was said above, copigmentation stabilizes the whole pigment. Experimental absorption properties of many systems have been published and bathochromic shifts, after the copigmentation is formed, were observed. Depending on laboratory conditions, the highest bathochromic shift was observed for malvin···sulfoquercetin (39 nm) and malvin···rutin (24 nm). The shift was lower than 20 nm for other systems<sup>78,79,81,144–147</sup>. We are currently theoretically assessing UV/Vis absorption properties of carefully chosen systems.

## 7. CONCLUSION

Computational methods have appeared well adapted to describe physical and chemical properties of polyphenols. They were used to describe, rationalize and highlight antioxidant activities and UV/Vis absorption properties of polyphenols. They also provided a new molecular picture of interaction with other pigments or large biomolecular systems, such as membranes or enzymes, and helped to elucidate biological activities of examined compounds at the molecular level.

Using the methods of (TD-) DFT with regular hybrid functionals, we identified main structural (highlighting the role of 2,3-double bond) and environmental (pH and solvents' effects) factors influencing the UV/Vis absorption properties of flavonolignans. It can help to understand possible and safe applications of these compounds as UV protectors or dyes. We also rationalized chemical processes related to oxidation processes on the electrode and antioxidant activity by theoretical descriptors. Screening of other newly synthesized compounds would be useful to identify promising agents with better antioxidant activities.

Color modulation plays an important role in food industry and the color is one of the main descriptors of many beverages. To thoroughly comprehend and tune color of *e.g.*, wines and ciders, it is important to understand underlying physical and chemical behaviors of anthocyanins and pyranoanthocyanins, which are found in such food products. TD-DFT calculations with B3P86 functional have shown to be a perfect tool to describe experimentally observed interesting features of hypso- and batho- chromic shifts *vs.* pH. Moreover, they also represent an accurate tool to describe noncovalent interactions (*e.g.*, copigmentation) with practical perspectives (*e.g.*, as food colorants). A careful geometry analysis of such pigment···copigment systems is mandatory to rationalize UV/Vis properties and corresponding excited states. The use of dispersion-corrected DFT methods (*e.g.*, B3P86-D2) is crucial to describe all phenomena related to noncovalent interactions and the use of  $\omega$ B97X-D functional is important to describe absorption properties of polyphenol complexes, in which electron transfer has a key role. We have closely collaborated with experimental groups and the use of such methods to perform our calculations succeeded in description of all spectral shifts observed experimentally. Nevertheless, there is still a place for methodological improvements since the methods use many approximations.

Polyphenol supramolecular assemblies are mainly stabilized by noncovalent interactions, where both  $\pi$ -stacking and H-bonding interactions play an important role. Geometries of such molecular assemblies often affect the association energies and corresponding optical properties. As already mentioned, calculations improved by description of dispersive effects may lead to better understanding of such assemblies and to better prediction of their physical-chemical properties. Implicit solvent models are often used in order to take solvation into account. Although this is shown to be a good compromise between accuracy and computational time, the main disadvantage is that this approach does not describe specific solute-solvent interactions. Therefore, more time-demanding approach allowing investigation of explicit solvent molecules around the system is often used, which can be assessed by QM/MM calculations. In ongoing project, we identified structural features of several pigment-copigment systems and we started a description of the systems in terms of association energies and UV/Vis absorption properties in comparison to known experimental data. This project would allow to assess the energy of association and to find the best copigment with the lowest association energy and with the highest bathochromic shift.

## 8. REFERENCES

1. Anouar, E. H., Gierschner, J., Duroux, J. L. & Trouillas, P. UV/Visible spectra of natural polyphenols: A time-dependent density functional theory study. *Food Chem.* **131**, 79–89 (2012).
2. Yang, S. H., Lin, J. K., Chen, W. S. & Chiu, J. H. Anti-angiogenic effect of silymarin on colon cancer LoVo cell line. *J. Surg. Res.* **113**, 133–138 (2003).
3. Jiang, C., Agarwal, R. & Lü, J. Anti-angiogenic potential of a cancer chemopreventive flavonoid antioxidant, silymarin: inhibition of key attributes of vascular endothelial cells and angiogenic cytokine secretion by cancer epithelial cells. *Biochem. Biophys. Res. Commun.* **276**, 371–378 (2000).
4. Jacobs, B. P., Dennehy, C., Ramirez, G., Sapp, J. & Lawrence, V. a. Milk thistle for the treatment of liver disease: a systematic review and meta-analysis. *Am. J. Med.* **113**, 506–515 (2002).
5. Dorai, T. & Aggarwal, B. B. Role of chemopreventive agents in cancer therapy. *Cancer Lett.* **215**, 129–140 (2004).
6. Pandey, K. B. & Rizvi, S. I. Plant polyphenols as dietary antioxidants in human health and disease. *Oxid. Med. Cell. Longev.* **2**, 270–278 (2009).
7. Beckman, C. H. Phenolic-storing cells: keys to programmed cell death and periderm formation in wilt disease resistance and in general defence responses in plants? *Physiol. Mol. Plant Pathol.* **57**, 101–110 (2000).
8. Novo, M. *et al.* Sulphur accumulation after *Verticillium dahliae* infection of two pepper cultivars differing in degree of resistance. *Plant Pathol.* **56**, 998–1004 (2007).
9. Di Meo, F., Anouar, E. H., Podloucka, P., Fabre, G. & Trouillas, P. Understanding antioxidant properties of natural compounds at the atomic scale. *J. serbian Soc. Comput. Mech.* **7**, 58–70 (2013).
10. Tsao, R. Chemistry and biochemistry of dietary polyphenols. *Nutrients* **2**, 1231–1246 (2010).
11. Rice-Evans, C. A., Miller, N. J. & Paganga, G. Structure-antioxidant activity relationships of flavonoids and phenolic acids. *Free Radic. Biol. Med.* **20**, 933–956 (1996).

12. Manach, C., Scalbert, A., Morand, C., Rémésy, C. & Jiménez, L. Polyphenols: Food sources and bioavailability. *Am. J. Clin. Nutr.* **79**, 727–747 (2004).
13. Zhu, W., Zhang, J. & Young, C. Y. F. Silymarin inhibits function of the androgen receptor by reducing nuclear localization of the receptor in the human prostate cancer cell line LNCaP. *Carcinogenesis* **22**, 1399–1403 (2001).
14. Williams, R. J., Spencer, J. P. E. & Rice-Evans, C. Flavonoids: Antioxidants or signalling molecules? *Free Radic. Biol. Med.* **36**, 838–849 (2004).
15. Friedman, M. Overview of antibacterial, antitoxin, antiviral, and antifungal activities of tea flavonoids and teas. *Mol. Nutr. Food Res.* **51**, 116–134 (2007).
16. Gažák, R., Walterová, D. & Křen, V. Silybin and silymarin - new and emerging applications in medicine. *Curr. Med. Chem.* **14**, 315–338 (2007).
17. Andersen, O. M. & Markham, K. R. *Flavonoids. Chemistry, Biochemistry and Applications. Angewandte Chemie International Edition* (CRC Press, 2006).
18. Hempel, J. *et al.* Flavonols and flavones of parsley cell suspension culture change the antioxidative capacity of plasma in rats. *Nahrung* **43**, 201–204 (1999).
19. Hirawan, R. & Beta, T. C-Glycosylflavone and lignan diglucoside contents of commercial, regular, and whole-wheat spaghetti. *Cereal Chem.* **88**, 338–343 (2011).
20. Feng, Y., McDonald, C. E. & Vick, B. A. C-Glycosylflavones from hard red spring wheat bran. *Cereal Chemistry* **65**, 452–456 (1988).
21. Green, C. O., Wheatley, A. O., Osagie, A. U., Morrison, E. Y. S. A. & Asemota, H. N. Determination of polymethoxylated flavones in peels of selected Jamaican and Mexican citrus (*Citrus* spp.) cultivars by high-performance liquid chromatography. *Biomed. Chromatogr.* **21**, 48–54 (2007).
22. Pan, G. G., Kilmartin, P. A., Smith, B. G. & Melton, L. D. Detection of orange juice adulteration by tangelo juice using multivariate analysis of polymethoxylated flavones and carotenoids. *J. Sci. Food Agric.* **82**, 421–427 (2002).
23. Hertog, M. G., Hollman, P. C. & Katan, M. B. Content of potentially anticarcinogenic flavonoids of 28 vegetables and 9 fruits commonly consumed in The Netherlands. *J. Agric. Food Chem.* **40**, 2379–2383 (1992).
24. Koh, E., Wimalasiri, K. M. S., Chassy, A. W. & Mitchell, A. E. Content of ascorbic acid, quercetin, kaempferol and total phenolics in commercial broccoli. *J. food*

- Compos. Anal.* **22**, 637–643 (2009).
25. Santos-Buelga, C. & Scalbert, A. Proanthocyanidins and tannin-like compounds – nature, occurrence, dietary intake and effects on nutrition and health. *J. Sci. Food Agric.* **80**, 1094–1117 (2000).
  26. Prior, R. L., Lazarus, S. A., Cao, G., Muccitelli, H. & Hammerstone, J. F. Identification of Procyanidins and Anthocyanins in Blueberries and Cranberries (*Vaccinium* Spp.) Using High-Performance Liquid Chromatography/Mass Spectrometry. *J. Agric. Food Chem.* **49**, 1270–1276 (2001).
  27. Tsao, R., Yang, R., Young, C. & Zhu, H. Polyphenolic Profiles in Eight Apple Cultivars Using High-Performance Liquid Chromatography (HPLC). *J. Agric. Food Chem.* **51**, 6347–6353 (2003).
  28. Arts, I. C. W., Putte, B. Van De & Hollman, P. C. H. Catechin Contents of Foods Commonly Consumed in The Netherlands. 1. Fruits, Vegetables, Staple Foods, and Processed Foods. *J. Agric. Food Chem.* **48**, 1746–1751 (2000).
  29. Arts, I. C. W., Putte, B. Van De & Hollman, P. C. H. Catechin Contents of Foods Commonly Consumed in The Netherlands. 2. Tea, Wine, Fruit Juices, and Chocolate Milk. *J. Agric. Food Chem.* **48**, 1752–1757 (2000).
  30. Tanaka, T., Takahashi, R., Kouno, I. & Nonaka, G. Chemical Evidence for the De-astringency (Insolubilization of Tannins) of Persimmon Fruit. *J. Chem. Soc. Perkin Trans. 1* 3013–3022 (1994).
  31. Guyot, S., Marnet, N., Laraba, D., Sanoner, P. & Drilleau, J.-F. Reversed-Phase HPLC following Thiolysis for Quantitative Estimation and Characterization of the Four Main Classes of Phenolic Compounds in Different Tissue Zones of a French Cider Apple Variety (*Malus domestica* Var. Kermerrien). *J. Agric. Food Chem.* **46**, 1698–1705 (1998).
  32. Mazur, W. M., Duke, J. A., Wahala, K., Rasku, S. & Adlercreutz, H. Isoflavonoids and lignans in legumes: Nutritional and health aspects in humans. *Nutr. Biochem.* **9**, 193–200 (1998).
  33. Simons, R., Gruppen, H., Bovee, T. F. H., Verbruggen, M. A. & Vincken, J.-P. Prenylated isoflavonoids from plants as selective estrogen receptor modulators (phytoSERMs). *Food Funct.* **3**, 810–827 (2012).



34. De-eknamkul, W. *et al.* QSAR study of natural estrogen-like isoflavonoids and diphenolics from Thai medicinal plants. *J. Mol. Graph. Model.* **29**, 784–794 (2011).
35. Djiogue, S. *et al.* Isoflavonoids from *Erythrina poeppigiana* : Evaluation of Their Binding Affinity for the Estrogen Receptor. *J. Nat. Prod.* **72**, 1603–1607 (2009).
36. Castañeda-Ovando, A., Pacheco-Hernández, M. de L., Pérez-Hernández, M. E., Rodríguez, J. A. & Galán-Vidal, C. A. Chemical studies of anthocyanins: A review. *Food Chem.* **113**, 859–871 (2009).
37. Horbowicz, M., Kosson, R., Grzesiuk, A. & Dębski, H. Anthocyanins of Fruits and Vegetables - Their Occurrence, Analysis and Role in Human Nutrition. *Veg. Crop. Res. Bull.* **68**, 5–22 (2008).
38. Biedermann, D., Vavříková, E., Cvak, L. & Křen, V. Chemistry of silybin. *Nat. Prod. Rep.* **31**, 1138–1157 (2014).
39. Pyszková, M. *et al.* Flavonolignan 2,3-dehydroderivatives: Preparation, antiradical and cytoprotective Activity. *Free Radic. Biol. Med.* **90**, 114–125 (2015).
40. Gažák, R. *et al.* Molecular mechanisms of silybin and 2,3-dehydrosilybin antiradical activity-role of individual hydroxyl groups. *Free Radic. Biol. Med.* **46**, 745–758 (2009).
41. Trouillas, P. *et al.* Mechanism of the antioxidant action of silybin and 2,3-dehydrosilybin flavonolignans: a joint experimental and theoretical study. *J. Phys. Chem. A* **112**, 1054–1063 (2008).
42. van Wenum, E., Jurczakowski, R. & Litwinienko, G. Media effects on the mechanism of antioxidant action of silybin and 2,3-dehydrosilybin: role of the enol group. *J. Org. Chem.* **78**, 9102–9112 (2013).
43. Křen, V. & Walterová, D. Silybin and silymarin - new effects and applications. *Biomed. Pap.* **149**, 29–41 (2005).
44. Singh, R. P. & Agarwal, R. Cosmeceuticals and silibinin. *Clin. Dermatol.* **27**, 479–484 (2009).
45. Anthony, K. & Saleh, M. Free Radical Scavenging and Antioxidant Activities of Silymarin Components. *Antioxidants* **2**, 398–407 (2013).
46. Tyagi, A., Agarwal, C., Harrison, G., Michael Glode, L. & Agarwal, R. Silibinin causes cell cycle arrest and apoptosis in human bladder transitional cell carcinoma cells

- by regulating CDKI-CDK-cyclin cascade, and caspase 3 and PARP cleavages. *Carcinogenesis* **25**, 1711–1720 (2004).
47. Ahlenstiel, T., Burkhardt, G., Kohler, H. & Kuhlmann, M. K. Bioflavonoids attenuate renal proximal tubular cell injury during cold preservation in Euro-Collins and University of Wisconsin solutions. *Kidney Int.* **63**, 554–563 (2003).
  48. Wang, M. J. *et al.* Silymarin protects dopaminergic neurons against lipopolysaccharide-induced neurotoxicity by inhibiting microglia activation. *Eur. J. Neurosci.* **16**, 2103–2112 (2002).
  49. Soto, C., Recoba, R., Barrón, H., Alvarez, C. & Favari, L. Silymarin increases antioxidant enzymes in alloxan-induced diabetes in rat pancreas. *Comp. Biochem. Physiol. - C Toxicol. Pharmacol.* **136**, 205–212 (2003).
  50. Al-Jassabi, S., Saad, A., And, M. S. A. & Al-Omari, A. The Role of Silymarin in Prevention of Alloxan-Induced Diabetes mellitus in Balb/C Mice. *Am. J. Toxicol. Sci.* **3**, 172–176 (2011).
  51. Svobodová, A., Zdařilová, A., Walterová, D. & Vostálová, J. Flavonolignans from *Silybum marianum* moderate UVA-induced oxidative damage to HaCaT keratinocytes. *J. Dermatol. Sci.* **48**, 213–224 (2007).
  52. Svobodová, A. *et al.* Attenuation of UVA-induced damage to human keratinocytes by silymarin. *J. Dermatol. Sci.* **46**, 21–30 (2007).
  53. Katiyar, S. K., Korman, N. J., Mukhtar, H. & Agarwal, R. Protective effects of silymarin against photocarcinogenesis in a mouse skin model. *J. Natl. Cancer Inst.* **89**, 556–566 (1997).
  54. Gu, M., Sivanandhan, D. & Rana P, S. Silibinin Protects against Photocarcinogenesis via Modulation of Cell Cycle Regulators, Mitogen-Activated Protein Kinases, and Akt Signaling. *Cancer Res.* **64**, 6349–6356 (2004).
  55. Agarwal, C. *et al.* Silibinin upregulates the expression of cyclin-dependent kinase inhibitors and causes cell cycle arrest and apoptosis in human colon carcinoma HT-29 cells. *Oncogene* **22**, 8271–8282 (2003).
  56. Katiyar, S. K., Mantena, S. K. & Meeran, S. M. Silymarin protects epidermal keratinocytes from ultraviolet radiation-induced apoptosis and DNA damage by nucleotide excision repair mechanism. *PLoS One* **6**, 1–11 (2011).

57. DiCenzo, R. *et al.* Coadministration of milk thistle and indinavir in healthy subjects. *Pharmacotherapy* **23**, 866–870 (2003).
58. Piscitelli, S. C. *et al.* Effect of Milk Thistle on the Pharmacokinetics of Indinavir in Healthy Volunteers. *Pharmacotherapy* **22**, 551–556 (2002).
59. Geier, J., Fuchs, T. & Wahl, R. Anaphylactic shock due to an extract of *Silybum marianum* in a patient with immediate-type allergy to kiwi fruit. *Allergologie* **13**, 387–388 (1990).
60. Kong, J. M., Chia, L. S., Goh, N. K., Chia, T. F. & Brouillard, R. Analysis and biological activities of anthocyanins. *Phytochemistry* **64**, 923–933 (2003).
61. Heinonen, I. M., Meyer, A. S. & Frankel, E. N. Antioxidant Activity of Berry Phenolics on Human Low-Density Lipoprotein and Liposome Oxidation. *J. Agric. Food Chem.* **46**, 4107–4112 (1998).
62. Meiers, S. *et al.* The anthocyanidins cyanidin and delphinidin are potent inhibitors of the epidermal growth-factor receptor. *J. Agric. Food Chem.* **49**, 958–962 (2001).
63. Rein, M. Copigmentation reactions and color stability of berry anthocyanins. (Academic dissertation.). (University of Helsinki, 2005).
64. Clifford, M. Anthocyanins - nature, occurrence and dietary burden. *J. Sci. Food Agric.* **80**, 1063–1072 (2000).
65. Bakker, J. & Timberlake, C. F. Isolation , Identification , and Characterization of New Color-Stable Anthocyanins Occurring in Some Red Wines. *J. Agric. Food Chem.* **8561**, 35–43 (1997).
66. Rentsch, M., Schwarz, M., Winterhalter, P. & Hermosín-Gutiérrez, I. Formation of hydroxyphenyl-pyranoanthocyanins in Grenache wines: Precursor levels and evolution during aging. *J. Agric. Food Chem.* **55**, 4883–4888 (2007).
67. Mateus, N., Oliveira, J., Haettich-Motta, M. & de Freitas, V. New Family of Bluish Pyranoanthocyanins. *J. Biomed. Biotechnol.* **2004**, 299–305 (2004).
68. Mateus, N. *et al.* A new vinylpyranoanthocyanin pigment occurring in aged red wine. *Food Chem.* **97**, 689–695 (2006).
69. Jingren, H. E., Santos-Buelga, C., Silva, A. M. S., Mateus, N. & De Freitas, V. Isolation and structural characterization of new anthocyanin-derived yellow pigments in aged red wines. *J. Agric. Food Chem.* **54**, 9598–9603 (2006).

70. Pissarra, J. *et al.* Isolation and structural characterization of new anthocyanin-alkylcatechin pigments. *Food Chem.* **90**, 81–87 (2005).
71. Mateus, N., Silva, A. M. S., Santos-Buelga, C., Rivas-Gonzalo, J. C. & De Freitas, V. Identification of anthocyanin-flavanol pigments in red wines by NMR and mass spectrometry. *J. Agric. Food Chem.* **50**, 2110–2116 (2002).
72. Mateus, N. *et al.* Isolation and Structural Characterization of New Acylated Anthocyanin-Vinyl-Flavanol Pigments Occurring in Aging Red. *J. Agric. Food Chem.* **51**, 277–282 (2003).
73. Oliveira, J. *et al.* Pyranoanthocyanin dimers: A new family of turquoise blue anthocyanin-derived pigments found in port wine. *J. Agric. Food Chem.* **58**, 5154–5159 (2010).
74. Oliveira, J., Mateus, N. & Freitas, V. De. Synthesis of a new bluish pigment from the reaction of a methylpyranoanthocyanin with sinapaldehyde. *Tetrahedron Lett.* **52**, 1996–2000 (2011).
75. Oliveira, J., Mateus, N. & de Freitas, V. Previous and recent advances in pyranoanthocyanins equilibria in aqueous solution. *Dye. Pigment.* **100**, 190–200 (2014).
76. Trouillas, P. *et al.* Stabilizing and Modulating Color by Copigmentation : Insights from Theory and Experiment. *Chem. Rev.* **116**, 4937–4982 (2015).
77. Boulton, R. The copigmentation of anthocyanins and its role in the color of red wine: A critical review. *Am. J. Enol. Vitic.* **52**, 67–87 (2001).
78. Eiro, M. J. & Heinonen, M. Anthocyanin color behavior and stability during storage: Effect of intermolecular copigmentation. *J. Agric. Food Chem.* **50**, 7461–7466 (2002).
79. Lambert, S. G., Asenstorfer, R. E., Williamson, N. M., Iland, P. G. & Jones, G. P. Copigmentation between malvidin-3-glucoside and some wine constituents and its importance to colour expression in red wine. *Food Chem.* **125**, 106–115 (2011).
80. Goto, T. & Kondo, T. Structure and Molecular Stacking of Anthocyanins- Flower Color Variatio. *Angew. C'hem. Int. Ed. Engl.* **30**, 17–33 (1991).
81. Baranac, J. M., Petranović, N. A. & Dimitrić-Marković, J. M. Spectrophotometric Study of Anthocyan Copigmentation Reactions. *J. Agric. Food Chem.* **44**, 1333–1336 (1996).

82. Brouillard, R. & Dangles, O. Anthocyanin molecular interactions: the first step in the formation of new pigments during wine aging? *Food Chem.* **51**, 365–371 (1994).
83. Lee, E. C. *et al.* Understanding of assembly phenomena by aromatic-aromatic interactions: Benzene Dimer and the substituted systems. *J. Phys. Chem. A* **111**, 3446–3457 (2007).
84. Geronimo, I., Lee, E. C., Singh, N. J. & Kim, K. S. How different are electron-rich and electron-deficient pi-interactions? *J. Chem. Theory Comput.* **6**, 1931–1934 (2010).
85. McGaughey, G. B., Gagné, M. & Rappé, A. K. pi -Stacking Interactions. ALIVE AND WELL IN PROTEINS. *J. Biol. Chem.* **273**, 15458–15463 (1998).
86. Grimme, S. Do Special Noncovalent  $\pi$ - $\pi$  Stacking Interactions Really Exist? *Angew. Chemie Int. Ed.* **47**, 3430–3434 (2008).
87. Koch, W. & Holthausen, M. C. *A Chemist's Guide to Density Functional Theory. Second Edition.* (Wiley-VCH Verlag GmbH, 2001).
88. Klein, M., Martinez, A. & Wang, X. P. On the Born-Oppenheimer Approximation of Wave Operators in Molecular Scattering Theory. *Commun. Math. Phys* **152**, 73–95 (1993).
89. Sherrill, C. D. An Introduction to Hartree-Fock Molecular Orbital Theory. 1–8 (2000). Available at: <http://vergil.chemistry.gatech.edu/notes/>.
90. Tsuneda, T. *Density Functional Theory in Quantum Chemistry.* (Springer Japan, 2014).
91. Sherrill, C. D. An Introduction to Configuration Interaction Theory. 1–55 (1995). Available at: <http://vergil.chemistry.gatech.edu/notes/hf-intro/>.
92. Šimová, L., Řezáč, J. & Hobza, P. Convergence of the interaction energies in noncovalent complexes in the coupled-cluster methods up to full configuration interaction. *J. Chem. Theory Comput.* **9**, 3420–3428 (2013).
93. Raghavachari, K., Pople, J. A., Replogle, E. S. & Head-Gordon, M. Fifth order Moeller-Plesset perturbation theory: comparison of existing correlation methods and implementation of new methods correct to fifth order. *J. Phys. Chem.* **94**, 5579–5586 (1990).
94. Andersson, K., Malmqvist, P.-A. & Roos, B. O. Second-order self-consistent perturbation theory with a complete field reference function. *J. Chem. Phys.* **96**, 1218–1226 (1992).

95. Davidson, E. R. & Feller, D. Basis set selection for molecular calculations. *Chem. Rev.* **86**, 681–696 (1986).
96. Frisch, M. J., Pople, J. A. & Binkley, J. S. Selfconsistent molecular orbital methods 25. Supplementary functions for Gaussian basis sets. *J. Chem. Phys.* **80**, 3265–3269 (1984).
97. Dunning, T. H. & Hay, P. I. in *Methods of Electronic Structure Theory. Volume 3* (ed. III, H. F. S.) 1–27 (Springer, 1977).
98. Jensen, F. Atomic orbital basis sets. *WIREs Comput Mol Sci* 1–23 (2012).
99. Bauschlicher, C. W. J. & Partridge, H. A comparison of correlation-consistent and Pople-type basis sets. *Chem. Phys. Lett.* **245**, 158–164 (1995).
100. Kryachko, E. S. Hohenberg-Kohn Theorem. *Int. J. Quantum Chem.* **18**, 1029–1035 (1980).
101. Bickelhaupt, F. M. & Baerends, E. J. Kohn-Sham Density Functional Theory: Predicting and Understanding Chemistry. *Rev. Comput. Chem.* **15**, 1–86 (2007).
102. Kohn, W., Becke, a D. & Parr, R. G. Density Functional Theory of Electronic Structure. *J. Phys Chem* **100**, 12974–12980 (1996).
103. Krukau, A. V., Scuseria, G. E., Perdew, J. P. & Savin, A. Hybrid functionals with local range separation. *J. Chem. Phys.* **129**, 1–7 (2008).
104. Grimme, S. Accurate description of van der Waals complexes by density functional theory including empirical corrections. *J. Comput. Chem.* **25**, 1463–1473 (2004).
105. Chai, J.-D. & Head-Gordon, M. Long-range corrected hybrid density functionals with damped atom-atom dispersion corrections. *Phys Chem Chem Phys* **10**, 6615–6620 (2008).
106. Grimme, S., Ehrlich, S. & Goerigk, L. Effect of the Damping Function in Dispersion Corrected Density Functional Theory. *J. Comput. Chem.* **32**, 1456–1465 (2011).
107. Grimme, S. Semiempirical GGA-Type Density Functional Constructed with a Long-Range Dispersion Correction. *J. Comput. Chem.* **27**, 1787–1799 (2006).
108. Grimme, S. *et al.* A consistent and accurate ab initio parametrization of density functional dispersion correction (DFT-D) for the 94 elements H-Pu. *J. Chem. Phys.* **132**, 154104 (2010).

109. Berger, O., Edholm, O. & Jahnig, F. Molecular Dynamics Simulations of a Fluid Bilayer of Dipalmitoylphosphatidylcholine at Full Hydration, Constant Pressure, and Constant Temperature. *Biophys. J.* **72**, 2002–2013 (1997).
110. Mackerell, A. D. & Banavali, N. K. All-Atom Empirical Force Field for Nucleic Acids: II. Application to Molecular Dynamics Simulations of DNA and RNA in Solution. *J. Comput. Chem.* **21**, 105–120 (2000).
111. Hornak, V. *et al.* Comparison of multiple AMBER force fields and development of improved protein backbone parameters. *Proteins* **65**, 712–725 (2006).
112. Sjöqvist, J., Linares, M., Lindgren, M. & Norman, P. Molecular dynamics effects on luminescence properties of oligothiophene derivatives: a molecular mechanics–response theory study based on the CHARMM force field and density functional theory. *Phys. Chem. Chem. Phys.* **13**, 17532–17542 (2011).
113. Sjöqvist, J., Linares, M., Mikkelsen, K. V. & Norman, P. QM/MM-MD simulations of conjugated polyelectrolytes: A study of luminescent conjugated oligothiophenes for use as biophysical probes. *J. Phys. Chem. A* **118**, 3419–3428 (2014).
114. Pedersen, M. N. *et al.* Damped response theory in combination with polarizable environments: The polarizable embedding complex polarization propagator method. *J. Chem. Theory Comput.* **10**, 1164–1171 (2014).
115. Olsen, J. M. H. & Kongsted, J. in *Advances in QUANTUM CHEMISTRY* (eds. Sabin, J. R. & Brandas, E.) **61**, 107–144 (Elsevier, 2011).
116. Schwabe, T., Olsen, J. M. H., Sneskov, K., Kongsted, J. & Christiansen, O. Solvation effects on electronic transitions: Exploring the performance of advanced solvent potentials in polarizable embedding calculations. *J. Chem. Theory Comput.* **7**, 2209–2217 (2011).
117. Olsen, J. M., Aidas, K. & Kongsted, J. Excited states in solution through polarizable embedding. *J. Chem. Theory Comput.* **6**, 3721–3734 (2010).
118. Granville, V., Křivánek, M. & Rasson, J. P. Simulated Annealing: A Proof of Convergence. *IEEE Trans. Pattern Anal. Mach. Intell.* **16**, 652–656 (1994).
119. Runge, E. & Gross, E. K. U. Density-functional theory for time-dependent systems. *Phys. Rev. Lett.* **52**, 997–1000 (1984).
120. Marques, M. A. L. & Gross, E. K. U. Time-Dependent Density Functional Theory.

- Annu. Rev. Phys. Chem.* **55**, 427–455 (2004).
121. Marques, M. A. L. *et al.* *Fundamentals of Time-Dependent Density Functional Theory*. (Springer Heidelberg, 2012).
  122. Harris, D. C. & Bertolucci, M. D. *Symmetry and Spectroscopy. An introduction to vibrational and electronic spectroscopy*. (Oxford University Press, 1978).
  123. Nepraš, M. & Titz, M. *Základy teorie elektronových spekter. Absorpční a luminiscenční spektra organických sloučenin v ultrafialové a viditelné oblasti světla*. (Praha Nakladatelství technické literatury, 1983).
  124. Zgierski, M. Z. Herzberg-Teller Interaction and Vibronic Coupling in Molecular Crystals. I. The Simple Model. *Phys. Status Solidi* **61**, 393–402 (1974).
  125. Orlandi, G. & Siebrand, W. Theory of vibronic intensity borrowing. Comparison of Herzberg-Teller and Born-Oppenheimer coupling. *J. Chem. Phys.* **58**, 4513–4523 (1973).
  126. Adamo, C. & Jacquemin, D. The calculations of excited-state properties with Time-Dependent Density Functional Theory. *Chem. Soc. Rev.* **42**, 845–856 (2013).
  127. Laurent, A. D., Adamo, C. & Jacquemin, D. Dye chemistry with time-dependent density functional theory. *Phys. Chem. Chem. Phys.* **16**, 14311–14972 (2014).
  128. Jacquemin, D., Planchat, A., Adamo, C. & Mennucci, B. TD-DFT assessment of functionals for optical 0-0 transitions in solvated dyes. *J. Chem. Theory Comput.* **8**, 2359–2372 (2012).
  129. Jacquemin, D. & Adamo, C. Computational molecular electronic spectroscopy with TD-DFT. *Top Curr Chem* 347–375 (2016).
  130. Antolovich, M., Prenzler, P. D., Patsalides, E., McDonald, S. & Robards, K. Methods for testing antioxidant activity. *Analyst* **127**, 183–198 (2002).
  131. Prior, R. L., Wu, X. & Schaich, K. Standardized Methods for the Determination of Antioxidant Capacity and Phenolics in Foods and Dietary Supplements. *J. Agric. Food Chem.* **53**, 4290–4302 (2005).
  132. Anouar, E. H. *et al.* Antioxidant properties of phenolic Schiff bases: structure-activity relationship and mechanism of action. *J. Comput. Aided. Mol. Des.* **27**, 951–964 (2013).
  133. Anouar, E. H. *et al.* Free radical scavenging properties of guaiacol oligomers: a



- combined experimental and quantum study of the guaiacyl-moiety role. *J. Phys. Chem. A* **113**, 13881–13891 (2009).
134. Trouillas, P., Marsal, P., Siri, D., Lazzaroni, R. & Duroux, J.-L. A DFT study of the reactivity of OH groups in quercetin and taxifolin antioxidants: The specificity of the 3-OH site. *Food Chem.* **97**, 679–688 (2006).
135. Di Meo, F., Sancho-García, J. C., Dangles, O. & Trouillas, P. Highlights on anthocyanin pigmentation and copigmentation: A matter of flavonoid pi-stacking complexation to be described by DFT-D. *J. Chem. Theory Comput.* **8**, 2034–2043 (2012).
136. Nave, F. *et al.* Influence of a flavan-3-ol substituent on the affinity of anthocyanins (Pigments) toward vinylcatechin dimers and proanthocyanidins (copigments). *J. Phys. Chem. B* **116**, 14089–14099 (2012).
137. Miller, B. R. *et al.* MMPBSA.py: An efficient program for end-state free energy calculations. *J. Chem. Theory Comput.* **8**, 3314–3321 (2012).
138. Genheden, S. & Ryde, U. The MM/PBSA and MM/GBSA methods to estimate ligand-binding affinities. *Expert Opin. Drug Discov.* **10**, 449–61 (2015).
139. Hou, T., Wang, J., Li, Y. & Wang, W. Assessing the Performance of the MM/PBSA and MM/GBSA Methods. 1. The Accuracy of Binding Free Energy Calculations Based on Molecular Dynamics Simulations. *J. Chem. Inf. Model* **51**, 69–82 (2010).
140. Aidas, K. *et al.* The Dalton quantum chemistry program system. *Wiley Interdiscip. Rev. Comput. Mol. Sci.* **4**, 269–284 (2013).
141. Trouillas, P. *et al.* *Optical properties of wine pigments: theoretical guidelines with new methodological perspectives.* *Tetrahedron* **71**, (Elsevier Ltd, 2015).
142. Bradshaw, D., Claridge, J. B., Cussen, E. J., Prior, T. J. & Rosseinsky, M. J. Design, chirality, and flexibility in nanoporous molecule-based materials. *Acc. Chem. Res.* **38**, 273–282 (2005).
143. Roesky, H. W. & Andruh, M. The interplay of coordinative, hydrogen bonding and  $\pi$ - $\pi$  stacking interactions in sustaining supramolecular solid-state architectures. A study case of bis(4-pyridyl)- and bis(4-pyridyl-N-oxide) tectons. *Coord. Chem. Rev.* **236**, 91–119 (2003).
144. Brouillard, R., Mazza, G., Saad, Z., Albrecht-Gary, A. M. & Cheminat, A. The

- copigmentation reaction of anthocyanins: A microprobe for the structural study of aqueous solutions. *J. Am. Chem. Soc.* **111**, 2604–2610 (1989).
145. Markovic, J. M. D., Petranovic, N. A. & Baranac, J. M. A spectrophotometric study of the copigmentation of Malvin with caffeic and ferulic acids. *J. Agric. Food Chem.* **48**, 5530–5536 (2000).
146. Alluis, B. & Dangles, O. Quercetin (=2-(3,4-Dihydroxyphenyl)-3,5,7-trihydroxy-4H-1-benzopyran-4-one) Glycosides and Sulfates: Chemical Synthesis, Complexation, and Antioxidant Properties. *Helv. Chim. Acta* **84**, 1133–1156 (2001).
147. Oszmiański, J., Bąkowska, A. & Piacente, S. Thermodynamic characteristics of copigmentation reaction of acylated anthocyanin isolated from blue flowers of *Scutellaria baicalensis* Georgi with copigments. *J. Sci. Food Agric.* **84**, 1500–1506 (2004).

# **A P P E N D I X**

## P U B L I C A T I O N I.

M. Pyszková, **M. Biler**, D. Biedermann, K. Valentová, M. Kuzma, J. Vrba, J. Ulrichová, R. Sokolová, M. Mojovic, A. Popovic-Bijelic, M. Kubala, P. Trouillas, V. Křen, J. Vacek, *Flavonolignan 2,3-dehydroderivatives: Preparation, antiradical and cytoprotective activity.* Free Radical Biology and Medicine 90 (2016) 114-125.

## PUBLICATION II.

E. Vavříková, V. Křen, L. Jezova-Kalachova, **M. Biler**, B. Chantemargue, M. Pyszková, S. Riva, M. Kuzma, K. Valentová, J. Ulrichová, J. Vrba, P. Trouillas, J. Vacek, *Novel flavonolignan hybrid antioxidants: From enzymatic preparation to molecular rationalization.* European Journal of Medicinal Chemistry. Submitted.

## P U B L I C A T I O N   I I I .

**M. Biler**, P. Trouillas, D. Biedermann, V. Křen, M. Kubala, *Tunable optical properties of silymarin flavonolignans*. *Journal of Photochemistry and Photobiology A: Chemistry* 328 (2016) 154-162.

## PUBLICATION IV.

A. Vallverdú-Queralt, **M. Biler**, E. Meudec, Ch. Le Guernevé, A. Vernhet, J.-P. Mazauric, J.-L. Legras, M. Loonis, P. Trouillas, V. Cheynier, O. Danglese, *p*-Hydroxyphenyl-pyranoanthocyanins: an experimental and theoretical investigation of their acid – base properties and molecular interactions. International Journal of Molecular Sciences 17 (2016) 1-19.

## PUBLICATION V.

M. Kubala, P. Čechová, J. Geletičová, **M. Biler**, T. Štenclová, P. Trouillas, D. Biedermann, *Flavonolignans as a novel class of sodium pump inhibitors*. *Frontiers in Physiology* 7 (2016) 1-10.